21st International HISWA Symposium on "Yacht Design and Yacht Construction"

Amsterdam, 15 & 16 November 2010

PROCEEDINGS

Edited by Piet W. de Heer

November 2010

Organized by HISWA - National Association of Watersport Industries in The Netherlands,
The International Trade Show of Marine Equipment METS 2010
Delft University of Technology

Photo cover: Ed Holt

Delft University of Technology
Ship Hydromechanics Laboratory

Printed by:

Service Point
Rooswijkseweg 311
Postbus 10000
1970 CA IJmuiden

Phone: +31 (0)251 495804
Fax: +31 (0)251 470002
Email: ijmond@servicepoint.nl

KONINKLIJKE BIBLIOTHEEK, DEN HAAG
Depot van Nederlandse Publicaties
Postbus 74
2501 AJ Den Haag

21st International Symposium on "Yacht Design and Yacht Construction": Proceedings of the 21st International Symposium on "Yacht Design and Yacht Construction", Amsterdam, 15 & 16 November 2010 – Delft University of Technology, Ship Hydromechanics laboratory, The Netherlands.
ISBN: 978-90-370-0010-8
Subject headings: Yacht Design, Yacht Construction

TABLE OF CONTENTS

Program Monday

Program Tuesday

Introduction

Session 1 – Jack Somer

Session 2 – Rene van Gilswijk

Session 3 – Mr. M. Krikke

Session 4 – Andy Glaughton

Session 5 – Jean Matthieu Boergeon

Session 6 – Guido Loeff

Session 7 – Jaap Gelling

Session 8 – Alex Meredith Hardy, Sylvain Julien & James Roy

Session 9 – I.M. Viola & R.G.J. Flay

Session 10 – H. Renzsch & K. Graf

Session 11 - Frederic Louarn & Paolo Manganelli

Session 12 - Roel ter Heide

HISWA Symposium 2010

Location: **Emerald Room, Amsterdam RAI**
Date: **November 15-16**

Program Monday November 15, 2010
Moderator: **Jack Somer**

08.30-10.00	Registration	
10.00-10.05	Opening	
10.05-10.45	"Recent and Future Developments in Mega Yacht Design" *Speaker: Jack Somer*	
10.45-11.00	Coffee Break	
11.00-11.45	"The Effect of the Choice of Building Material on the Sustainability of a Yacht" *Speaker:* Rene van Gilswijk	*
11.45-12.30	"On the use of adhesion techniques in the maritime industry?" *Speaker: Mr M. Krikke (Adhesion project)*	
12.30-13.30	Lunch Break	
13.30-14.15	"The Development of a new America's Cup Rule" *Speaker: Andy Glaughton*	*
14.15-15.00	"The Development of the Hydroptere" *Speaker: Jean Matthieu Boergeon*	
15.00-15.15	Coffee Break	
15.15-16.30	"Control on Comfort Onboard Yachts in Anchoring Conditions" *Speaker: Guido Loeff*	*
16.30-17.00	"New Concepts in the Design of Fast Ships" *Speaker: Jaap Gelling*	
17.00-17.30	"Recent Regulatory Changes and their Impact on the Design of Large Yachts" *Speaker: Alex Meredith Hardy*	
17.30-18.30	Reception	

Program Tuesday November 16, 2010
Moderator: Jack Somer

09.00-09.45	"On Water Pressure Measurements on a Modern Asymmetric Spinnaker" *Speakers: I.M. Viola & R.G.J. Flay*
09.45-10.30	"Fluid Structure Interaction Simulation on Spinnakers - Towards Simulation Driven Design" *Speakers: H. Renzsch & K. Graf*
10.30-10.45	Coffee Break
10.45-11.30	"A simplified slamming analysis model" *Speaker: Paolo Manganelli*
11.30-12.15	"Diesel Electric Propulsion Systems for Yachts" *Speaker: Roel ter Heide*
12.15	Closing

*) Not available at time of printing

INTRODUCTION.

Dear Delegates,

For the 21 th time now we organize the International HISWA Symposium on Yacht Design and Construction here in the RAI Congress Centre in Amsterdam.

It is always a not directly visible but substantial amount of work that has been put in the selection of topics and papers for this conference. Much of this work is carried out by the Scientific and Paper Committee.
This time the Organizing Committee and the Scientific Committee have joined their efforts to focus a serious part of the contents of the presentations on sustainability and related “green” subjects. I think that, looking at the contents of the papers, that this is now well balanced with other interesting topics related to the high tech end of the yacht design and yacht building industry. As always there is a good mix between science and industry and this is completely in line with our slogan: “the HISWA Symposium, where science meets industry”

This is the right place to thank all the authors for their considerable efforts to produce these presentations and the written contributions for the Proceedings. Without their efforts the symposium would not have been possible.

In addition I certainly wish to express my gratitude towards our sponsors here. You can find their logo’s on the cover of the Proceedings. In our effort to keep the delegate fee affordable and also to allow a considerable group of students from all kind of education institutions to take part at even lower cost, their financial contributions are very important and very much appreciated.

Let me finish with stating that I hope that the gathering of people, involved in design, research or construction of yachts at the actual Symposium days will be as interesting and fruitful as ever.

Jan Alexander Keuning
Chairman of the Organizing Committee
International HISWA Symposium on Yacht Design and Construction

ADHESION: *Adhesive bonding in ship structures*

Authors:

Marnix Krikke; Centre for Maritime Technology and Innovation

Ramona Steenbreker; Adhesion Institute - Delft University of Technology

Bernd-Jan Bekkers; Damen Schelde Naval Shipbuilding

Introduction

Shipbuilding companies in The Netherlands need to have a range of technologies available to provide innovative engineering solutions for their shipbuilding projects. These solutions enable the effective production of various types of complex and multifunctional ships that have to meet very demanding requirements. For light weight constructions and for constructions composed of various materials the welding technology reaches its limits. Adhesive bonding offers a promising alternative for these constructions, be it that the technology is not readily available for typical maritime applications. To implement advanced technology of adhesive joints with class approval in shipbuilding practice a new research project 'Adhesion' was initiated within the Netherlands Maritime Innovation Programme. The project consortium consists of 13 collaborating organisations representing the various stakeholders - shipyards, a company producing adhesives, engineering firms, knowledge institutes and classification societies. The project includes development of a design and engineering methodology, an experimental program on structural elements and development and testing of demonstrators. Four cases, representing typical maritime structures and combinations of materials, were selected and documented. A first series of orientating elementary experiments have just been completed. It was concluded that the tested adhesive bonds were of such quality that these bonds can be used for durable applications.

Literature review

A literature survey has been conducted to review the current state of art of adhesive bonding in maritime applications.

Only a minority of papers were found for the specific cases. Most papers dealt with different adherent materials. For application in marine environments, adhesively bonding ship structures involves more than just replacing the currently used methods like bolting and welding. Not all structures are suitable for adhesive bonding. However, for some structures, consisting of dissimilar metals, adhesive bonding is an excellent joining technique. For adhesive bonding to be introduced successfully, the designs need to be specifically tailored to optimize the loading condition of the adhesive (maximizing shear and minimizing peel). Care must be taken in pre-treatment of the substrates and application of the adhesives in an actual manufacturing environment. Experience and knowledge on applications in other sectors, like the automotive or aerospace industry will be beneficial to shipbuilders. In these sectors the technology for design and engineering of durable adhesively bonded joints is further advanced.

The current challenges of the successful application of adhesive bonding in maritime applications lie within the prediction and validation of the long term behaviour of adhesive bonded joints. Experiments should be developed which show that a joint fulfils the long term requirements. The literature survey also disclosed that research in adhesively bonded joints

in maritime applications is mainly focussed on numerical prediction methods. More attention should be given to the physical understanding of adhesive bonded joints, using known analytical solutions.

The literature survey concluded that very limited literature is available that contains knowledge directly applicable to the specific maritime cases. However, information from other sectors in which adhesively bonded joints are applied may be effectively translated to the shipbuilding industry. This does require an effort from the shipbuilding engineers to change designs details to optimize the mechanical loading of the adhesives. From the literature review it is recommended to start using adhesively bonded joints in secondary structural parts to gain practical experience with both the design as well as the production process, and to choose structures in which application of adhesive bonding can have a significant benefit, either economically or for maintenance reasons.

Advantages and disadvantages of adhesive bonding

The main *advantages* of adhesive bonding of ship structures, compared to other joining techniques are:

Design: The adhesive bonding technique may lead to reduction in weight of construction and increase in application of different materials. A larger design space for light weight ship constructions is thereby achieved. The bonds are providing electric and galvanic isolation, which prevents corrosion. Due to the flexibility of the bond the mechanical damping is high, which reduces vibrations.

Production: The flexibility of production will be higher, because bonding may be applied during all building stages. Modifications in the final stage of production will be realized with less time and cost due to reduced pre- and after treatment compared to welding.
Cleaner working conditions

The main *disadvantages* of adhesive bonding of ship structures, compared to other joining techniques are:

Design: Limited practical knowledge is available on the behavior of adhesive bonds applied to ships during the life cycle in relation to production specifications. Application in constructions critical to fire safety is limited due to reduction of bond strength at high temperatures.

Production: Adhesive bonding is not yet a fully accepted joining technique in shipbuilding. Experience shows that employees used to welding have to pass a high threshold to adopt adhesive bonding technology. Very different production techniques have to be exploited, such as: mixing, application (times), strict cleaning procedures, curing times. Adhesive bonding requires also a better control of dust and temperature of the production environment. Especially for on site repairs conditions may be hard to control. Finally the qualification of bonded constructions is more demanding due to limited knowledge on inspection methods.

During the project all these critical aspects will be addressed, with emphasis on removing obstacles and adapting technology to the specifics of maritime constructions.

The project objectives

In shipbuilding practice adhesive bonding applications are scarce, and knowledge in this area is fragmented. For wider applications and up scaling of adhesive bonding techniques the

available knowledge and know how at the shipyards is insufficient. The knowledge centres and engineering companies have extensive knowledge in other areas, but have to adjust their knowledge to the specific character of ships operating in demanding maritime conditions and to the limitations and particulars of the shipbuilding process.

For that reason the Adhesion project was initiated with the overall objective to implement technology of classified adhesive joints in shipbuilding practice. The following more specific objectives have been formulated:

- To develop and provide knowledge and guidance to designers and engineers of maritime constructions on how to engineer constructions in which adhesive bonding is applied;
- To determine the effect of the shipyard process and conditions on the most appropriate bonding technology;
- To transfer know how of practical adhesive bonding applications to shipyard production and repair employees;
- To identify the technical and economic potential of large scale applications of bonding technology to light weight maritime constructions.

A case based experimental research approach has been chosen to achieve the above mentioned goals. Knowledge will be gained and a methodology is being developed by analysing and redesigning a few typical cases. Each selected case represents a class of typical maritime constructions, fulfilling a combination of functions and subject to a limited range of loading conditions. The cases have to be applicable to various ship types. For example, one of the cases consist of the adhesive bonding of a structure on top of another structure, which could represent a mast on a superstructure or a superstructure on a hull, where different material combinations will be investigated.

The project outline

Based on detailed investigations of selected cases, load spectra and other functional requirements are determined. From these cases the specifications for several test series are derived. These test series range from elementary specimen tests to three dimensional structural details. Based on the results of elementary specimen testing, combinations of surface treatment and adhesion material will be chosen. Construction cases will be redesigned an tested extensively. Finally a demonstrator will be developed. Results of previous test series will contribute to a technical and economical evaluation of an upscaling of the demonstration case. The effects of shipyard conditions will be determined by comparing specimen produced in ideal and realistic conditions. In short, the following characteristics of bonds will be researched:

- Initial mechanical behavior
- Durability: corrosion (influence of moisture, salt water)
- Durability: the influence of cyclic ageing

All knowledge gained in this project will be included in a guidance document describing a design and engineering methodology. This document has to provide support in the selection of materials and bonding methods, the introduction of selected material and bonding methods into the overall and detailed design. The selected cases will be used to guide the development of a design and engineering methodology. This result will be a design and engineering handbook and course material. The guidance procedure will be detailed throughout the project. A major issue is to develop procedures for qualification of adhesive bonding, that may ease the certification process for bonded constructions.

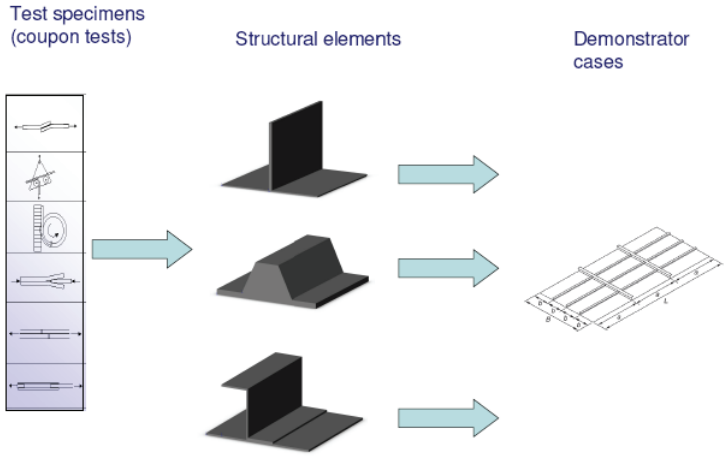

The final project task is a technical and economical evaluation of the new techniques compared to the traditional joining techniques. The knowledge, methodology and know-how developed in this project will enable the project partners to design light weight constructions in which robust adhesive bonds are applied.

The partners in the Adhesion project are:

- Two knowledge institutes (TU Delft Aerospace and TU Delft 3ME), who will provide technology and perform tests;
- A world leading company in adhesive bonding (Henkel) will bring in the latest developments in bonding technology and products;
- Two engineering firms will guide the partners in engineering solutions (Airborne and Lightweight Structures);
- Six shipyards are participating in this project (two IHC yards; three yards of Damen and Oceanco).
- Two classification societies (Bureau Veritas and Lloyds Register) will monitor the technology development and advice on the certification process.

The introduction of this new technology will reduce the building time and cost of engineering and building of ships, through higher efficiency and increased flexibility in the building process and through decreased risk in producing lightweight constructions.

The Adhesion project started in January 2009 with a lead-time of 32 months. The first series of orientating experiments within the project have been completed. The test results show the effect of various general used primer systems to the strength and durability of the adhesive bonding applications. Especially the thickness of the primer is a very important parameter. The interaction between a number of selected adhesive bonds and primers is of such high quality that these bonds could be used for durable applications.

Accelerated ageing tests will be executed to explore the durability of specific primer and adhesive bonds combinations. Various preliminary treatments (grinding, sandblasting, grit-blasting, laser cleaning, etc.) will be examined during these experiments. The intention is to compare the accelerated ageing test samples to the real life influence of the environment and through that to validate the computer models that predict the actual lifetime of the adhesive bonds.

Following the elementary testing, specimen testing will be done in a laboratory and will be repeated in shipyard environments. This will contribute to the education of the designers, engineers and production personnel of the participating companies on the subject of designing and production of adhesive joints. The results will be included in a project database.

Transfer of knowledge

A selected group of designers, engineers is offered theoretical and practical adhesive bonding workshops in laboratory conditions. The workshop addresses the following topics: Where and when can I use adhesive bonding? What are the consequences for my construction? What is the durability and not in the last place: the price? What are the safety factors? how to select the right adhesive for the job? and how do I determine the optimal pretreatment. etc.

The production personnel is offered comparable workshops with emphasis on production aspects. These workshops address the following topics: how do I know if my surface is clean enough?, what is the green time of my adhesive?, what to do if the surface is found to be damp?, how do I control the adhesive bond line?, and how do I visually determine if an adhesive bond is OK or not?

Within this project and with the support of M2i the Adhesion institute has therefore developed a program for employees that will apply the adhesives in practice, to ensure they have the proper knowledge and skills. The Adhesion Institute, organises for that reason these workshops on ‘European Adhesive Bonder level (EAB)’ that can be compared to the well-known welding courses. In these workshops, lectures are given on the properties of adhesives and their application in practice, as well as pre-treatments, design, safety, quality control and durability. The workshops include a practical part, where participants learn to apply adhesives and test these bonds in a certified laboratory.

Conclusions

Adhesive bonding has a large potential within the shipbuilding sector. The project Adhesion accelerates the introduction of adhesive bonding in this sector. The firsts test series have shown promising results.

A major issue is the behaviour of adhesive bonding over time in a demanding maritime environment. Procedures have to be developed to ease certification of bonded constructions.

More information about the Adhesion project:

Centre for Maritime Technology and Innovation,	**DAMEN SCHELDE NAVAL SHIPBUILDING (DSNS)**
Boudewijn Hoogvelt	Bernd-Jan Bekkers
Innovation manager	bj.bekkers@damennaval.com
+31 6 5068 1908	

l'HYDROPTERE: A story of a dream

JM Bourgeon, S Dyen, D Moyon, D Schmäh, R Amacher, D Colegrave, Hydroptère Design Team

M Calmon, M Farhat, P Fua, K Startchev, G Bonnier, J-A Månson, V Michaud, A Sigg, M Oggier, MO Deville, O Braun, ML Sawley, L Blecha, J Cugnoni, Ecole Polytechnique Fédérale de Lausanne (EPFL), CH

SUMMARY

In 2009, l'Hydroptère broke the symbolic barrier of 50 knots and became the world fastest sailing boat over both 500 meters and 1 nautical mile. This major achievement relied on the high skills of the sailing team but also on technical advances of the boat, resulting from long years of studies and development. This achievement is also an open window to a new goal: flying around the world.
In the present article, we present this long and incredible story, highlighting the different steps, the technology involved, and the background of that project..

NOMENCLATURE

d	Level of immersion (m)
G_{Ic}	Griffith's critical strain energy release rate (J)
q	Angle of refraction (°)
P,Q	Pixel distributions
p	Static pressure (Pa)
p_v	Vapour pressure of water (2300 Pa)
ρ	Density of water (997 kg m^{-3})
s	Cavitation number ($= \frac{p - p_v}{\frac{1}{2}\rho V^2}$)
V	Flow velocity (m s^{-1})
2D	Two-dimensional
3D	Three-dimensional
CVLab	Computer Vision Laboratory
DMA	Dynamic Mechanical Analysis
DSC	Differential Scanning Calorimetry
EPFL	Ecole Polytechnique Fédérale de Lausanne
FE	Finite Element
LIN	Computational Engineering Laboratory
LMAF	Laboratory of Applied Mechanics and Reliability Analysis
LMH	Hydraulic Machines Laboratory
LTC	Laboratory of Polymer and Composite Technology
UD	Unidirectional tape
UFO	Unidentified Floating Object

1. PRINCIPLE

l'Hydroptère is a sailing trimaran using the lift of hydrofoils in a whole sense, i.e. using them to balance completely the weight of the boat and to pull the hulls out of the water from a minimum boat speed, thus reducing drastically hydrodynamic drag and raising performance to high levels.

2. HISTORY

2.1 BEGINNING

In 1987, with the help of Eric Tabarly, Alain Thébault met engineers from Dassault Aviation in order to imagine a new sailboat, now able to fully flight thanks to new composite materials.
Thebault had to wait until 1992 before starting the building of his boat, the time to experiment on several reduced scale models and to convince partners to follow him in that crazy project.
l'Hydroptere was launched in 1994 and the first fly was a full success, with a nice stability and high speeds reached for that time.

2.2 10 years of reliability

During the ten years following the first flight, l'Hydroptère knew three major crashes.
Indeed, because of this totally new way of sailing, the strengths viewed by the different pieces of the boat were unknown.

1995: Breakage of the leeward crossbeam. After that first crash, in the same way than in aeronautic world, engineers understood they had to set up a full measurement system, in order to record data and better understand the loads viewed by the boat.

1998: Lose of the leeward foil, after the breakage of a link bolt.

2002: Breakage of the windward crossbeam during an offshore sailing at high speed in rough see. Then the team understood it would never be possible to prevent the boat from every peak loads. The solution was to set up shock absorber between the foil and the crossbeam in order to protect the boat structure in every sailing condition.

2.3 10 years of performance quest

In 2004, the team launched a fully reliable boat, with a well-calculated structure, inboard systems to run a full time survey of the loads, and shock absorber to prevent the boat from damages.

Then the team may concentrate on one goal: be the fastest sailboat for offshore sailing.
We made the choice to validate different steps in our quest:

- Costal sailings
- Speed
- Offshore sailings

2005: First costal record. l'Hydroptère crossed the Channel faster than aviator Louis Blériot in 1909, sailing from Dover to Calais in 34 minutes and 24 seconds, at an average speed of over 33 knots.

2006: l'Hydroptère unfortunately collided with an Unidentified Floating Object (UFO) during a Cadiz to San Salvador crossing record attempt. Afterward, Swiss nationals Thierry and Adrien Lombard saved the project and established a contact between the Hydroptère Team and the Ecole Polytechnique Fédérale de Lausanne (EPFL), giving rise to a scientific partnership.

2007: Launch of new version of l'Hydroptère, with new planning floats and a new rigging.

Two new world speed sailing records:
→ 500m/D class record – 44.81kts
→ 1Nm outright record – 41.69kts

Costal records attempts on SNSM (Saint-Nazaire/Saint-Malo) and Brittany Ferries (Plymouth/Roscoff).

The team discover both high speed and offshore potential of the concept.

2008: Studies for the outright speed record over 50kts. In partnership with EPFL, the team work on several domains, mainly hydrodynamics in order to solve cavitation problem, but also on aerodynamic and structural behaviour issues.

Despite nice numerical and experimentation results, the crew met difficulties to stabilize high speed on 500 meters. Indeed, because of instabilities of wind and see conditions (gust, waves), the foil shape needed to be more versatile.
In high windy conditions, with wind gust over 45kt, and after a peak speed of 56.36kts reached, l'Hydroptère capsize the 21st of December 2008.

2009: The design team find the problem of the instability in the behaviour of the boat. In specific conditions of incidence and immersion of the windward foil, at very high speed, a coupling between the twist of the crossbeam and the load on the foil appear.
With a new shape of the foils, the team solved that problem and the crew manage to reach the speed goal over their deeper objectives with two new world records:
→ 4 September 2009: Outright speed record over 500m – 51.36kts
→ 8 November 2009: An incredible outright speed record over 1Nm – 50.17kts

2010 and after: Back to the offshore. After the speed step, the team concentrate on a new one, sailing offshore at high speed.

To reach that goal, the team can experiment offshore thanks to l'Hydroptère, test improvements and measure phenomenon.

Moreover, the team members designed and launched the 8th of October 2010 a new 35 feet catamaran on Geneva Lake. This new boat is the result of years of studies and learning on the oldest boat. This new flying catamaran is a true laboratory that will permit the engineers to better understand the behaviour and the different solutions available.

3. BACKGROUND

3.1 COMPANY

Hydroptère is two companies: Hydroptère France located in Paris with office and shipyard in Brittany, and Hydroptère Suisse located in Lausanne with office just close to EPFL.

3.2 TEAM

Since the beginning of the project, Alain Thébault has been accompanied by passionate professionals from the marine and aeronautical fields. An extraordinary team composed of sailors, scientists and technicians has been created to design, develop and make the boats fly:
- A Sports Team based in La Trinité sur Mer with 8 engineers, technicians and sailors.
- A Design Team based in Lausanne with 5 engineers.
- An Operational Team based in Paris with 2 persons in charge of the communication and the finance.
- A strategic support from 8 engineers on a voluntary basis – called the "Papés" – from high-tech industrial companies (Dassault, Airbus, Assystem...).

3.3 PARTNERS

Two mains sponsors permit the dream going on:
- The swiss bank LOMBARD ODIER

- The swiss watchmaker AUDEMARS PIGUET

4. THE STUDIES

To achieve such outstanding performance with wind as the only driving force, the Hydroptère Team has required to decrease air resistance of all the boat's aerodynamic elements and to improve both shape and tuning of the sails in order to obtain as much propulsive force as possible. But the main challenge is to obtain sufficient lift force from the hydrofoils despite phenomena encountered at high speed like cavitation and ventilation that can lead to hydrodynamic load instabilities. Moreover, structural design, materials choice and manufacture are the main factors affecting the safety and stability of the yacht and can significantly affect its overall performance. In such a trans-disciplinary project, the global design and optimization process usually requires a significant number of inputs and hypotheses coming from different fields like fluid dynamics for the determination of the wide range of loading conditions, or materials science and solid mechanics for the determination of the failure criteria of the materials that can be used. Knowing these design criteria, an iterative design-simulation-optimization process can then be employed to progressively turn an innovative design concept into a highly sophisticated and high-performance hydrofoil yacht.

4.1 MATERIALS

To minimize the weight of the structure while answering to the needs of the design, it is necessary to carefully evaluate and optimize the properties of materials and of their assembly in conditions that are very close to ship yard practice (humidity, temperature, lay-up and processing time, part shape, etc...). Several studies were thus performed to gain confidence and potentially reduce safety factors in the part design.

4.1.1 MANUFACTURING PROCESSES

Most parts of the boat are made of carbon-epoxy composites, either as monolithic parts or as sandwich structures with honeycomb cores. Several processing methods are used, depending on the part design, from lay-up of wet-impregnated fabrics or prepregs cured under vacuum bag only, to prepregs cured in an autoclave. For all these, several studies were carried out to select the best process, including the cure schedule, and to check the part quality after processing. Additional studies were carried out to analyse the influence of the off-axis plies in the final part properties in bending. Occasionally, analyses were carried out on processed parts, especially if potential defects are suspected: visual inspections by micrographs or curing stage by Differential Scanning Calorimetry (DSC) and Dynamic Mechanical Analysis (DMA) for example. A constant interaction between the boat builders, the Hydroptère Design Team and the lab is crucial to obtain best results.

4.1.2 SANDWICH STRUCTURES

A specific study was carried out to compare the design values with experimental results for honeycomb sandwich structures processed with Nomex Flexcore under vacuum bag only (Figure 1). The final aim was to determine how this anisotropic honeycomb affects the properties of the final sandwich of the hull and provided experimental values for simulation model.

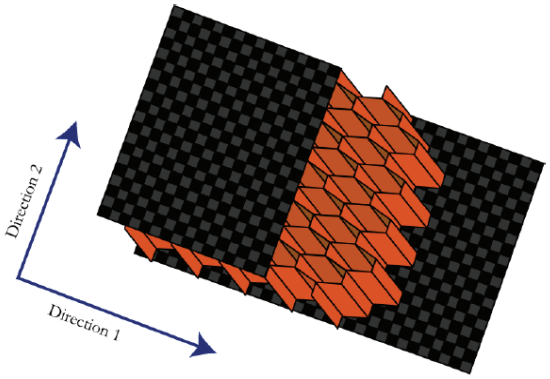

Figure 1: Anisotropy of the Nomex Flexcore and the two main directions

For this, samples consisting of skins only, then full sandwich structures were manufactured and tested in tension, compression and shear for the skins, and in four points bending with several span lengths for the sandwich beams in order to calculate the shear modulus of the core in the two main directions. A careful comparison of the experimental values, with the estimated values from the skins and core properties was carried out and used in the simulated model.

4.1.3 THREADED JOINTS

Several metallic parts are attached to the composite parts through threaded joints, for example the mast railing. A study was conducted to assess the strength of these joints, as a function of the composite type (unidirectional UD vs. quasi-isotropic), the screw material (stainless steel vs. composite), the presence of an insert or not, and how it is assembled (glued screw, screw with release agent and glued). Joints were made, and a testing device was produced that allowed the screws to be tested by extracting them with a force perpendicular to the composite plane. Results show as expected that it is important to reinforce the joint location by quasi-isotropic lay-up (Figure 2). Also, direct threading with a proper tool, with a glue layer, gives the best results. However, a request could be that joints can be removed easily for dismounting and repair. The use of a release agent before gluing the screw does not decrease the ultimate strength, even if the screw is un-screwed and re-screwed. These results do not take into account aging effects. If the screw is to be removed “frequently”, a glued insert can be safely used, albeit with a weight penalty.

(a)

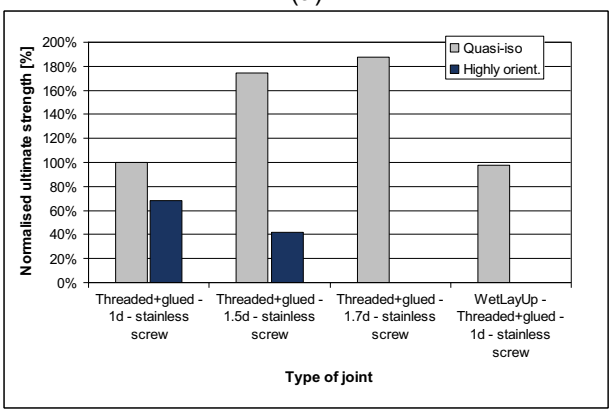

(b)

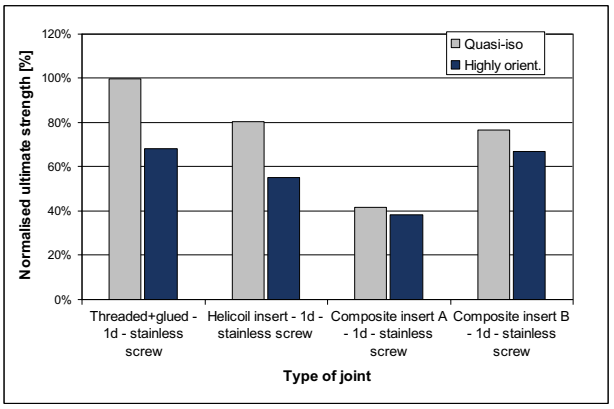

Figure 2: Comparison of the pull-out force for several types of joint
(a) Thread length effects
(b) Thread type effects
(100% reference value correspond to stainless steel screw threaded in quasi-isotropic laminate, with embedment length of the screw diameter)

4.1.4 BONDING

An extensive study was carried out to optimise the surface treatment of titanium for bonding to composite parts. This is crucial to make sure these bonds are designed properly, and the effect of aging is taken into account. For this, comparative measurements of fracture strength and Griffith's critical strain energy release rate G_{Ic} were carried out on adhesive bonded joints with three surface treatments of titanium. Tests were performed un-aged and along thirteen weeks of accelerated aging in salted or de-ionized water at 50°C. Thermo-mechanical measurements were carried out on the epoxy Araldite 420 adhesive alone, with the same aging conditions.
From these results, the best practical solution for the performance and lifespan of the bonded joint was determined. A combined surface treatment of sanding, degreasing and chemical etching shoed the best durability, whereas a treatment using a sulphuric anodic oxidation in addition showed the best adherence before aging. On the whole, bonded joints showed a high variability and a fall of their properties from 30 to 70% at the end of aging according to the surface treatment.

A numerical method for dimensioning was proposed by means of a finite element implementation with a cohesive zone model in Abaqus. This method was validated by simulation of two representative mechanical tests corroborating the experimental results. Experimentally determined failure criteria as well as aging effects and safety factors were thus taken into account in the finite element model.

4.2 STRUCTURE

For precise predictions of the dynamic behavior of the yacht, a detailed and accurate model of the structure is required. However, because of the large number of variables (material properties, geometry and assembly) and their inherent uncertainties, the developed FE model had to be thoroughly validated on the basis of real structural tests. A series of tests have been conducted first on components and then on the whole yacht. The static deformations of key elements were measured under various loading conditions to determine the most important stiffness values and a detailed modal analysis of the foils alone and the whole yacht was carried out.

The measured stiffness's and Eigen frequencies were then used to update the FE model parameters in order to achieve a good agreement between the numerical predictions and the real behaviour of the structure. A FE model optimization method was developed and interfaced with the Abaqus solver to automate the parameter updating procedure and maximize the accuracy of the numerical model (Figure 3).

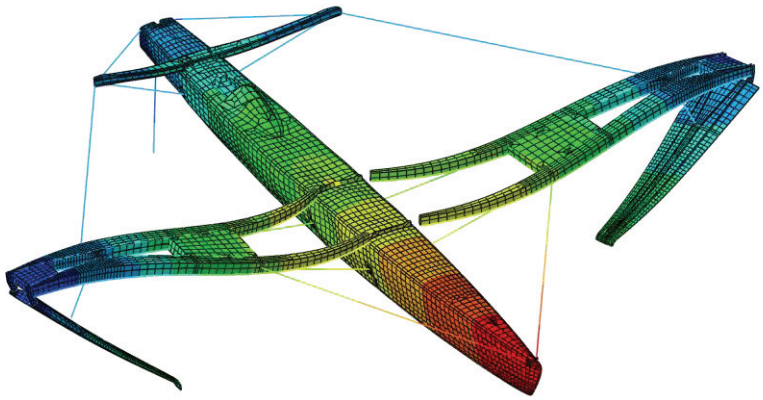

Figure 3: Numerical modal analysis of the whole l'Hydroptère structure using the calibrated model

The calibrated FE model was also used to provide important modal analysis data to the Hydroptère Design Team in order to study the hydrodynamic stability (divergence / flutter) of the rear stabilizator at high speed (Figure 4).

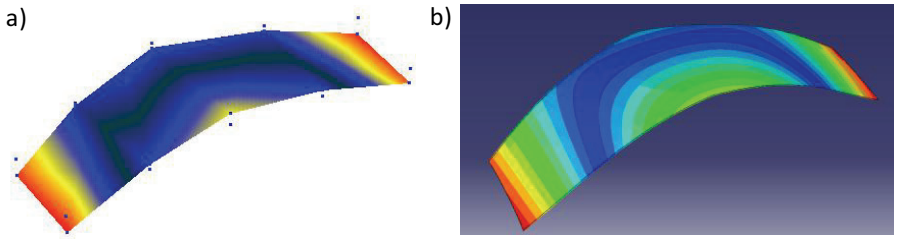

Figure 4: Experimental modal analysis of the rear horizontal stabilizator (a) and predictions using the calibrated model (b)

4.3 ONBOARD MEASUREMENT SYSTEMS

4.3.1 PRESENTATION

A measurement system on board provides the sailors with real time values and is divided into four sub-systems:

- Stress and positioning sensors
- Navigation unit
- Inertial unit
- Video system

The stress measuring and positioning system is composed of 54 sensors, placed on various strategic points on the boat. It includes four types of recordings:

- Strain gauges, measuring local stress, which permit the analysis of the efforts sustained by the structure of the boat
- Accelerometers
- Rotation sensors
- Pressure sensors

All these sensors are connected to HBM digiCLIP digital amplifiers.

The navigation unit indicates the environment in which l'Hydroptère evolves, speed, angle, direction of real and apparent winds, and the GPS positioning of the boat.

The IXSEA Octans inertial unit gives the boat's attitudes, roll, pitch, surge, yaw and dig in, as well as their speeds and accelerations, with great precision.

The video system has been added using Cosworth Pi VIDS2 video recorder, and a few cameras, in order to analyse in real time the submerged depth of immersed appendages, as well as the structure deformation, with video-imaging techniques.

All the values from the four sub-systems are spread in a CAN bus and recorded in a synchronised way into a logger box (Cosworth Pi Sigma LLB data logger), as well as copied to a ruggedized computer (Lemer Pax Posibox) in order to:

- Display with visual and sound effects to inform the test engineer on the applied strain, with an alarm signal if necessary
- Process the data through basic mathematical tools or more powerful tools such as filtering or the Fourier transform.

The real-time data are an essential aid to steer the carbon bird over the irregular air-water interface and after every sail test the collected data is analyzed to make improvement for the next sailing day. Those recordings could also be compared off-line to the estimates of the flight simulator, and serves as a database for improvements or new designs.

4.3.2 COMPUTER VISION EXTENSION

Only the resultant of the hydrodynamic loads on the foil is deduced from the jack load. This resultant is the product of the hydrodynamic pressure distribution over the submerged surface of the foil. Thus, high load over only a tip of the foil could lead to the same jack load than a smaller load spread over the whole foil. The knowledge of the submerged depth of the foil allows refining the true effect of hydrodynamic loads.

The principle of the foil immersion detection was derived at the Computer Vision Laboratory (CVLab). The definition of the level of immersion uses the refraction phenomena. It consists in moving along the edge of the foil, and looking for a change of slope due to the refraction of the submerged part (Figure 5). The method, simple in its principle, could be quite challenging in its application since a lot of perturbations could disturb the detection: changing light condition, reflections or spray drops on lens resulting in blurred images.

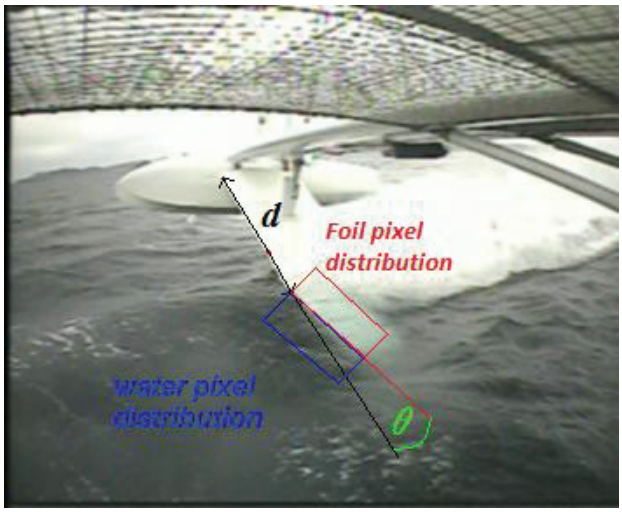

Figure 5: Definition of level of immersion using refraction phenomenon and Kullback-Liebler divergence

The algorithm is based on the maximization of a function of the Kullback-Liebler divergence [3] between pixel distributions *P* and *Q* of the non-submerged or submerged parts of the foil, and water (histogram of pixels), given a level of immersion *d* and an angle of refraction *θ*:

$$F(d,\theta) = \frac{D_{KL}(P,Q) + D_{KL}(Q,P)}{2}$$

$$= \frac{1}{2}\sum_{0}^{255} P(i)\log\frac{P(i)}{Q(i)} + Q(i)\log\frac{Q(i)}{P(i)}$$

The results from this tool can be quite interestingly compared with other synchronised measures

4.4 HYDRODYNAMICS

4.4.1 HYDRODYNAMIC PHENOMENA

4.4.1 (a) Cavitation

The cavitation phenomenon is the formation of vapour cavities within a flowing liquid due to excessive decrease of local pressure [4]. It may occur in a variety of hydraulic systems such as hydraulic turbines and pumps, ship propellers and space rocket inducers. Cavitation may be the source of severe erosion and vibration as well as alteration of hydrodynamic performances.
In the specific case of l'Hydroptère riding at 50 knots, it is almost impossible to avoid cavitation occurrence. As the boat speed increase, cavitation may suddenly appear with a drastic drop of the hydrodynamic lift and a substantial increase of drag and structural vibrations. In this case, the safety may be seriously compromised. Nevertheless, we have worked out the design of the foils to make that phenomenon appearing later and with fewer consequences.

4.4.1 (b) Ventilation

Ventilation is a phenomenon in which air from above the free surface is sucked into a low-pressure zone below the surface. It is of course more important in very low-pressure zones, such as those that can lead to cavitation, and both phenomena are thus strongly interacting. Most often, air from above the surface is guided along the suction side, leading to a drop in lift (as well as in drag, although this is of lesser importance for hydrofoils) [5].

Hydroptère team use numerical simulation and experiments on l'Hydroptère boat in order to define the best solutions to solve ventilation problem.

4.4.2 NUMERICAL SIMULATIONS

Using FLUENT, cavitation was initially investigated by simply "contouring" the low-pressure zones below the vapour pressure; this approach provided interesting but only qualitative results. Another possible approach, using a "mixture" model did not provide adequate results, with a clear tendency to predict very large cavitation zones. More successful was the use of ANSYS CFX with a three-phase flow model. For ventilation, both solvers appeared to perform well, although the convergence properties of CFX were found to be better.

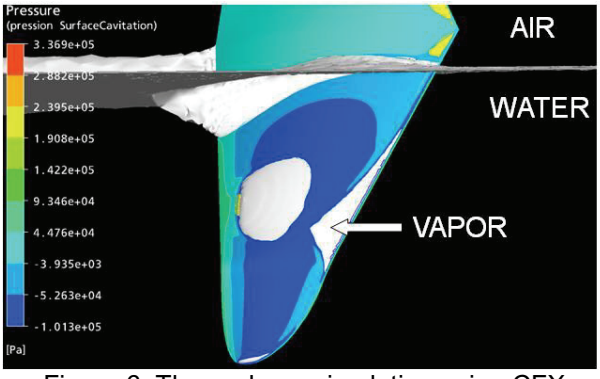

Figure 6: Three-phase simulation using CFX

4.4.3 VALIDATION OF SIMULATIONS

Model scale tests involving three different phases of fluids (air, liquid water and water vapour) are extremely difficult to perform. For validation purposes, phenomena were divided and simulation directed towards two-phase flow cases: cavitation or ventilation alone.

In order to investigate the cavitation phenomenon in the case of l'Hydroptère foils, laboratory tests were carried out at the Hydraulic Machines Laboratory (LMH). 1/10 scaled models of both foils and

rudder/stabilizer portions were mounted in the middle of 150 mm x 150 mm square test section of the EPFL high speed cavitation tunnel. A maximum speed of 50 m/s may be reached at the test section inlet and the pressure may be adjusted from 0.02 to 1.6 MPa. Cavitation can then be easily controlled, either enforced or avoided.

To allow for accurate scale up, the flow velocity was set to 15 m/s and the *s* value corresponded to l'Hydroptère speed of 50 knots under atmospheric pressure. For these conditions, a turbulent boundary layer develops on the foil and Reynolds effects may be neglected.
As illustrated on Figure 7, attached cavitation occurs on the foil. The location of the cavity detachment and its length depend strongly on the angle of attack. For low angles (left), cavitation departs downstream to the leading edge and extends rapidly beyond the trailing edge. In this regime, the flow is rather "smooth" with low induced vibration. As the angle is increased (right), the cavitation appears even for higher *s*, and its detachment moves upstream with growing amplitude of the cavity pulsation. The sheet cavitation turns into the so-called cloud cavitation, which is associated with large lift fluctuation and induced vibration.

In the design process, profile sections, distribution and angles of attacks of the foils of l'Hydroptère were optimized to avoid the occurrence of cloud cavitation.

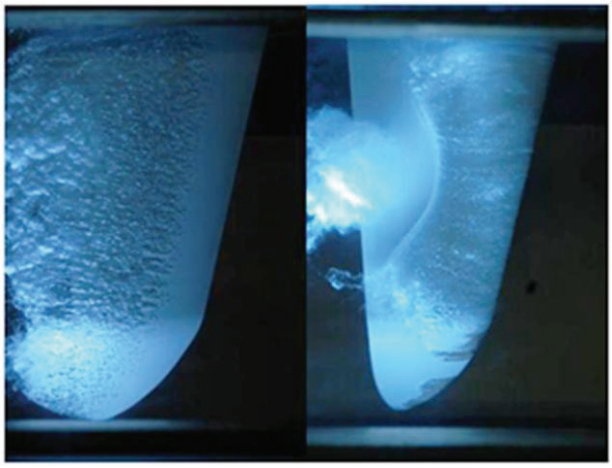

Figure 7: Cavitation trends
(Left: low *a* and $\bar{s}$=26;
Right: high a and $\bar{s}$=87)

Initial validation studies were based on direct visual comparison between experimental photos and simulated images for the same flow conditions. Although this is only qualitative, it already gives a good idea of the ability to capture the presence of cavities, their extent and shape, the inception trends, etc.

More quantitative validation was performed through the variation of hydrodynamic loads according to cavitation extent. The experimental loads were determined by mounting the foil on a calibrated 5-axis balance, and compared with the simulated loads.

Ventilation is a more complex phenomenon to validate, since the hydrodynamic tunnel is not suitable for ventilated tests. In fact, really few towing tank can reach the high speed required to reveal interesting effects.

The first step was again directed to visual comparisons to obtain a qualitative assessment, but on the true scale of the prototype. The shape of the wave elevation around the real foils was compared with pictures taken from onboard video recording system.

A second step was the analysing of the loads measured on the foil. Indeed the ventilation will change the arm level of the load, and consequently the measure on the jack. Thanks to that measure combined with video recording, we can analyse the ventilation appearing and effects.

4.5 3D SIMULATOR

To help the design of new solutions, the performance predictions, and the knowledge of the loads for structural design, the team develop since many years a 3D simulator of l'Hydroptère.
At the beginning, this tool was only considering foils working in sea with unidirectional swell.
But more and more developments are added in order to be as close to the reality as possible. It means different way of developments:
- Swell (crossed swell)
- Floats (Archimedean, planning hulls)
- Structure behaviour

And, with the growing of computer power, we can even imagine to take into account hydrodynamics phenomenon like cavitation or ventilation..

5. CONCLUSIONS

In direct association with the Hydroptère Design Team, several laboratories at EPFL have contributed to a number of optimizations of l'Hydroptère that have enabled the sailing team to achieve the world sailing speed records. Several FE models of the structure have been developed and updated. Specific materials have also been developed, produced and tested in various conditions with the aim to optimize the structural behaviour and provide new design solutions. Onboard measurements of structural deformation and foil immersion used to validate and refine the design loads and operation scenarios have proved to be very important in the fine optimization of the yacht. Various foils were tested at reduced scale in a high-speed water tunnel, and the results used to validate numerical simulations.

The collaboration between l'Hydroptère and EPFL continues with further challenging objectives for both sailors and researchers. Several studies have already been directed in order to help the team to achieve larger goals: Offshore records with the absolute dream to fly around the world!

6. ACKNOWLEDGEMENTS

L'Hydroptère is supported by Lombard Odier, and Audemars Piguet.

L'Hydroptère benefit from the scientific partnership with l'EPFL, and the technical partnership with Lancelin and HBM.

We should acknowledge all the students who have contributed to many stages of this collaboration, among: M. Tinguely, M. Reclari, D. Burgstaller, A. Ratouis, P. Gaillard, O. Pacot, C. Dufour, C. Legris, R. Gubler, M. Henry, K. Lilla, J. Michalik, L. Monnard, J. Ostlund, A. Varol, F. Dujonc, G.A. Benvenuti, L. Genolet, M. Ferrario, C. Brière, B. Golaz...

7. REFERENCES

7. REFERENCES

1. FLUENT and CFX User's Manuals, *ANSYS, Inc., USA*
http://www.ansys.com/

2. Abaqus User's Manual, *Dassault Systèmes SIMULIA, USA*
http://www.simulia.com/

3. KULLBACK, S., and LEIBLER, R. A., 'On Information and Sufficiency', *The Annals of Mathematical Statistics*, 22(1):79-86, 1951

4. BRENNEN, C. E., 'Cavitation and Bubble Dynamics', *Oxford University Press, USA*, 1995
http://resolver.caltech.edu/CaltechBOOK:1995.001

5. HOERNER, S. F., 'Fluid-dynamic drag', 1965

8. AUTHORS BIOGRAPHY

Jean-Mathieu Bourgeon is R&D Manager, **Stéphane Dyen** and **Davy Moyon** are Fluid Dynamics Engineers**, Daniel Schmäh** is Composite Materials Engineer, **Robin Amacher** is Naval Architect, and **Damien Colegrave** is Test Engineer at Hydroptère SA.
http://www.hydroptere.com/

Martin Calmon and **Mohamed Farhat** are respectively Assistant and Senior Scientist at the Hydraulic Machines Laboratory (LMH) of the Ecole Polytechnique Fédérale de Lausanne (EPFL). **Mohamed Farhat** is heading the research group on cavitation and interface phenomena.
http://lmh.epfl.ch/

Pascal Fua, Konstantin Startchev and **Guillaume Bonnier** are respectively Director, Engineer and Assistant at the Computer Vision Laboratory (CVLab) of the EPFL.
http://cvlab.epfl.ch/

Jan-Anders Månson, Véronique Michaud, Antoine Sigg and **Marc Oggier** are respectively Director, Professor and Assistants at the Laboratory of Polymer and Composite Technology (LTC) of the EPFL.
http://ltc.epfl.ch/

Michel Deville, Olivier Braun and **Mark Sawley** are respectively Professor Emeritus (former Director) and Scientists at the Computational Engineering Laboratory (LIN) of the EPFL
http://lin.epfl.ch/

Luc Blecha and **Joël Cugnoni** are respectively Postdoctoral Researcher and Research Associate at the Laboratory of Applied Mechanics and Reliability Analysis (LMAF) of the EPFL. **Luc Blecha** is now Chief Technical Officer at Almatech.
http://lmaf.epfl.ch/

"Recent Developments in the Design of Fast Ships"

by

J L Gelling *High Speed Craft DAMEN SHIPYARDS*

J A Keuning *Shiphydromechanics Department Delft University of Technology*

1. INTRODUCTION.

The combination of high forward speeds and waves of any significance has since considerable time been a serious challenge for designers and operators of fast ships. The possibility of a fast ship to maintain its intended high forward speed in those conditions is a serious measure for its operability. For decennia Damen Shipyards has put considerable effort in improving the operability of fast ships in a seaway. The last two decades this has resulted in a close cooperation with the Ship hydromechanics Department of the Delft University of Technology. As a result of this cooperation some successful new concepts have been developed and brought to the market.
In the present paper an oversight of these developments will be presented and some results obtained with these new concepts when compared with existing contemporary designs will highlighted.

2. PROBLEM DEFINITION.

From full scale experience it is known for a long time that severe motions and in particular high vertical accelerations are the main reason for speed reduction of fast ships in a seaway. This speed reduction occurs primarily in head and bow quartering waves. Due to the large motions and the sometimes very high peaks in the vertical accelerations during impacts most crews apply voluntary speed reduction in order to maintain workable conditions on board of their ships, in order to prevent possible structural damage to the ship and in order to be able to guarantee the safety of the crew and the ship.
Principal reasons for these phenomena to occur in particular with fast ships originate from the fact that, both for practical and economical reasons, most fast ships are generally small, say smaller then 50 meters length over all, and therefore the waves they are sailing in are relatively large. Also due to the high forward speeds in head waves the frequency of encounter is high, which has a very negative effect on the acceleration levels on board of these ships.
For a long time the emphasis in the design of fast ships however has been put on the minimal obtainable resistance at the required maximum speed. This had to be obtained in calm conditions. Operation of the ships in a seaway was for a long time not considered as an important design issue. In some design areas, such as the fast ferries markets, the search for improved seakeeping behavior was found in the design

and application of ever larger vessels. By doing so the mentioned deviancies in the behavior in waves could be partly overcome, but this is not a solution applicable in most of the other areas of application of fast ships. The focus on calm water performance has lead to particular trends in the fast ship designs, such as low deadrise, low length to beam ratios and relatively short and heavy hulls, i.e. low length – displacement ratios. These trends however showed unfavorable for the behavior of these fast ships in a seaway. So when these ships moved their operational areas from the more sheltered inland waters to the more exposed sea areas a new design philosophy had to be developed.

3. THE DEVELOPMENT OF NEW DESIGN CONCEPTS

An important role in this new development, at least within the Damen and DUT cooperation, was played by the results obtained from a considerable amount of full scale measurements carried on board various fast Patrol Boats and SAR vessels of different sizes on the North Sea. As reported by Keuning in Ref [1] it became obvious that improving the operability in head waves meant reducing the peaks in the vertical accelerations on board as much as possible. Not the significant (or "average") value of the vertical accelerations proved to be the prime factor for the crews to voluntary reducing the speed of the ship but the occurrence of the more scarcely high vertical peaks or slams. Avoiding these high peaks therefore became a primary driving factor in the designs.
To demonstrate this the next Figure is introduced. In this Figure 1 the distribution of the peaks in the irregular time signal of the vertical accelerations of a fast ship is presented. The horizontal scale represents the change of occurrence and is "transformed" according to the Rayleigh distribution, the vertical scale presents the magnitude of the vertical accelerations in meters per second squared.

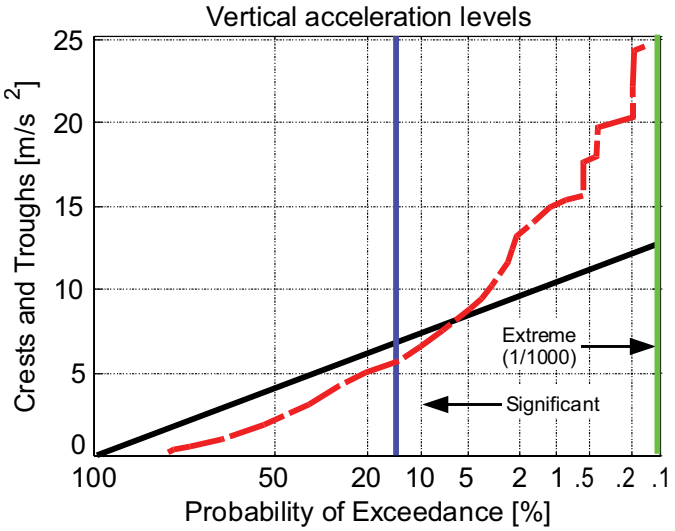

Figure 1: Distribution of peaks and troughs of an acceleration signal

The wish to avoid the high peaks in the acceleration signal for improved operability in a seaway means that a distribution according to the black (straight) line is very much to be preferred above the distribution following the red line. This holds true even though the significant value corresponding with the black distribution line is higher then that of the red line.

These insights lead to the development and introduction of the Enlarged Ship Concept (ESC) in 1995, see Ref [1] and Ref [2]. First by the so called "simple ESC 4100" in which just the length was increased without changing the section and bow shape of the design and which proved already a considerable improvement over the conventional designs. This concept was subsequently followed by the development of the more improved concept called "TUD 4100" in which the improved bow geometry was introduced. These were subsequently followed by the more radical new design concept called the "AXE 4100" applying the philosophy in full of the AXE Bow Concept (ABC) in 2001, see Ref [3] and [4]. Based on an extensive research project FAST 1 carried out in 2003 by the Shiphydromechanics Department of the Delft University of Technology jointly sponsored by Damen, Royal Netherlands Navy, US Coast Guard and MARIN all relevant aspects of the behavior of the ABC in waves from any direction were analyzed and evaluated. This showed such promising results that Damen decided to introduce the ABC designs on the market in 2006 and these designs have been very successful indeed.

The philosophy behind these concepts is that first of all the length should be brought back into design. By increasing the length without changing the beam, the forward speed and the functionality of the design, the L/B ratio becomes larger, the L/DISP ratio also becomes larger and there a more suitable place available for positioning the important areas on board such as the wheelhouse or passenger areas can be found, i.e. the ESC 4100. By increasing the length without changing the functionality also more space (void space) becomes available enabling the design of the hull shape more from an optimal hydromechanics point of view.

To avoid severe impacts during sailing in waves the hydrodynamic lift generated at the fore sections of the hull have to be reduced. Also the dominant wave exciting forces for fast ships has been proven to be the so called non linear Froude Kriloff forces. These have to be reduced as far as possible, which is achieved by the introduction of changes in submerged volume below and above the waterline both in the horizontal and the vertical direction. This results, in particular at the bow, in taking care that only small changes in submerged geometry at the forward sections of the hull do occur when these sections are moving in and out of the water due to provoked motions in the incoming waves. This leads to very sharp bows with non flared sections and very deep fore foots with possibly a negative contour. The sheer line is significantly raised to generate more freeboard forward and so increase the reserve buoyancy. To illustrate this the lines of a Conventional, a ESC and a ABC design are depicted in the Figure 2. A more detailed description of these design concepts has been presented by Gelling at the 19th HISWA Symposium see Ref [5].

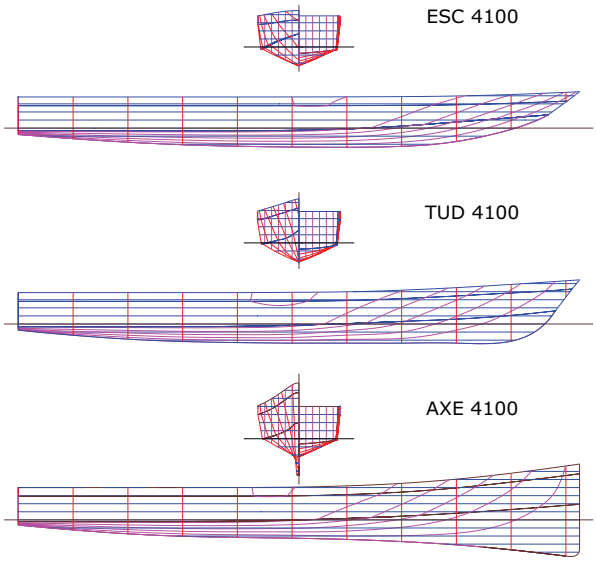

Figure 2: The lines plans of the simple ESC, the improved ESC (TUD 4100) and the ABC designs

The improvements obtained with these designs in the vertical accelerations are clearly demonstrated by the results from a comparative study presented in Figure 3. Here the distributions of the peaks in the vertical accelerations at the bow of the three concepts sailing at high speed in head waves corresponding to a Seastate 5 on the North Sea are plotted on basis of a Rayleigh distribution scale. From these plots it is obvious that the application of the ESC and the ABC design philosophy leads to a significant reduction of the high peaks with limited occurrence, i.e. the right hand side of the figure is much lower. In particular the AXE 4100 is superior in this respect. This leads to a large improvement in the operability of these craft. These theoretical results are in the meantime fully confirmed by full scale experience with the actual ships.
On the market both concepts are very successful. This is amongst others things demonstrated by the fact that from the ESC design more then 75 have been sold since 1997 and from the ABC design more then 30 since its introduction in 2007.

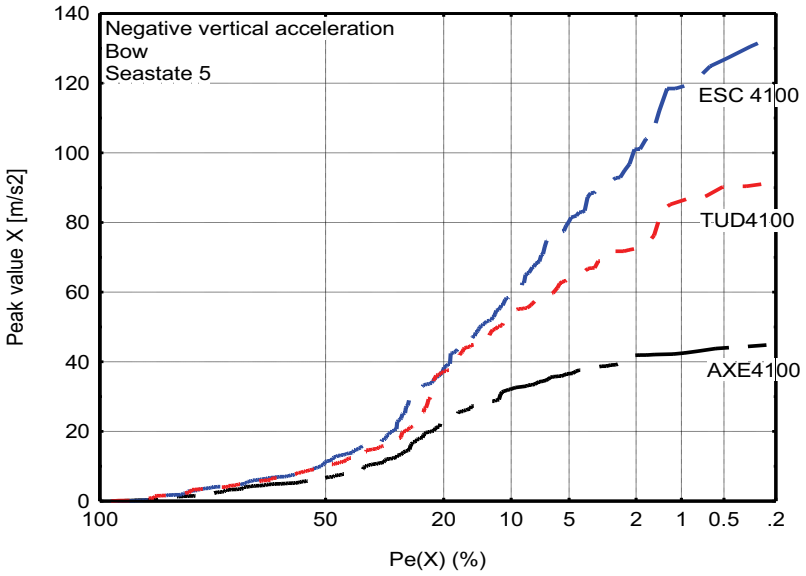

Figure 3 The comparison of the distributions of the vertical accelerations at the bow for the new design concepts.

The ESC has been built primarily in the function of Patrol Boat in the range from 40 till 60 meters length over all with speeds ranging from 22 to 30 knots. The Axe bow designs range from 30 till 60 meters length over all and are primarily used as Fast Crew Suppliers, Fast Yacht Support Ships and more recently Patrol Boats. Some typical examples are depicted in the Figure 4.

Figure 4 The AXE Bow Concept applied as Fast Yacht Support vessel (left) of 50 m length and the ESC as 42 m Patrol Boat (right)

One of the particular beneficial aspects of the application of the AXE Bow turned out to be the circa 20% lower fuel consumption in waves compared with conventional ships due to the considerable lower added resistance due to the waves.

These good results obtained with the designs with the AXE Bow lead to a new research project in 2009 into the possible application of this concept in catamarans. An important aspect was if and if so which modifications had to be introduced for application of the concept with catamarans.
In the last decade a considerable demand has come from the market for relatively small catamarans with improved seakeeping performance. These have to be operated from low up to moderate sea states in particular for application as service vessels for the offshore wind mill farms at the North Sea. Typical length of these vessels is in the 20 meter range and typical speeds are up to 25 knots in calm water. In addition to the usual requirements for low levels of vertical accelerations and small motions the improvement in the seakeeping behavior of the catamaran has also to be found in the avoidance of wetdeck slamming. This put special focus on the design of the hull shape.
The solution for the optimized catamaran hull design was found in applying the Enlarged Ship Concept first and so to extend the overall length from 20 to 25 meters. Then the AXE Bow concept was applied on both hulls. To avoid wet deck slamming the vertical motion of the fore ship had to be introduced in such a way that when sailing into the wave to deck was lifted but without violent accelerations. So a special geometry has been designed between the hulls to introduce the wave forces gently but not to eliminate them completely. Finally the avoidance of the wet deck slamming was found in cutting away the fore most part of the wet deck about 20% of the overall length. This was also made possible by the application of the enlarged ship concept.
The lines plan of the “TwinAxe” catamaran concept is depicted in the Figure 5

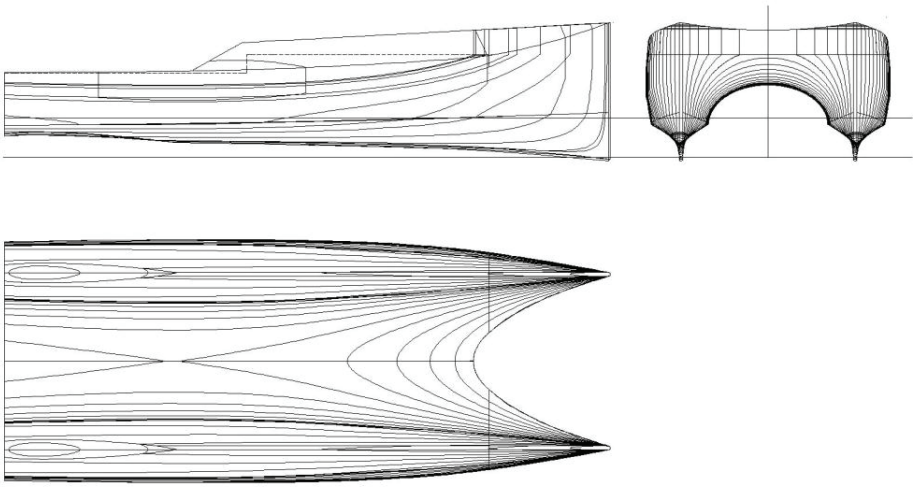

Figure 5 The linesplan of the TwinAxe Catamaran concept.

The research project aimed at a comparison between the TwinAxe concept and a comparable conventional catamaran. It was decided that the comparison between the two designs would be focused on the resistance in calm water and the heave and pitch motions and vertical accelerations in head waves. In addition the possible tendency for bow diving in following seas was also investigated for both designs.
The calm water resistance of the two designs is compared in the Figure 5. From these results it is obvious that the resistance of the TwinAxe is lower than that of the conventional catamaran. This is in particular due to the higher L/B ratio of the hulls and their bigger separation. A typical cross over is found at 25 knots.

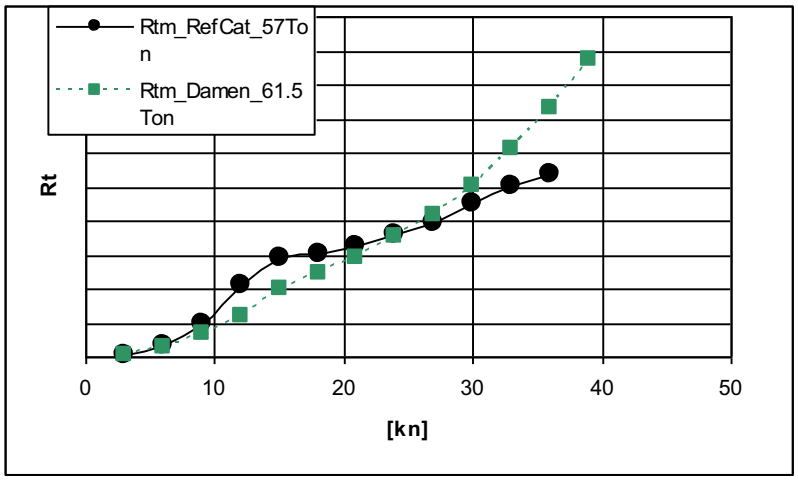

Figure 5 Calm water resistance of the TwinAxe and the Conventional Catamaran.

From the results in waves only the vertical accelerations at a location 10% of the Loa aft from the bow are shown. The tests have been carried out in a typical North Sea Seastate and at a forward speed of 25 knots. These results are depicted in Figure 6.

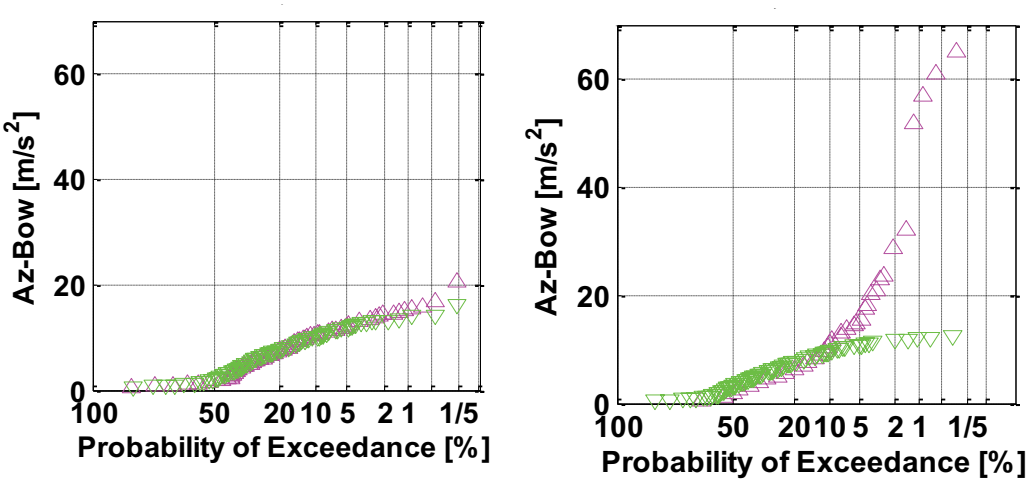

Figure 6 The distribution of the vertical accelerations at the bow for the TwinAxe Catamaran (left) and the Conventional Catamaran (right) at 25 knots in irregular waves with significant wave height Hs of 1.5 meters.

The enormous gains achieved in the vertical acceleration levels obtained with the application of the TwinAxe concept are rather obvious.
It is also well worth to mention that in all the conditions tested, i.e. with significant wave heights ranging from 1.0 to 2.5 meters and forward speed of 25 knots any wet deck slamming with the TwinAxe did not occur. In the following sea conditions no bow diving occurred also.
Although the development time of this new catamaran concept was rather short the obtained results were so promising that already a couple of these catamaran designs have been sold. A typical rendering of one of these designs is depicted in the Figure 7.

Figure 7. Rendering of the TwinAxe Catamaran as windmill support ship

Another application of the new concepts was found in the design of a possible new Search And Rescue (SAR) vessel for the Royal Dutch Lifeboat Institute (KNRM). At present they are looking for a possible replacement of their existing fleet of 18.5 meter long RIB vessels capable of a forward speed of maximum 35 knots and to be used on the North Sea in all weather conditions. Due to the special functionality of these SAR boats and their possible use in very extreme environmental conditions some modifications to the original AXE Bow design had to be made. The new SAR boats should have improved seakeeping performance when compared to the present ones when head and bow quartering seas are concerned. In all other conditions they should at least have similar performance and preferably better. Particular attention had to be paid to the possible occurrence of broaching in stern quartering seas. Also the tendency to bow diving in extreme following waves should be considered. Finally the maneuverability of these SAR ships in severe waves, both head and following, should be an issue. The boats should also be self righting.
Based on these requirements a new design has been developed. Particular point in the design were the enlargement of the hull, the application of the AXE bow but without

the typical negative sloped contour (downwards) forwards because these SAR boats should be able to take the ground frequently and violently. For safety and maneuverability reasons the boats are equipped with waterjets of ample power. The tube along the entire length of the hull is there for fendering reasons mainly. The most striking difference with the existing boats is the very fine bow with increase sheer and freeboard. Compared with the existing boats the deadrise is increased and the L/B ratio of the hull also. A rendering of this design is depicted in Figure 8.

Figure 8 Proposal for a new SAR vessel for the KNRM with Loa = 21 m and Vs = 35 knots

From an extensive series of experiments carried out with a model of this new design and a model of the existing boat in the towing tank it has been demonstrated that a considerable improvement in the head seas conditions has been achieved with the new concept, without any loss of performance in following and stern quartering conditions.

4. DEVELOPMENT OF NEW ACTIVE CONTROLS

In addition to these new concept developments also research has been carried out in the area of active control for fast ships. This originates from the effect that both the size and the high forward speed of these craft make the use of actively controlled fins etcetera very attractive. Two typical examples with promising results will be mentioned here:

- an actively controlled trim flap or interceptor at the transom of the boat to control pitch, heave and vertical accelerations and
- a retractable vertical bow rotor below the bow of a fast ship to improve directional control and reduce the roll- and yaw motion in stern quartering and following waves.

The idea of controlling the ship motions with an active control on the trim flaps at the transom is not new. In 1984 Wang Ref [7] ,amongst others, published experimental and computational results of a hard chine planing hull equipped with actively controlled trim flaps. In his research he already showed that considerable gains could be obtained with this control.

Recently Rijkens has extended this research with model experiments to determine the forces and moments delivered by both active flaps and active interceptors at the transom. The results of these systematic series of experiments have been used to extend the calculation procedure used in the mathematical model for the motions of fast ships in waves. The type of flaps and interceptors investigated by Rijkens are depicted in the Figure 8.

And the results he obtained with the flaps on the vertical accelerations at the bow are depicted in Figure 9 for the tests with and without flaps.

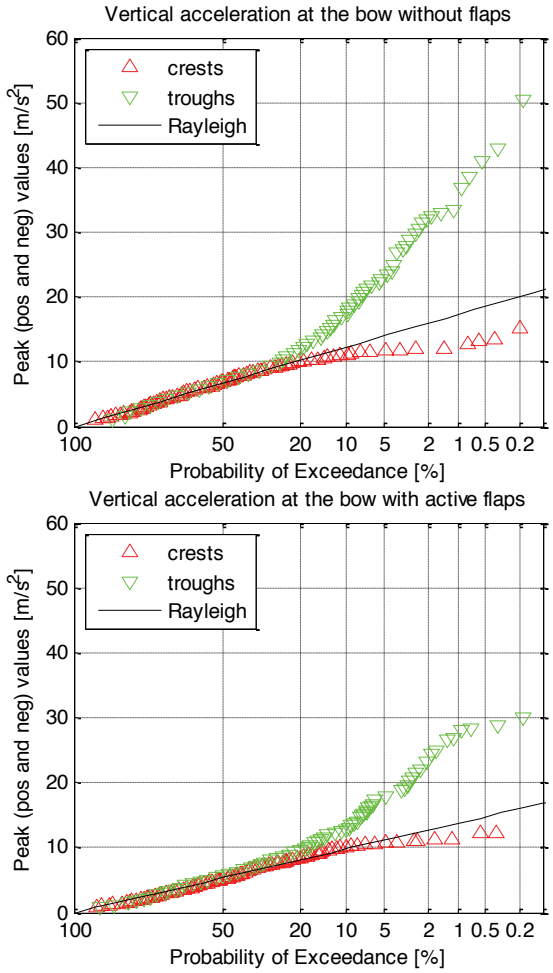

Figure 9 Vertical accelerations at the bow with and without active control on the flaps

Finally a new device has been developed for controlling the roll and yaw motions of fast ships in stern quartering waves.

It is known from full scale experience and model experiments that quite a few fast ship concepts are sensitive for severe combined roll and yaw motions in stern quartering waves sometimes even leading to complete loss of control and a broach. This is aggravated once again by the fact that most fast ships are relatively small compared with the surrounding waves. The phenomenon of the broach will not be fully explained here but a extended description can be found in Ref [8].
The Vertical Bow Rotor (VBR) device is a vertical and retractable Magnus Rotor underneath the bow of a ship, preferably an AXE Bow because the very geometry of such a bow easily enables the housing of such a device. A additional benefit of the AXE Bow and VBR combination is that the VBR cylinder is and will remain deeply submerged when the ship is heaving, rolling and pitching in large waves. A Magnus Rotor has the property to generate very efficiently a very high lift force when the cylinder is put into rotation. The combination of the forward velocity of the ship and the rotation of the cylinder produces a lift force perpendicular to the forward velocity of the ship. By changing the rotations per minute (RPM) of the rotor and/or the direction of rotation the lift force can be fully controlled both in magnitude and direction. Almost like a rudder but than more efficient. The VBR in this application is made retractable because in those situations or conditions in which its application is not necessary she can be easily retracted and so effect of the rotor on the ship resistance remains. A typical configuration of such a rotor is depicted in the Figure below.

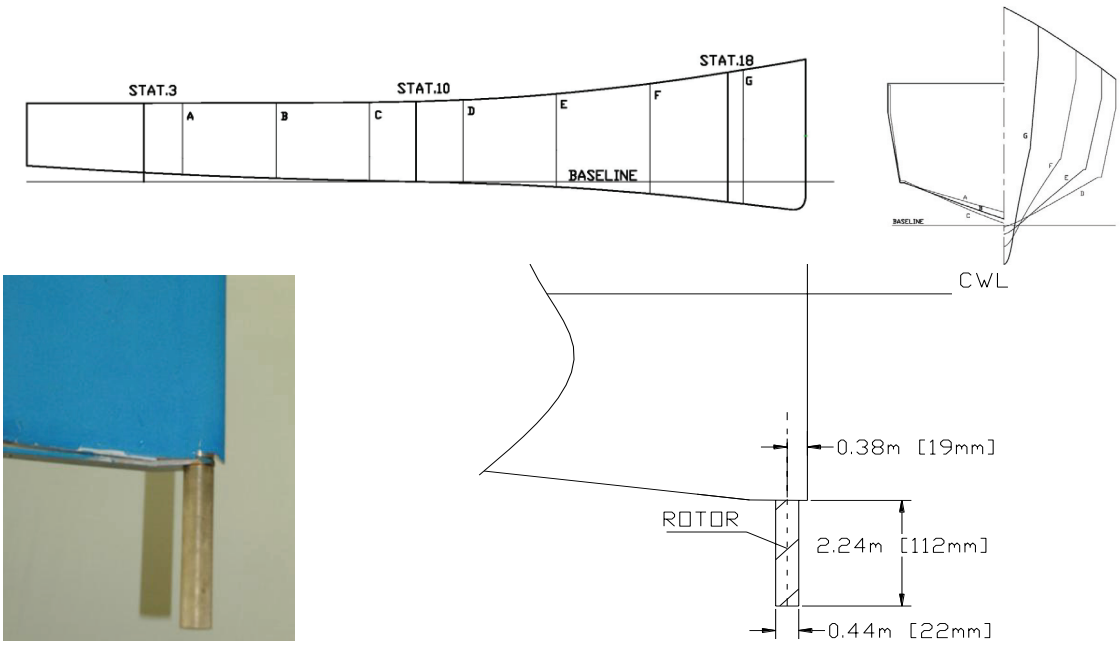

Figure 9 : The configuration of the VBR at the AXE Bow of a 35 meter LOA Fast Patrol boat (dimensions rotor full scale)

To investigate the effect of the VBR on the dynamic behavior of a fast patrol boat in stern quartering waves extensive experiments have been carried out in the Ship Motion Basin of MARIN in Wageningen. The ship tested was a 35 meter Length over all Fast Patrol Boat from DAMEN and the VBR was dimensioned based on an extensive systematic test with various rotors in the towing tank of the Delft University of Technology. A few of the results are presented here. They show the effect of the VBR on the roll and the yaw motion in an irregular sea with a significant wave height of 2.5 meters and a peak period Tp of 7.6 seconds, a typical North Sea spectrum energy distribution over the frequency range. The waves are coming from 315 degrees (stern quartering) and the ship travelled at a forward speed of 22 knots. From earlier tests it was found that this was the worst combination of waves, heading and forward speed. The distribution plots show the crests and troughs of roll and the yaw motion with and without the VBR.

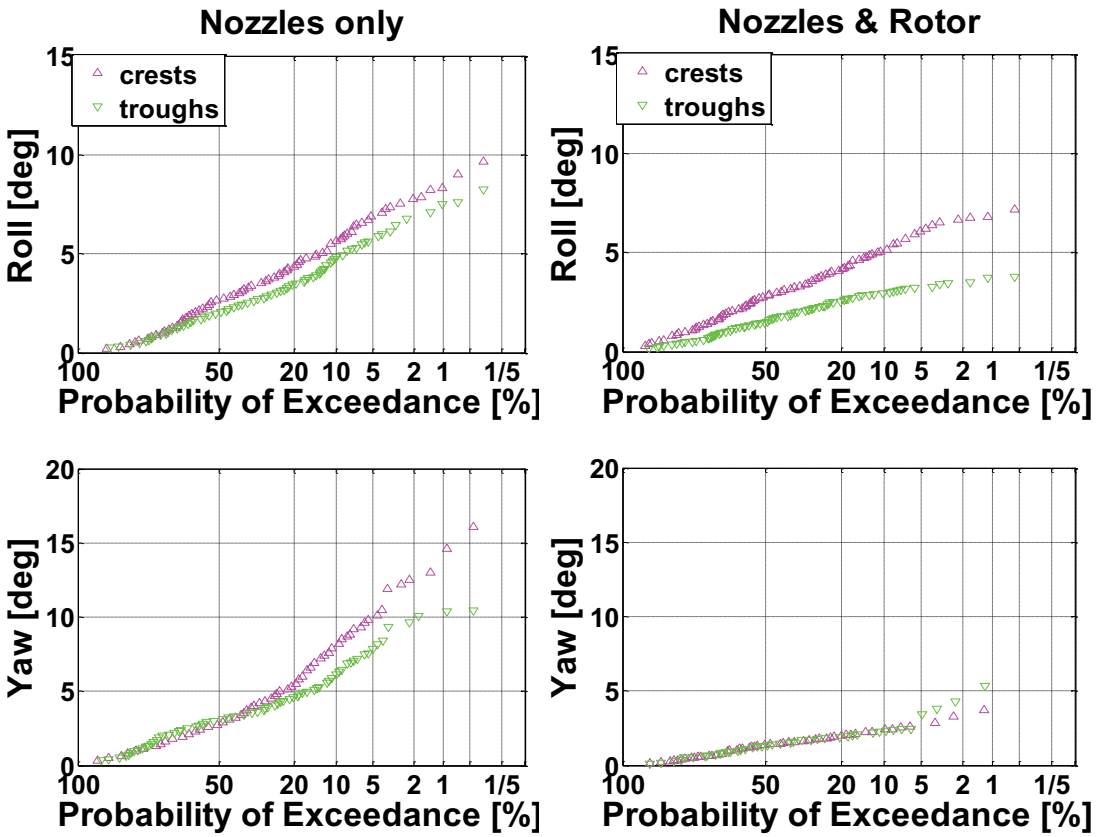

Figure 10 Distribution of roll and yaw motions in stern quartering seas with Hs = 2.5 meter at 22 knots with and without VBR

These results show that a reduction of almost 40 % on average in the roll motion and of almost 60% in the yaw motion can be achieved in those conditions.
To investigate the extended application of the VBR also measurements have been carried out in Seastate with 3.5 meters significant wave height, conditions in which the ship without the active VBR now and then broached. These results are presented on a different

way in the following figures, i.e. in the Figure 11 as Significant Double Amplitudes (SDA) of the motions and as Maximum Plus and Minus amplitudes in Figure 12.

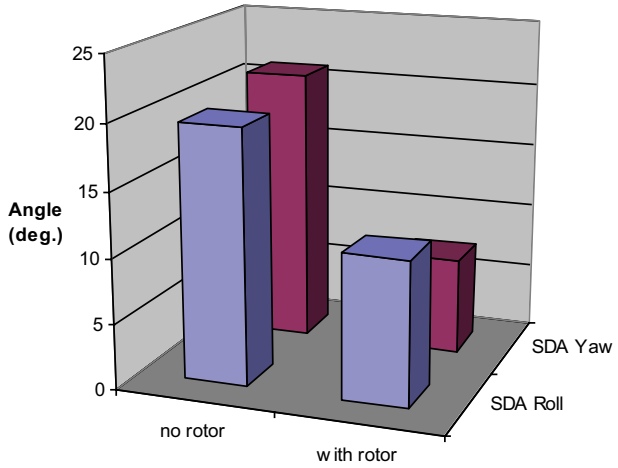

Figure 11 Significant Double Amplitude for Roll and Yaw with and without the Bow Rotor at 22 knots in a seaway from a angle of incidence of 315 degrees and with a significant wave height of 3.5 meters

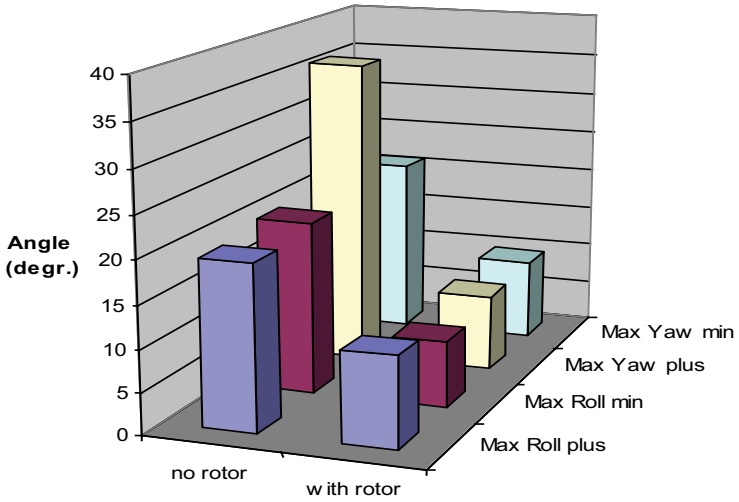

Figure 12: Maximum Roll and Yaw angles with and without the Bow Rotor at 22 knots in a seaway from an angle of incidence of 315 degrees with a significant wave height of 3.5 meters.

From these results it can be concluded that the introduction of the VBR has very positive effects on the controllability and the reduction of the roll and yaw motions in stern quartering seas. The operability of fast vessels in those conditions can be very much improved by application of the VBR. In the conditions tested the vessel used for the experiments did not ever experience any broaching behavior with the VBR activated whilst without the VBR some broaches did occur. Although not specifically investigated yet it appears that the use of the VBR is especially suited in combination with the AXE Bow

5. CONCLUSSIONS

The High Speed Craft area lends itself very much for improvements in design. In particular improving the operability in general of fast ships in a seaway is a very interesting field of research and development. Some noticeable results have been achieved in this area over the last decade's trough intensive cooperation between universities and research institutes with the industry. It is to be expected that if this cooperation is continued and intensived in the years to come new and very fruitful results will be achieved again.

REFERENCES

[1] Bosch, J.J. van den
"*Tests with two planing boats in waves"*
TU Delft Laboratorium voor Scheepsbouwkunde,
Report 238, june 1969

[2] Blok, J.J. and Roeloffs, H.W.
'The influence of the Forebody Deadrise on the performance in a Seaway"
MARIN Report No 49207-1-HT april 1989

[3] Keuning, J.A.
"Nonlinear Heave and Pitch Motions of Fast Ships in Irregular Head Waves"
ASNE High Speed Marine Vehicles Conference, Washington, June 1992

[4] Keuning, J.A.
"The Non Linear Behavior of Fast Monohulls in Head Waves"
PhD Thesis, Delft University of Technology, September 1994

[5] Keuning, J.A. and Pinkster, J
"Optimization of the Seakeeping Behavior of a Fast Monohull"
FAST Conference Proceedings 1995

[6] Keuning, J.A. and Pinkster, J.
"Further Design and Seakeeping Investigations into the Enlarged Ship Concept"
FAST Conference Proceedings 1997, Sydney Australia

[7] Keuning, J.A. , Pinkster,J. and Walree, F. van
"Further Investigation into the Hydrodynamic Performance of the AXE Bow Concept"
Proceedings of the WEGEMT Conference on High Performance Marine Vehicles September 2002 Ischia, Italy

[8] Keuning, J.A., Toxopeus, S. and Pinkster, J.
"The Effect of Bow Shape on the Seakeeping Performance of a Fast Monohull"
FAST Conference Proceedings Southampton, September 2001

[9] Ooms, J and Keuning, J.A.
"Comparitive Full Scale Trials of Two Fast Rescue Vessels"
International Conference SURV 4 , 13&14 may 1997 Gothenburg

[10] Keuning, J A and Visch, G
The Application of a Vertical Bow Rotor on an AXE Bow
FAST Conference Athens, Greece 2009

Recent Regulatory Changes and their Impact on the Design of Large Yachts

***Alex Meredith Hardy**, Naval Architect, BMT Nigel Gee Ltd*
***Sylvain Julien**, Naval Architect, BMT Nigel Gee Ltd*
***James Roy**, Yacht Design Director, BMT Nigel Gee Ltd*

ABSTRACT

The Large Commercial Yacht Code (LY2) has in the last decade become the de facto standard for the design and construction of large yachts. However the code is limited to a passenger number of 12 and a gross tonnage of 3000 GRT, implying a maximum length of approximately 85m LOA. In recent years, the number of large motor yachts outside of these boundaries has been steadily increasing making them subject to full SOLAS passenger ship regulations in addition to other pertinent conventions. This SOLAS based regulatory frame work has recently been subject to a period of significant change with the entry into force of a number of new regulations and conventions. It was recognised that gaining quantified insight into the impact of these on large yacht design would be of value to the industry, allowing refinement of design methods and procedures.

This paper investigates several new or recently updated regulations and conventions all of which will have varying degrees of impact on large yacht design practices and arrangements. These include SOLAS harmonised probabilistic stability, MARPOL fuel tank protection, MARPOL exhaust emissions, the Maritime Labour Convention and the Ballast Water Convention.

Each topic has been assessed in order to extract and summarise the relevant areas with regard to large yachts. Where possible the paper quantifies the effect the new regulations will have on yachts offering naval architects and designers insight as to how current design practices will need to change to ensure compliance.

1. INTRODUCTION & BACKGROUND

The large yacht market (>30m in length) has seen rapid growth in the last ten years. On average this has been 13% per annum year on year and over 300% overall. Not only has the number of yachts designed and built increased significantly so too has their size.

The majority of these large yachts are restricted to carrying 12 passengers and are less than 3000 GRT in order that they can be regulated under the Large Yacht Code (LY2). This code was developed in the early 1990's by yacht industry policy makers and was based on SOLAS Cargo Ship, Load Line Regulations and others. These standards incorporated sufficient equivalencies to allow the freedom and flexibility in design that yachts need in order to satisfy an owner's desire for individuality.

In recent years the size of yachts in the upper segment of the industry (as large as 160m in length) has become such that they are now outside of this regulatory framework and are subject to full SOLAS passenger ship regulations as well as other pertinent regulations. A limited number of yachts have been successfully designed and built to these regulations and there are now moves being made by the industry policy makers to develop specific regulations for these vessels based on equivalences to SOLAS, as had been done for the smaller yachts with the LY2 code.

However the SOLAS based regulatory framework is currently undergoing a period of change. Forthcoming ratification and entry into force of recent and future regulations will have a significant impact on the layout of SOLAS certified passenger ships and therefore the yachts in the upper segment of the industry. For several regulations no equivalency will be sought by the policy makers, specifically the introduction of probabilistic damaged stability for passenger ships, the Ballast Water Management Convention, MARPOL Regulation 12A (protection of fuel tanks), MARPOL Exhaust Emissions Compliance and the soon to be ratified Maritime Labour Convention 2006.

BMT Nigel Gee has undertaken a research project to investigate the implications of these future regulations on the layout of large yachts and how current design practices will need to change in the future to deal with the regulatory changes. Although the paper is focussed on yachts of 3000 GRT plus, some of the regulations discussed will also apply to smaller yachts, particularly the Maritime Labour Convention.

2. THE MARITIME LABOUR CONVENTION

The Maritime Labour Convention (MLC) 2006 has been created to form a single coherent instrument embodying as far as possible existing up-to-date maritime labour conventions, recommendations, and principles. The convention is governed by the International Labour Organisation (ILO) and will enter into force after ratification by at least 30 Members with a total share in the world gross tonnage of ships of at least 33%. It is

predicted to reach the required ratification level by mid 2011 and will apply to yachts ordinarily engaged in commercial activities (charter yachts). It is believed that the ILO also mean to include yachts owned by businesses or companies. This differs from the interpretation of 'commercial' by some Flags and may not be enforced by those administrations.

This convention covers many topics with regard to seafarer working conditions. However the main concern with regard to design is the minimum size requirements for crew cabins. This is currently an area of contention between the ILO and the yachting industry and if enforced as written, will have major implications on the design of yachts less than 65m. This will impact on yachts constructed after the date that the convention comes into force for the member state concerned. MLC Standard A3.1.20 allows member states to exempt vessels less than 200 GRT from the accommodation area requirements. The MCA have indicated that they intend to apply accommodation requirements on this size of vessel through other codes such as the Small Commercial Vessel Code [1].

To assess the impact that implementation of the MLC would have on 200 GRT+ yachts, BMT Nigel Gee carried out a crew accommodation study. This applied the MLC requirements to crew cabins, officer cabins and messes of 15 large yachts between 40m -100m LOA regulated under both LY2 and full SOLAS as passenger ships. The results are shown in Figure 2.1.

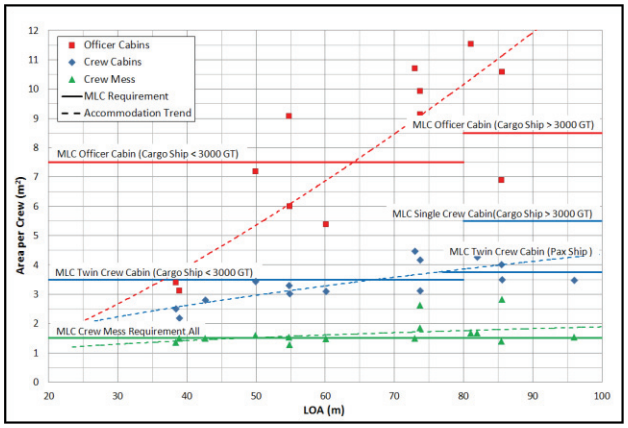

Figure 2.1 – Accommodation Study Results

Looking at LY2 yachts (less than 3000 GRT) it was found that yachts below 65m (approx 1150 GRT) were not meeting the crew cabin requirements. At the lower end of the scale (35m) crew cabins were approximately 65% of the area required. For yachts built to SOLAS cargo ship rules larger than 3000 GRT the MLC requires all crew to be in single cabins. This is not current industry practice and would have serious implications for future yachts of this type, effectively doubling the number of crew cabins. For full SOLAS passenger ship yachts the crew cabin threshold was 77m (approx 1800 GRT). When investigating the officer cabin area requirements it was found that the MLC threshold was 62m (typically 1000 GRT). A significant problem in smaller vessels was that only the captain had an officer cabin. LY2 states that there should be between three and five officers on a yacht. MLC requires all these to have officer sized cabins. On a separate study of two 40m yachts, the combined effect of the officer and crew requirements reduced the number of guest cabins from four to two. This has a large impact on cabin arrangements and crew/guest balance of a yacht resulting in significant loss of function of the vessel. The MLC requirement for crew messes is 1.5m^2 per person. It was found that yachts over 45m generally already comply. In smaller vessels some increase in mess size may be required.

It is clear from this study that the MLC will have a significant impact on the commercial viability of yachts less than 65m (approx 1150 GRT). The yachting industry is currently involved in coordinated dialogue with the ILO through representatives such as the PYA, SYBAss, ICOMIA and MYBA as well as the UK MCA. The ILO is aware of the problem. The hope is that yachts will be recognised by the ILO as a special case and equivalent accommodation standards with reduced area requirements can be drawn up and agreed upon. This would consider that yacht crew generally have en-suite bathrooms and long periods in port compared to other seafarers. There is no guarantee from the ILO at this stage that a special case will be made for yachts. Although the current advice is that future designs should meet the requirements of the MLC as written, it should be borne in mind that the equivalent standard for yachts under development may come into effect. What is fairly certain is that with either route seafarer cabins will be larger than current standards. Discussions are ongoing, so watch this space.

3. PROBABILISTIC STABILITY

The probabilistic stability method has been under development since the early 1960s. It was first adopted in 1990 as the damaged stability method for dry cargo ships. From 1995, considerable efforts were made to provide a harmonised probabilistic stability standard applicable to all ships. In 2005 MSC 194(80) was adopted to form what is commonly referred to as SOLAS 2009. This stability standard entered into force on 1st January 2009, and is applicable to all passenger ships as well as cargo ships over 80m built from that date. The aim of the new probabilistic standard is to provide an equivalent level of safety to SOLAS 90 [2].

3.1 ATTAINED AND REQUIRED INDEX

Unlike deterministic stability, the probabilistic method uses a risk based approach assessing the probability of damage and the severity of the consequences. The calculation assesses this across all compartmentation on the vessel. The final result is expressed by the Attained Index value 'A', the maximum value of which is 1.00.

This can be thought of as a percentage of total safety. Practically, no vessel is 100% safe so it is necessary to define some level of acceptable safety. This is defined by the Required Subdivision Index 'R'. The method that defines 'R' is a function of the size of the vessel, number of persons on board and configuration of the lifesaving equipment. Table 3.1 compares the typical complement of a yacht compared to a passenger ship. It can be seen that the complement of a yacht does not increase significantly with length compared to a passenger ship. Figure 3.1 shows how 'R' varies with length considering these typical values.

Length [m]	50	100	150
Yacht - Total Complement	54	81	96
Passenger Ship - Total Complement	200	525	1425

Table 3.1 – Comparison of Typical Complements

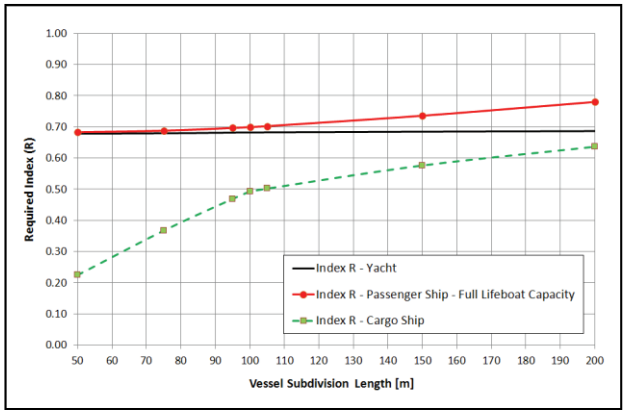

Figure 3.1 – Comparison of Required Index R

It can be seen that 'R' remains relatively constant as the yacht length increases. Whilst the subject of equivalency to SOLAS 90 is outside of the scope of this paper, it can be seen that the gap in safety between a typical passenger vessel and a yacht increases with vessel length. This is a significant difference to the SOLAS 90 standard where the level of safety is the same whatever the number of people onboard. Additionally, with the probabilistic method, catastrophic damage cases with a low probability of occurrence can exist whilst not reducing 'A' sufficiently to cause the vessel to fail. There is currently debate within the wider industry as to whether the probabilistic method is equivalent to the previous deterministic standards. As a result, probabilistic stability standards still include deterministic requirements for passenger ships to guarantee minimum stability characteristics following minor damage. This adds further to an already complex set of regulations.

3.2 AIM OF THE WORK

The primary aim of the research carried out by BMT Nigel Gee was to see how the naval architect can assess large yacht designs, with confidence, at a preliminary design stage. Unlike deterministic methods, the probabilistic calculations are unintuitive. It is hard to get a feel for how changes during the preliminary design process will influence the Attained Index. As a result, in the early design stages it is difficult to be confident that the final design will pass. As a result, the aim of the work carried out was to ascertain what the major influences on the Attained Index are, and what level of subdivision must be defined in order to have confidence that a vessel will pass.

3.3 SIGNIFICANT INFLUENCES ON 'A'

Three draughts are defined for the calculations, Deepest Subdivision, Partial Subdivision, and Light Service draught. The deadweight distribution in each case is undefined and totally reliant on the judgement of the naval architect. It is important at the preliminary design stage that a practical VCG is used for each case to get a realistic Attained Index.

The margin line concept is not applied in probabilistic stability. The survivability of the craft in any single flooding scenario is considered to be zero if any part of a horizontal evacuation route on the bulkhead deck is submerged. It is important that preliminary positions of evacuation routes are defined as they can have a significant effect on 'A', especially in yachts with stepped bulkhead decks.

The subdivision arrangement, and the level of detail represented, has a major influence on the final result. As would be expected, representing all major transverse subdivisions is the most efficient way to increase the Attained Index. Longitudinal subdivision can result in large reductions in Attained Index due to asymmetric flooding. Horizontal subdivision can both improve and reduce the result depending on its location compared to the waterline. In order to better understand how sensitive the Attained Index was to the level of subdivision modelled, a study on a 95m and 85m yacht was undertaken. Starting with the as built fully defined subdivision arrangement, subdivision definition was progressively removed in a methodical manner and the Attained Index assessed at each stage. Table 3.2 describes the levels of subdivision assessed.

Table 3.2 – Levels of Subdivision Investigated

Stability Model	Compartmentation Description
As built	As built, highest level of complexity.
Option 0	Removal of small double bottom, central tanks. Main longitudinal subdivisions maintained.
Option 1	As option 0 but with cross connection of all wing spaces to eliminate any asymmetric flooding effects.
Option 2	Removal of all longitudinal subdivision and transverse tank ends in the double bottom (excluding main WT bulkheads). No subdivision below the tender bay deck.
Option 3	Removal of double bottom and tender bay floor. Only main transverse bulkheads represented.
Option 4	As option 3 with every other main transverse bulkhead between the forward engine room bulkhead and the forepeak bulkhead removed.
Option 5	Only aft peak, forepeak and engine room bulkheads defined.
Option 6	Only aft peak, forepeak and forward engine room bulkhead defined.

Figure 3.2 shows the Attained Index achieved at each stage of subdivision as a percentage of the 'as built' vessel.

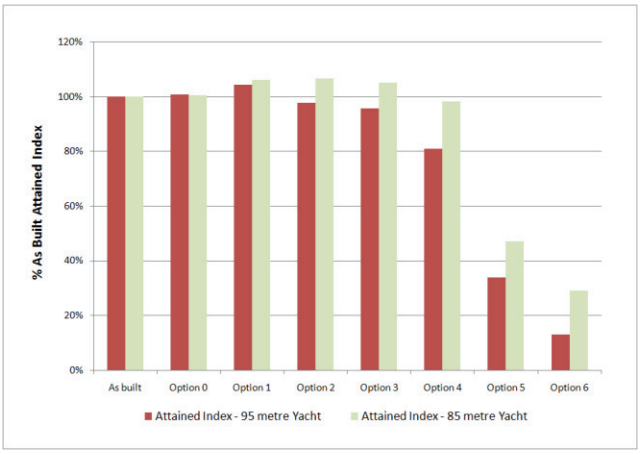

Figure 3.2 – Results of Subdivision Study

The most significant conclusion was that there is a danger of calculating an overly optimistic result unless all asymmetric flooding is considered. For a preliminary design where longitudinal subdivision is not defined a margin must be used (10% for typical levels of asymmetric flooding). It was found that removing small central bottom tanks does not significantly alter 'A'. These do not need to be considered at a preliminary design stage. To obtain a sufficiently valid Attained Index the following should be modelled; collision, aft peak and intermediate main transverse bulkheads, tender bay deck and any subdivision resulting in asymmetric flooding.

3.4 PRELIMINARY DESIGN METHODOLOGY

From this body of work, a methodology was developed to allow the naval architect to use the probabilistic method effectively for yachts at the preliminary design stage and have confidence in the Attained Index before all levels of subdivision are defined. This is based on the assumption that below the main deck, the majority of large yachts follow a generic layout, illustrated approximately as shown in Figure 3.3.

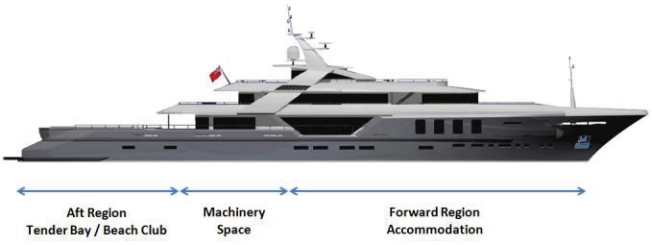

Figure 3.3 – A Generic Yacht Arrangement

A brief summary of the methodology is discussed.

- Step 1 - Even in the earliest design stages with a preliminary general arrangement the following subdivision should be defined; collision bulkhead, aft peak bulkhead, extents of tender bay, vertical location of tender bay deck, extents of engine room, and bulkhead deck geometry. Define the position of evacuation routes on the bulkhead deck.
- Step 2 – Define the loading conditions for the required draughts ensuring calculated VCGs are realistic.
- Step 3 – Optimise the main transverse subdivision in the forward region and check the position of engine room and tender bay bulkheads are suitable. This can be done by inspecting the contribution to the attained index for each compartment. If the tender bay is not overly large then the Attained Index may now meet the required index. However, as no asymmetric flooding has been considered it cannot yet be concluded that the vessel will pass.
- Step 4 – Add double bottom.
- Step 5 – Optimise subdivision in the aft region. This step applies when tender bays or beach clubs are overly large. Additional subdivision below the tender deck can allow a limited increase in the size of tender bays. On completion of this step the aim should be to have an attained index with sufficient margin over the required index (at least 10%) as longitudinal subdivision has yet to be considered.
- Step 6 – Introduce longitudinal subdivision. This will primarily be dictated by the tank arrangement. Void wing spaces should be cross connected to minimise asymmetric flooding. The Attained Index at this stage should be a good representation of the final Attained Index.

Ultimately, whether the exact methodology above is adopted or not, it is critical for the naval architect to understand the influence of the various principal levels of subdivision within a design. It is only through intimate understanding of the calculation and intermediate results that contribute to the Attained Index, that the subdivision can be optimised.

4. MARPOL REGULATION 12A

The MARPOL Convention covers pollution of the marine environment by ships. MARPOL Annex I covers the prevention of pollution by oil. Regulation 12A is an amendment which entered into force in August 2007. The purpose of the regulation is to minimise the quantity of oil lost from a vessel following damage from grounding or collision. This is achieved by enforcing a certain level of oil fuel tank protection. The new regulation applies to all ships with a fuel oil capacity of greater than 600m^3 delivered on or after 1st August 2010. The regulation provides two methods through which suitable oil fuel tank protection can be achieved.

4.1. PROTECTED FUEL TANKS

This method achieves adequate protection by positioning fuel tanks a required distance (typically 0.76m – 1.1m for

large yachts) from the hull shell of the vessel effectively creating a double skin.
There are several issues associated with protected fuel tanks that are likely to discourage naval architects from pursuing the protected fuel tank route. The current yacht practice of using double bottom fuel storage is beneficial because it makes use of awkward, otherwise unusable void spaces. The protected tank method effectively creates more void space. Figure 4-1 shows a possible protected fuel tank arrangement. In order to accommodate an equivalent capacity of fuel the tank top height has to be increased significantly. In the example shown an additional 75% of volume was required compared to a pre regulation arrangement. This significantly impacts internal accommodation volume and the deck arrangement of the vessel. Wing tanks and tanks near the bow and stern, where there is high curvature, become very ineffective. The structural design and production of such a protected fuel tank arrangement would be significantly more challenging than current bottom arrangements, especially in areas of hull curvature. The additional tank boundary and supporting structure will increase structural weight. The increase in the double bottom height also shifts the decks above increasing lightship VCG impacting on stability and aesthetic profile. Deadweight VCG is also increased.

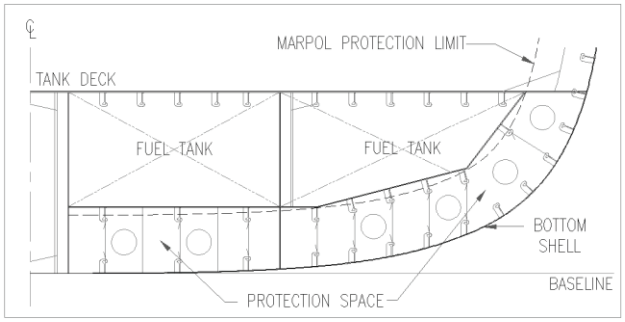

Figure 4-1: A Protected Tank Arrangement

4.2 ACCIDENTAL OIL FUEL OUTFLOW

The second method of compliance is a performance based method involving a probabilistic analysis of the fuel tank arrangement focussing on the likelihood of damage to each tank, and the subsequent quantity of oil that would be lost. A certain score must be achieved to demonstrate the required level of protection.

The main advantage of the outflow performance standard is that fuel tanks can remain in contact with the hull shell in line with current yacht design and production practices for double bottoms. However, the arrangement of tanks is severely restricted in order to pass the outflow standard and needs to be considered from the outset of the design process. The calculation effectively achieves protection by driving the designer to position tanks in areas where probability of damage is low, and where outflow resulting from damage will be minimal. From the authors experience it has been found generally that to achieve a suitable outflow score tanks need to be positioned in the bottom away from the shell sides. Tanks may also need to be deeper than is current normal practice, in some cases extending up to the deck above the inner bottom. The main two factors that influence the impact on vessel design is the overall fuel capacity and longitudinal tank distribution (fuel LCG). As the requirements for either become more extreme, flexibility in the arrangement is quickly lost. Where this is the case, tank top heights will generally increase impacting internal accommodation volume and the deck arrangement of the vessel.

Other points to note are that impact on vessel lightship and deadweight VCG is less significant than with protected fuel tanks. The outflow result can also be improved by subdividing or making fuel tanks smaller. This will drive up the number of tanks resulting in a more complex, heavier fuel transfer, bunkering and supply systems.

4.3. COMPARISON STUDY

A study was carried out that looked at these two methods and investigated the requirements and the impact of each method when applied to large yacht design. The impact was assessed and quantified for two concept designs by looking at the effect on various design parameters. These where the number of bunker tanks (an indication of complexity), fuel LCG (ability to control design trim and LCB), fuel VCG (impact on deadweight VCG) and the lower deck height (to indicate impact on deck arrangement and lightship VCG). The lower deck is the deck above the tank deck.

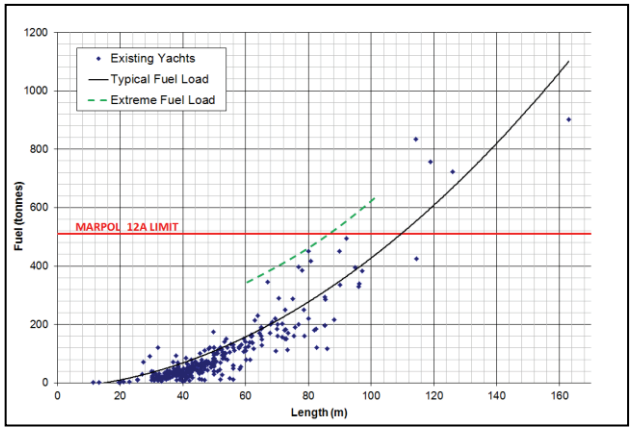

Figure 4-2: Regulation Threshold Length

An initial assessment of existing yachts was made to identify what size yacht the 600m^3 fuel threshold is reached. This showed that 110m was the typical size, and in extreme cases as small as 85m. See Figure 4-2. These two sizes of yacht where used as the subject of the quantitative study, each with a design fuel load of 600 m^3. The results for the parameters investigated are shown in Table 4-1. From the results of the study it can be seen that in general the number of bunker tanks, the fuel VCG and the lower deck height are less for the oil outflow method. It can be seen that for the typical threshold yacht (110m) the impact on these three parameters is minimal. However, there was a significant restriction on fuel LCG.

It was found that a suitable fuel LCG of 43.5%LWL could be achieved, but any further forward and an increase in tank top height would be required. A pre-12A arrangement could achieve a fuel LCG 6% further forward with no need to increase tank top height. The ability to adjust fuel LCG is useful during the design process to achieve suitable trim and LCB. The loss of flexibility needs to be considered from the outset of a design. It can be seen that the protected tanks method can achieve more flexibility in fuel LCG (about 2%), but the designer has to balance the benefit of this with the increased impact on build complexity, stability and internal arrangement. A further point to note is that the required bottom clearance for protected tanks is calculated from beam. Therefore as vessels get larger the protected fuel tanks method will impact more on the internal volume and arrangement of the ship.

85m Motor Yacht	Pre-Reg. 12A Unrestricted Tanks	Reg. 12A Protected Tanks	Reg. 12A Oil Outflow
No. of Bunker Tanks	12	13	10
Fuel LCG (%LWL)	43.5	43.5	41.9
Fuel VCG/Reduction GM (m)	1.81	2.22 / 0.08	1.95 / 0.03
Lower Deck Height (m)	4.70	5.10	5.10

110m Motor Yacht	Pre-Reg. 12A Unrestricted Tanks	Reg. 12A Protected Tanks	Reg. 12A Oil Outflow
No. of Bunker Tanks	10	12	10
Fuel LCG (%LWL)	49.4	45.3	43.5
Fuel VCG/Reduction GM (m)	1.48	2.55 / 0.09	1.49 / 0.00
Lower Deck Height (m)	4.70	5.20	4.70

Table 4-1: Study Results

The results considered in this paper are for two specific vessels. They have been presented to illustrate some of the issues that must be considered, but it should be noted that every yacht is different with their own design priorities. What can be said with certainty is that Regulation 12A is a dominant factor that must be considered at an early stage.

5. BALLAST WATER CONVENTION

The International Convention for the Control and Management of Ships' Ballast Water and Sediments (BWM) has been developed to control the transfer of harmful and invasive aquatic organisms and pathogens through ships' ballast water and sediments. This has become a significant problem due to the expanded trade and traffic volume over the last few decades. The effects in many areas of the world have been devastating. Data shows that the rate of bio-invasions is continuing to increase at an alarming rate. Effects such as invasive fouling and extinction of local fish stocks have been reported. The convention was adopted by the IMO in Feb 2004 but has not yet entered into force. The BWM will enter into force 12 months after it has been ratified by not less than thirty States, constituting not less than thirty five per cent of the gross tonnage of the world's merchant shipping fleet.

All yachts with seawater ballast will have to comply with Regulation D-2 of the convention by 2016. Some flags may implement the Regulation on new yachts (constructed in or after 2009) before that date. Regulation D-2 is the Ballast Water Performance Standard which states the required water quality that must be achieved for any ballast water that is being discharged. An acceptable water quality is defined by achieving maximum numbers of various micro-organisms per volume of water. To meet this standard, ballast water will need to be treated.

A review into the types and availability of systems suitable for yachts was undertaken. In general treatment units available use a two stage process which first filters the water and then sterilises it. The methods of sterilisation vary between manufacturers, examples being UV light, electrolysis, additives, and oxidation. With the aid of a technology review carried out by Lloyds' Register [3] it was found that the availability of suitably sized units for yachts was seriously restricted at this time. Most systems have been developed for large commercial vessels. From the research carried out, only one approved system was found that offered a low enough capacity to be suitable on a yacht. An assessment was carried out to ascertain the impact of installing such a system by looking at the size, weight and required power demand. For a 90m yacht the system would need a footprint area of approximately $3m^2$, weigh 1.5t (wet) and use 15 kW of power. Apart from the additional space requirements in what are usually already very tight machinery spaces, it was concluded that the impact of installing the system on a large yacht would be relatively small.

As a result of the review it was concluded that there is a lack of availability of suitably sized, approved systems for a yacht application. Considering the current status, the most sensible course of action at this stage would be to reserve space in current yacht designs for a ballast water treatment unit but not install it. Once the convention is ratified, it is likely there will be more choice of products for large yachts thus allowing the most suitable system to be installed.

6. MARPOL EXHAUST EMISSIONS

Regulations governing the prevention of air pollution from ships are dealt with in Annex VI of MARPOL. The main pollutants relevant to yachts are those emitted from engine exhausts such as nitrogen oxides (NOx), sulphur oxides (SOx) and particulate matter (PM). These cause harm to the environment as well as human health.

IMO Resolution MEPC 176 (58) contains amendments to Annex VI which will see higher emission standards

coming into force. These are the addition of tier II and tier III nitrogen oxide limits, more onerous sulphur content limits on fuel oil and the establishment of Emission Control Areas (ECA).

An ECA is an IMO approved geographical area where there is a need or requirement to reduce the level of emissions from ships. More stringent emission limits for NOx, SOx or both will be applied in these areas. An ECA is a progression from the Sulphur ECA (SECA) which was used in previously enforced regulations. SECAs are already established for the Baltic Sea and the North Sea including the English Channel. These areas are subject to SOx requirements only and will only become subject to NOx requirements if re-designated by the IMO. A new ECA (subject to NOx and SOx) has however been recently adopted. This will come into effect in 2011 and covers all areas within 200 miles of the US and Canadian coastline. It is possible that other areas such as the Mediterranean could also become ECAs. As yachts spend the majority of their time near to the coast it is likely that the more stringent regulations required in the ECAs will have a significant effect on yachts.

Regulation 14 of Annex VI deals specifically with the sulphur content of fuel oil used onboard ships. The maximum limits allowed are to be reduced over time. Globally the intention is to reduce the fuel sulphur limit to 0.5% by 2020. In ECAs and SECAs the intention is to reduce the sulphur limit to 0.1% by 2015. The sulphur requirements will not have any significant impact on yachts as it is generally the case that large yacht engines are high speed diesel types which use marine gas oil (MGO). MGO is a high quality diesel grade which has low sulphur content. As a result of preceding EU and US sulphur regulations on automotive fuels, MGO with a sulphur content below the MARPOL 0.1% limit is becoming more widely available. Use of this fuel will negate the need for 'add on' sulphur treatment systems for yacht exhausts.

Regulation 13 of Annex VI is concerned with NOx emissions from marine diesels with a power output greater than 130kW. The regulation limits the weight of NO_2 that can be emitted per kW hour of engine operation. The gram/kWhr limits specified are a function of engine RPM. There are three different limits (tiers) which will be introduced with varying time frames. Figure 6-1 shows the requirements for the three NOx tiers. Table 6-1 shows how the three NOx tiers will be implemented, and to which engines they will apply. It can be seen that the tier III requirements only apply to vessels built after the 1st Jan 2016 whilst operating inside an ECA.

In light of the new regulation, engine manufacturers have been carrying out development programs in order to optimise the combustion process and improve engine emissions sufficiently to meet the tier I and tier II NOx requirements. Some suppliers to the yacht market are already offering tier II compliant engine models. As a result, tier II compliance can be achieved simply through appropriate engine selection. However, at present, tier III requirements are beyond the capabilities of 'on engine' technology. There are several 'add on' technologies being developed that may in the future offer a viable treatment method for reducing NOx emissions to meet tier III requirements. These include exhaust gas recirculation and water emulsification technologies. However, currently there is only one that is technically proven to reduce NOx sufficiently to tier III requirements. This is Selective Catalytic Reduction (SCR).

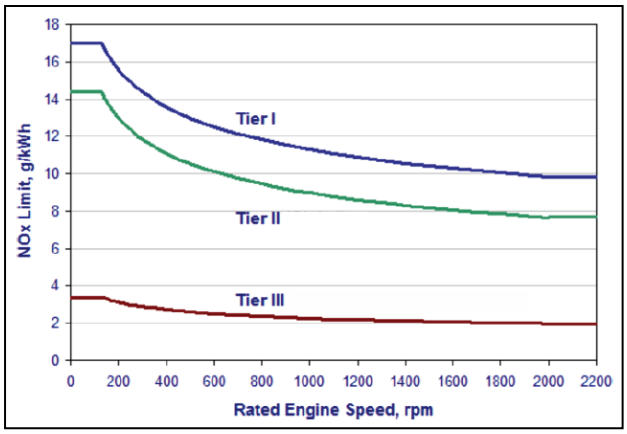

Figure 6-1: Tier I, II & III NOx Emission Limits

Engine Installation	Outside ECA	Inside ECA
Engine installed on a ship constructed before 1st Jan 1990	-	-
Engine installed on a ship constructed Jan 1990 - Jan 2000 which is smaller than 5000 kW or 90 litres per cylinder	-	-
Engine installed on a ship constructed Jan 1990 - Jan 2000 which is larger than 5000 kW and 90 litres per cylinder	Tier I	Tier I
Engine installed on a ship constructed 1st Jan 2000 - 1st Jan 2011	Tier I	Tier I
Engine installed on a ship constructed after 1st Jan 2011	Tier II	Tier II
Engine installed on a ship constructed after 1st Jan 2016	Tier II	Tier III

Table 6-1: Implementation of NOx Emission Limits

SCR is a treatment technology where urea or ammonia is sprayed into the hot exhaust gas before flowing through a catalyst. This causes a reaction which causes the NOx gases and the reactant to breakdown into harmless nitrogen and water. The reaction is relatively sensitive to temperature but can achieve good results; it is claimed up to 98% reduction in some cases. This technology is currently in service, and has been shown to be effective on ships and some yachts. The SCR system can be combined with a soot and particle filter which reduces soiling and odour on deck. At present this type of system seems the most appropriate for future yacht applications. The number of manufacturers able to supply the yacht industry is currently very low.

A SCR system proposal was developed with a manufacturer for a 100m concept yacht with 4 x 2900kW propulsion engines in order to assess the impact of installing such a system. The reactor/filter unit, fitted in

each exhaust line, is the central system component. The units are positioned in a similar fashion to a silencer. Each unit is of significant size (2m x 1.7m x 1.9m) and weighs 1.5 tonnes. This could increase engine room or casings sizes impacting on accommodation space. The unit does provide some noise attenuation (15 – 25 dB) but not enough to meet high yacht standards. Silencers are still required which will add to the arrangement complexity. The urea reactant for the system has to be stored in a tank onboard. The urea is injected via a supply pump and dosing unit. These items and the associated additional piping will add to engine room space requirements and weight. Urea consumption rates are reported to be between 3% - 7% of fuel consumption by volume. It should be noted that the de-NOx process only needs to be running when a vessel is inside an ECA. Generators will also require exhaust treatment when running in an ECA. A 100m yacht with a fuel capacity of 500 tonnes spending a large proportion of time in an ECA would require a urea capacity of 32 tonnes. This is a significant increase in the deadweight of a yacht. A look at current urea prices shows that it is available for GBP 0.28 /litre. This is fairly inexpensive and will not increase running costs of a yacht significantly.

In conclusion, the installation of an SCR system on a large yacht will have a significant impact in two main areas; space and weight. The size of the units and its ancillary equipment will compound the problem of tight engine room arrangements already found on yachts. It is likely that accommodation space will be lost to compensate. An approximate design displacement increase for such a system on a 100m yacht will be in the order of 45 tonnes (well over 1% of displacement for a 100m).

It should be remembered that the implementation date for tier III is still 5 years off. This will allow further development of current products which may see the impact on large yachts reduce. It should be noted that the automotive industry is well advanced in SCR development indicating that the potential emergence of new technologies is less likely. A close eye should also be kept on the NOx tier III review in 2012-13 which will verify the final implementation schedule for the tier III requirements after considering the available technology.

7. SAFE RETURN TO PORT

Safe Return to Port (SRtP) is a set of amendments incorporated into SOLAS that entered into force in July 2010. They were developed following concerns over the ability to safely evacuate passengers (including elderly and injured) to lifeboats and rescue craft on ships with high passenger densities. The SRtP amendments aim to improve survivability of passenger ships so that, in the event of a casualty, people can stay safely on board as the ship proceeds to port. SRtP applies to all passenger ships that have a length (deepest subdivision load line) greater than 120m, or three or more Main Vertical Zones (MVZs). For a yacht the transition between two and three MVZs will generally occur in vessels with a waterline length no greater the 104m.

Considering that large yachts have low passenger densities and generally operate near to shore, the SRtP requirements seem overly onerous. It has been indicated by industry policy makers that SRtP will not be applied to passenger ships carrying 36 passengers or less.

8. CONCLUSIONS & THE FUTURE

All of the regulations considered in this paper will have some impact on the design of large yachts. Perhaps the most conspicuous is the MLC, the unknown future outcome of negotiations and the potential impact it could have on yachts between 200 – 1150 GT. The new emissions and ballast regulations demonstrate how increasing environmental responsibility is leading to more and more equipment being squeezed onto vessels, inevitably adding weight and altering the balance of accommodation space and machinery space on yachts. The increased protection of fuel tanks will result in more loss of accommodation space and reduced flexibility of design. In an effort to improve safety, the new SOLAS probabilistic stability also adds complexity to the design process. The challenge facing yacht design teams has certainly increased.

It should be noted that each of the six regulations studied have been considered in isolation. In reality MARPOL Regulation 12A will have some influence over probabilistic stability performance and vice versa. Also the combined effect of the BWM Convention and the MARPOL emissions requirements will have a compounding influence on engine room size. The aim of this paper has been to demonstrate the likely impact of these new regulations. It is not until industry responds and subsequent future designs emerge that the true impact will be known.

The large yacht industry is currently in the consultation process for the Passenger Yacht Code (PYC). This is being developed by members of the Red Ensign Group and in a similar vein to LY2, will provide a code for yachts carrying between 13 – 36 passengers on international voyages. It is hoped the code will take into account that some aspects of the SOLAS and Load Line regulatory framework are impractical in the context of yachts of this type considering their operating profiles and layouts compared to commercial passenger ships. This would allow designers to have more freedom in certain areas than is currently the case and remove previous ambiguities from interpretation for yachts. However, looking at a draft version published, it is not believed that any of the regulations discussed in this paper will be subject to any equivalences or concessions

in the code except for SRtP. The code is due to be presented to the IMO in November 2010.

9. REFERENCES

[1] 'Application of the MLC 2006 – United Kingdom Policy', MCA, http://www.mcga.gov.uk/c4mca/...2006/mcga.ds-ssh-mlc-definitions

[2] A. Papanikolaou & E. Eliopoulou, 'Impact of New Damage Stability Regulations on Ship Design' Proc. 2nd Int. Maritime Conference on Design for Safety, Sakai-Osaka, October 2004.

[3] 'Ballast Water Treatment Technology – Current Status', Lloyds' Register, February 2010.

10. AUTHORS' BIOGRAPHIES

Alex Meredith Hardy is a Naval Architect at BMT Nigel Gee. He has worked on a wide range of projects including commercial and military vessels. More recently he has focussed on large yachts as an active member of the design team for several yacht projects.

Sylvain Julien is a Naval Architect at BMT Nigel Gee. He is involved in a wide range of naval architectural duties from the concept design stages through to the detail design stages, including hull lines development, stability calculations, performance predictions, and model testing.

James Roy is the Yacht Design Director at BMT Nigel Gee Ltd. He is responsible for development of the companies' yacht design activities and managing conceptual and preliminary design work as well as consultancy services.

Ignazio Maria **Viola**[1] & Richard GJ **Flay**[2]

ON-WATER PRESSURE MEASUREMENTS ON A MODERN ASYMMETRIC SPINNAKER

Proceedings of the 21st International HISWA Symposium on Yacht Design and Yacht Construction, 15th-16th November 2010, Amsterdam, The Netherlands

Abstract

The present paper presents full-scale pressure measurements on sails set in downwind conditions. Pressure distributions were measured on a pressure-tapped asymmetric spinnaker. The sail was designed for Emirates Team New Zealand, a potential challenger for the 34th America's Cup, when it was expected to be sailed in AC33-class yachts. Pressure distributions were measured for several sail trims, and at three apparent wind angles, on both sides of the sail. Pressure distributions are discussed and correlated with the flow field. Full-scale pressure distributions are compared with wind-tunnel measurements. Good agreement and few differences were found.

1. Introduction

Sail aerodynamics has been widely investigated in the last century. Sails made from different materials and made in different shapes have been compared with on-water tests, wind tunnel tests and numerical codes. These three approaches allow different aspects of sail aerodynamics to be investigated. Unfortunately, each of them has some limitations, and none of them are able to substitute for the other two. The present paper investigates sail aerodynamics in downwind sailing conditions from on-water tests.

COMPUTATIONAL FLUID DYNAMICS

In the past few decades, numerical codes have become the most commonly used research tool for sails. In the 60s, potential-flow codes were used for 2D horizontal sail sections. In following years, the fast growth of computational resources led to Navier-Stokes codes being used more and more frequently. Nowadays, while potential-flow codes are widely used for upwind sailing conditions, Navier-Stokes codes are most commonly used for downwind conditions. In fact, in upwind conditions, sails are designed to operate near the maximum lift/drag ratio and, therefore, the flow has an attached boundary layer on most of the sail surface. Potential-flow codes, which are unable to model separated boundary layers, can compute aerodynamic forces with a reasonable accuracy in upwind conditions. Conversely, in downwind conditions, sails are designed to operate near the maximum lift and, therefore, they have more cambered sections and higher pressure gradients. The boundary layer separates before the trailing edge over a large part of the sail surface due to the high adverse pressure gradients. To correctly compute the aerodynamic forces, separation has to be computed correctly by modelling the viscosity of the fluid. Therefore, Navier-Stokes codes are commonly used to model downwind conditions.

Due to the relatively high sail Reynolds number, nowadays Direct Navier-Stokes simulations cannot be used in sail aerodynamics, even when very large computational resources are available (Viola & Ponzini, 2009). Therefore, Reynolds Averaged Navier-Stokes (RANS),

---

[1] Formerly Yacht Research Unit, The University of Auckland (New Zealand);
Since Sep. 2010, School of Marine Science and Technology, Newcastle University (UK).

[2] Yacht Research Unit, The University of Auckland (New Zealand);.

Large Eddy Simulations (LES) or Detached Eddy Simulations (DES) techniques have to be used to model the small-scale turbulence neglected by the limited grid resolution. These techniques use based on heuristic equations, which need to be validated with experimental measurements. Validations should be repeated every time the modelled geometry or the fluid characteristics are changed significantly. Therefore, wind-tunnel tests have to be performed for this purpose.

WIND TUNNEL TESTS

Wind tunnel tests allow the designer to have a real-time aerial view of the flying sails. Smoke visualization or other similar techniques allow streaklines to be visualised very efficiently. At the Yacht Research Unit, forces are measured with a 6-component balance located inside the boat model. It is common practice to use flexible sails, which can be trimmed remotely. Therefore, the change of forces and streaklines with change in the sail trim can be appreciated immediately. In most of the wind tunnels where sail aerodynamics is investigated, special devices allow the flying shapes to be detected. Thus the aerodynamic forces and flying shapes are recorded simultaneously. This increases the repeatability of the measurements and allows differences between sails and trims to be better appreciated. It also allows flying shapes to be modelled with numerical codes and computed forces to be compared with measured forces. However, validating numerical simulations just with forces is not ideal. In fact, the pressure distribution on sails might be computed incorrectly even when the computed resultant aerodynamic forces agreed with the measured force. This is because different pressure distributions can lead to the same global aerodynamic force. For this reason, in recent years, a great deal of effort has been put into measuring pressure distribution on sails with the aim of validating numerical codes (Viola & Flay, 2009; Viola et al, submitted).

Using flexible sails in wind tunnel tests allows different trims to be investigated. The deformation of the mast should be correctly modelled because it has a significant affect on the sail shape and on the sail position with respect of the longitudinal boat axis. Wind tunnel tests are usually performed at wind speeds between 2 m/s and 5 m/s. In wind tunnels with large test sections, the model-scale is of the order of 1/10 of full-scale. As a consequence, in order to achieve the full-scale Reynolds number, the wind tunnel wind speed should be 10 times higher than the full-scale wind speed. Unfortunately however, the maximum wind tunnel wind speed is usually equal to or less than the full-scale wind speed. This is because the flexible sails and rigging do not allow testing in high-speed conditions, as they would break!

The attitude of a sail flying high and far from the yacht depends on the ratio between the pressure distribution and the gravity force. Therefore, the weight of the model-scale sails should be chosen to achieve the same full-scale ratio between the pressures forces and the gravity force. This criterion leads to the choice of a very light model-scale sailcloth. However, since, the sail is a membrane, such a lightweight cloth would stretch a considerable amount due to the loads it be subjected to, and this change in shape would alter the aerodynamic loading. Unless the mast is especially bendy, where it needs to bend in the wind tunnel tests, the mast is usually modelled in its deformed “sailing” shape and, often, the sail is cut to its “flying” shape. Thus the wind tunnel tests the sails in the correct flying attitude, and thus properly simulates full-scale.

ON-WATER TESTS

Both numerical simulations and wind tunnel tests are simplified models of the complex full-scale conditions. When yachts sail, the dynamic movements of the yacht and of the sails are considerable. Moreover, the yacht sails through the turbulent atmospheric boundary layer, which leads to a time dependent flow pattern. The sails are continuously trimmed to take into account the dynamic movements of the yacht, the sails, and the change in the wind speed and direction. All these dynamic effects are modelled with difficulty (and consequently with low

accuracy) in CFD, and are normally not modelled in wind tunnel, except in special "dynamic" tests.

Because of the complexity of these dynamic effects, on-water tests are very difficult to perform and suffer from poor repeatability, thus leading to large uncertainty in the results. Firstly, the fully three-dimensional time dependent wind flow, in which the yacht sails, cannot be measured. For instance, if an anemometer were fixed on the top of the mast to measure the three wind velocity components, the measurement would be affected significantly by the influence of the sail trim. Moreover, even if the flow field was known at a location near the top of the mast, the apparent wind speed and direction changes significantly between the top of the mast and sea level, due to the apparent wind vector being formed by subtracting the yacht velocity off the true wind velocity, and their differences vary considerably between the foot and head of a sail.

Both forces and pressures can be measured onboard. As mentioned above, measuring the pressure distributions is preferable to measuring forces, as it gives a much more complete description of the loading process. It is more difficult to measure pressure measurements in downwind conditions than in upwind sailing conditions because the Apparent Wind Speed (AWS) is lower in the former case. The differential pressure across sails is of the order of magnitude of the dynamic pressure, which is, for instance, about 5.5 Pa for a 3 m/s AWS. To measure a pressure distribution along a sail section, pressure variations smaller than about 1 Pa should be measured. However, in one minute, the wind typically oscillates by about ±0.5 m/s, which leads to dynamic pressure oscillations of about ±2 Pa. Moreover, pressures can change by several Pascals per minute due to the incoming atmospheric turbulence.

Therefore on-water pressure measurements automatically take into account these dynamic effects, which are neglected or poorly modelled by numerical modelling and wind tunnel experiments, but on the other hand, the complexity of the real system makes the measurements quite complicated and, thus, less accurate.

2. The State of the Art of Pressure Measurements on Sails

Sail aerodynamics has been widely investigated with numerical modelling. From the 1960s to the end of the last century, most of the computations were performed using potential flow codes. In the past 10 years, RANS codes became very popular for studying downwind sails. A review of potential flow and RANS applications is presented in Viola, 2009. Over the past few years, only a few LES or DES applications on sails have been published (Wright et al., 2010; Braun & Imas, 2008) but the most important research institutes in sail aerodynamics are all investigating these techniques.

Viola & Flay, 2009, reviews wind tunnel force measurements on downwind sails, while Viola & Flay, 2010, reviews pressure measurements on sails performed on-the-water and in a wind tunnel. In the following paragraphs, a complementary review of force and pressure full-scale experiments on sails is provided.

Force measurements have been performed more rarely in full-scale than in wind tunnels, due to the difficulty and cost. Milgram et al, 1993, at the Massachusetts Institute of Technology (MIT), introduced the innovative concept of an instrumented framework structure located inside the 35-foot yacht *Amphetrete*. The frame connected the rigging to the hull and was instrumented with a 6-component balance that measured the aerodynamic forces in equilibrium with the hydrodynamic forces. Masuyama & Fukasawa, 1997, at the Kanazawa Institute of Technology, developed a similar concept on the yacht *Fujin*. These two papers are mainly oriented towards investigating the aerodynamics of yachts. Conversely, the research described by Hochkirch and Brandt, 1999, at the Berlin University was mainly focused on the hydrodynamics of yachts. They applied a similar "framework structure" concept to the 33-

foot yacht *Dyna*, as well as having an additional anemometer, and were able to measure the hydrodynamic forces on the yacht appendages.

Full-scale pressure measurements were performed for the first time by Warner and Ober, 1925, at the Massachusetts Institute of Technology (the tests were performed between 1915 and 1921). The authors used U-tube pressure manometers on the S-class yacht *Papoose*. Much later, Flay and Miller, 2006, reported the lessons learned by the Yacht Research Unit (YRU) of the University of Auckland in measuring pressures on the sails of the Farr1020-class yacht *Shokran*. The first pressure distribution with a large number of pressure taps (25 per side) was presented the same year by Puddu et al., 2006, from the University of Cagliari, Sardinia. The authors measured the pressures on the mainsail of a Tornado-class catamaran. Graves et al., 2008, measured the pressures on the mainsail of a IACC-class yacht, but only 5 pressure taps were used. The first modern pressure measurements (after Warner and Ober in 1925) on head sails was recently performed by Viola & Flay, in press. The authors measured pressure distributions on the mainsail and the genoa of the 24-foot yacht *Aurelie,* designed by Sparkman & Stephens.

As far as is known by the authors, pressure distribution on downwind sails have never been published. The present paper presents the first pressure measurements on an asymmetric spinnaker. The measurements were performed on a 1/3rd model-scale sail, which was designed for a 90-foot America's Cup class (AC33) yacht. The sail was tested on a 25-foot Platu25-class yacht.

3. Method

THE SAILS

In the late 2008s and early 2009s, it was not clear which yacht class would be used in the 34th America's Cup, and when and where the race would be held. Emirates Team New Zealand, the winner of the previous Louis Vuitton Cup, was investigating the design of the most likely class for the next event. The YRU, which is Emirates Team New Zealand's Official Scientific Advisor, asked North Sails New Zealand to manufacture a 1/3rd scale AC33-class asymmetric spinnaker for on-water testing. The spinnaker was built with 4 horizontal panels, which were sewed together with an overlap of about 100 mm at each joint. The overlapped panels made 3 horizontal pockets where 21 pressure taps per pocket were located, and the pockets were used to contain the tubes. Figure 1 shows a schematic drawing of the pressure taps located along the three overlapping joints.

The pressure taps were very flat thin plastic cones with base and top surface diameters of 50 mm and 40 mm, respectively. The cone height was 5 mm. The pressure taps had a hole in the centre of the top surface which connected to a metal 2 mm diameter tube protruding out the side of the tap, as shown in Figure 2. PVC tubes connected to the pressure taps conveyed the pressures to the transducers located inside the yacht cabin. The tubes from all the pressure taps were threaded to the luff (leading edge of the sail) inside the horizontal pockets and then down to the tack (corner of luff and sail foot) inside an additional vertical pocket.

The pressure distributions were measured on the leeward side while sailing on starboard tack (wind coming from the right hand side of the yacht), and on the windward side when sailing on the port tack (wind coming from the left hand side of the yacht). No pressure measurements were performed on the mainsail. Future research should aim to measure the pressure on the two sails simultaneously. The mainsail used in the on-water tests was a standard Platu25-class mainsail.

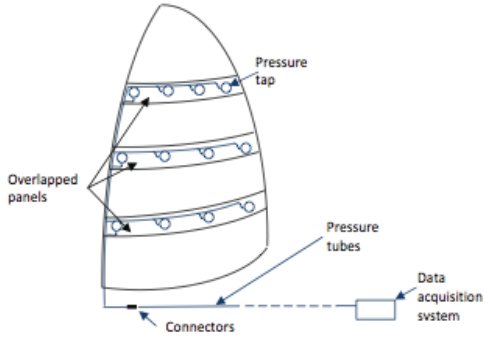

Figure 1: Schematic layout of the pressure-tapped sail (edited from Watier, 2010).

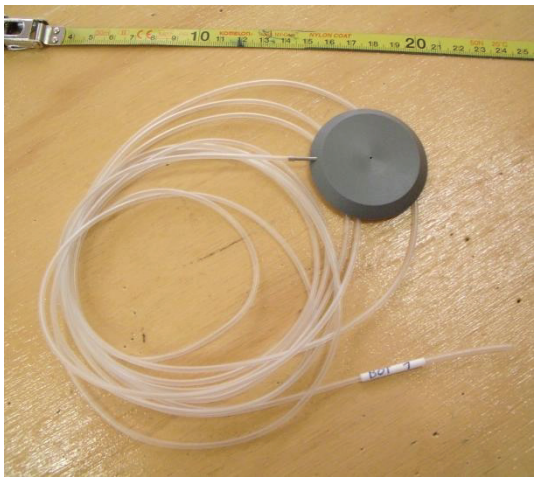

Figure 2: Pressure tap with pressure tube connected.

THE PRESSURE SYSTEM

The tubes were connected to the transducers, which were well protected inside the cabin. The pressure transducers had a range of ±450 Pa and a resolution of 9.25 mV/Pa with an accuracy better than ±0.5 Pa. Additional details describing the pressure system are provided by Fluck et al., in press. All the transducers were pneumatically connected to a reference static pressure tube. The tube was 10 m long and the end of the tube was located inside a porous box in a cabinet inside the cabin, which assured that the air inside the box had negligible velocity. The reference static pressure p_∞ was compared with the static pressures measured by Pitot-static probes fixed to a pole on the stern of the boat. The pole was about 2 m high and several Pitot-static probes were fixed onto it. The anemometers were deliberately pointed in different directions. All the static and the total pressures from the Pitot-static probes were connected to the transducers inside the cabin. When the boat was at the wharf, the pressure differences between p_∞ and the static pressures measured on the pole were found to be negligible, as expected. Conversely, the differences between the static pressures were larger while sailing. This was assumed to be due to the influence of the sails on the static pressures measured on the pole. For this reason, the reference static pressure p_∞ was taken to be that measured inside the cabin, and not by the probes on the pole.

Pressures were acquired at 100 Hz for 90 seconds. High frequency fluctuations would have been damped by the long tubes (up to 20 m long) and hence a higher sampling frequency would have resulted in additional and redundant stored data.

Pressures were measured using two different approaches. In the first case, pressures were measured with the yacht sailing in the most stable sailing state as possible, with the sails in a fixed state of trim and the yacht on a constant course. Pressures were recorded and averaged on the sampling period. In the second case, pressures were measured while one sail condition was changed at a constant rate. For instance, over 90 s the sail was trimmed in from fully eased to hard in. For these test cases the pressures were averaged in sets of about 15 s and the resulting 6 average values were used to show the pressure variation with the sail trim.

MEASURING THE DYNAMIC PRESSURE

The dynamic pressure was measured with the Pitot-static probes fixed onto the pole on the stern of the yacht. The pole was on the port side when pressures on the windward side of the sail were measured, and on the starboard side when pressures on the leeward side of the sail were measured. The pole was also inclined at about 20° from the vertical axis of the yacht, so

that the Pitot-static probes were always leaning to windward from the yacht. Figure 3 shows the pole supporting the probes while sailing upwind after the tests. It was found that the pressures measured by the Pitot-static probes on the pole were less affected by the sail trim, than when the pole was 2 m above the head of the mast.

Initially, a single pivoting Pitot-static probe was mounted on the pole. In a previous experiment (Viola & Flay, in press.), where pressures were measured on upwind sails, the wind was able to align the pivoting anemometer used with the wind direction. This setup was not appropriate for the present test, however, because the AWS was not high enough to align the anemometer into the wind. Therefore, three fixed Pitot-static probes aligned in different directions were used. The total-pressures from all three anemometers were measured at each acquisition. Then the pressure measured by the Pitot-static probe most aligned with the wind local wind direction was used as the reference dynamic pressure q_∞. In the present paper, q_∞ was between 4 and 40 Pa.

The AWA was measured with the standard on-board instrumentation located at the top of the mast.

4. Results and Discussion

Figure 4 shows the Platu25-class yacht sailing with the pressure-tapped asymmetric spinnaker. In the full-scale AC33-class yacht, the top of the spinnaker is at the same height as the top of the mainsail. Therefore, the measurements were performed with the mainsail lowered (one reef was taken) from the hoist shown in Figure 4, so that the heads of both sails lined up during the measurements. As a consequence, the lower centre of effort of the mainsail led to a lower heel angle of 10°, than that shown in Figure 4.

Three AWAs and several sail trims were measured. The full-scale asymmetric spinnaker was designed to be sailed at about AWA=80° in light air. The Platu25-class yacht does not have a very large transverse stability, and therefore an AWA of 80° resulted a fairly small angle to be sailed with a spinnaker. Two additional AWAs were tested, namely 120° and 170°.

The pressure signals were remarkable unsteady. In fact, it was not possible to keep a constant sail trim and to sail a constant course. When a gust arrived, the AWS increased and so did the heeling moment. The yacht began heeling and the helmsman reacted immediately to change the course to increase the AWA. The yacht then straightened up and accelerated due to the reduction in hydrodynamic resistance. The increased boat speed led to a lower AWA and the sail then had to be trimmed in. As soon as the gust passed by and the yacht slowed down, the sail became over-trimmed and it had to be eased. Therefore, the AWA and the sail trim were changing continuously. The frequency and the amplitude of the changes in the course and in the sail trim are certainly larger on small yachts, such as the Platu25 class, than on large yachts, such as the AC33 class, and thus much care has to be taken in transferring the results obtained on a tender keel boat to a more stable large keel boat with a relatively much heavier keel.

The dynamic movement of the sail led to vertical wrinkles, which were continually appearing and disappearing. The wrinkles were often in the same positions on the sail. Peaks and hollows in the averaged pressure distributions along horizontal sections in relation to these wrinkles are discussed later.

The pressure measurements are presented in terms of pressure coefficient Cp, defined as the difference between the pressures measured by the pressure taps on the sail and the reference static pressure p_∞, measured inside the cabin, divided by the reference dynamic pressure q_∞, measured by the selected Pitot-static probe on the pole. The pressure distributions presented have been smoothed to present general trends.

Figure 3: Pole supporting the Pitot-static probes (shown while sailing upwind after the tests).

Figure 4: The yacht and the pressure-tapped sail. The black bands show the locations of the pressure taps.

GENERAL PRESSURE DISTRIBUTION TRENDS

Pressure distributions on sails can be explained in terms of classical aerodynamic theory for thin airfoils. In a middle height section, the flow direction can be considered mainly in the chord-wise direction. If the local flow at the leading edge is tangent to the sail, then the angle of attack is named *ideal angle of attack*. In this case, the stagnation point is at the leading edge, where the pressure is nearly equal to the dynamic pressure and $Cp \approx 1$. On the leeward side, *Cp* decreases along the chord until about the maximum curvature of the sail, and then increases again until roughly $Cp \approx 0$ if there is no trailing edge separation, or until $Cp \approx -1$ if there is trailing edge separation. On the windward side, the flow is slow and *Cp* is nearly the stagnation pressure for most of the chord length. At the trailing edge, *Cp* decreases to match the leeward-side trailing-edge pressure.

If the flow at the leading edge presents a positive angle with the leading-edge sail profile, a leading-edge separation bubble occurs. At the leading edge, the flow separates on the leeward side of the sail and reattaches in the first quarter of the chord length. The pressure on the leeward side decreases abruptly near the leading edge, and then increases until roughly the reattachment point. Further downstream, the pressure decreases again due to the sail curvature and then increases after the maximum sail curvature. The pressure increase can lead to trailing edge separation. If separation occurs, the pressure recovery is interrupted and the pressure remains constant and equal to the so-called *base pressure*. Figure 5 shows a schematic drawing of the flow field and the correlated pressure distribution.

As far as the flow does not stall, the higher the angle of attack, the higher is the suction near the leading edge. At high angle of attacks, the leading edge suction peak is much higher than the cambered-related suction peak and, thus, the second is not visible. When the flow stall and the flow does not re-attach downstream, the leading edge suction peak decreases. At very

high angle of attacks, higher than the stall angle, the pressure becomes almost constant and equal to the base pressure.

The stall angle on the mid section of an asymmetric spinnaker is above 20°. On an equal two-dimensional section, the stall angle would have been significantly lower. On three-dimensional sails, the tip vortices take a large amount of flow from the windward side to the leeward side, increasing the pressure on the leeward side. Therefore, the flow is able to reattach downstream at high angle of attacks. More details about the pressure distribution on downwind sails can be found on Viola & Flay 2009 and 2010.

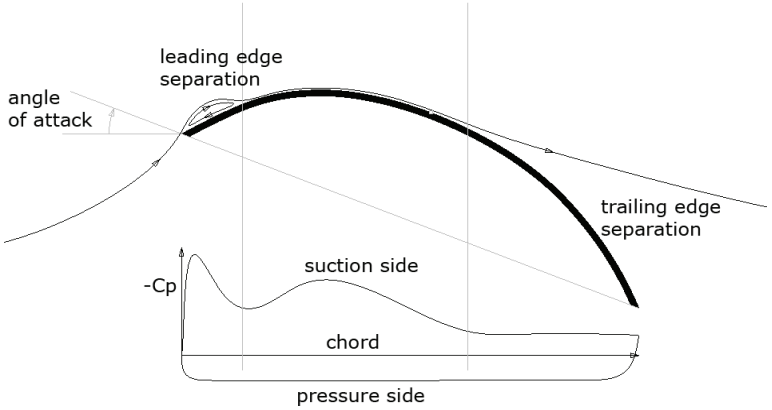

Figure 5: Schematic drawing of the flow field and of the correlated pressure distribution.

PRESSURE DISTRIBUTIONS FOR DIFFERENT TRIMS

Figure 6 shows *Cps* on the leeward side of the 3 horizontal sections of the asymmetric spinnaker. *Cps* are plotted along the curve length for each sail section and for 4 different sail trims. The sail is initially eased as much as possible (*max eased* trim in Figure 6). The low angle of attack on the top sections of the sail leads to flapping of the leading edge. The pressures on the top section ($3/4^{th}$ of the sail height) show that the sail is trimmed at the *ideal angle of attack*. On the lower sections, a leading edge suction peak occurs, and the *Cp* shows a suction peak within the first quarter of the sail. In the second half of the curve length, trailing edge separation occurs and the *Cp* becomes almost constant.

When the sail is trimmed in just enough to stop the luff from flapping (trim *eased* in Figure 6), a leading edge suction peak occurs on the top section. Sailors would generally consider this the optimum trim. On the middle and bottom sections, the suction peak decreases due to movement of the trailing edge separation point upstream along the curve length. On the top section near the trailing edge, *Cp* decreases up to -3. This pressure trend is unexpected and should be investigated further. It could be related to the interaction of the asymmetric spinnaker with the mainsail, or to a local stable vortex with a significant reverse velocity at the trailing edge. It should be noted that a similar trend has never been measured in wind-tunnel tests, as far as the authors are aware. On trimming further in, (from trim *tight* to *max tight* in Figure 6), stall occurs and the leading edge suction peak decreases. *Cp* becomes almost constant and is equal to -1.

On the windward side (Figure 7), *Cp* is almost independent of the sail trim and, therefore, *Cp* measured at the optimum trim only is shown. *Cp* is less than 1 at the trailing edge, which shows that at the stagnation point there is a significant span-wise velocity component. Along the chord length, *Cp* decreases only near the trailing edge, where it matches *Cp* on leeward side. Because the pressure tap closest to the trailing edge was about 100 mm from the trailing edge, the last measured *Cp* on the leeward side is not equal to the last measured *Cp* on the windward side.

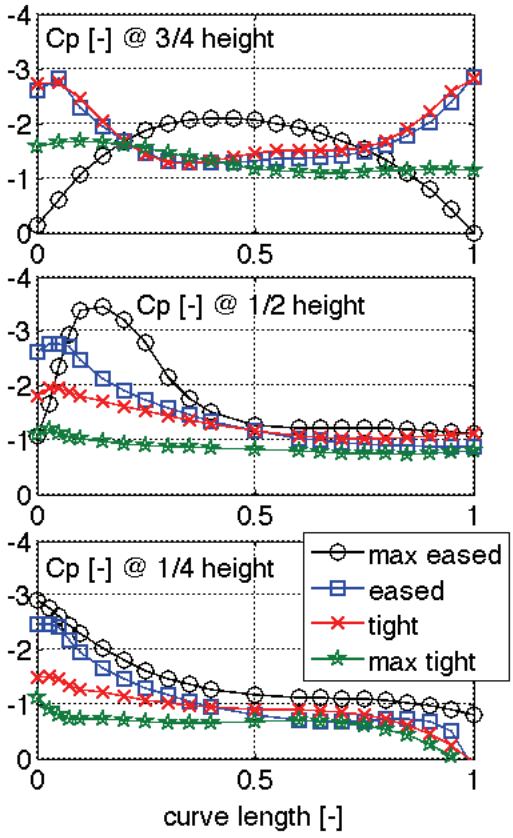

Figure 6: Leeward *Cp* on the 3 sail sections for 4 sail trims.

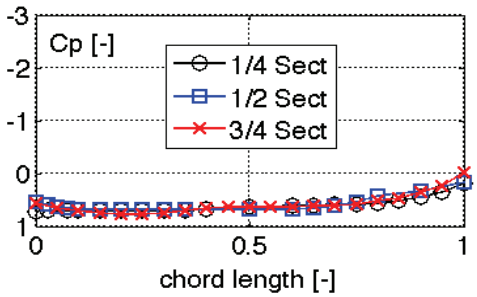

Figure 7: Windward *Cp* on the 3 sail sections.

PRESSURE DISTRIBUTIONS FOR DIFFERENT AWAS

Figure 8 shows *Cps* on the leeward side of the 3 horizontal sections of the asymmetric spinnaker. The sail was re-trimmed to the optimum trim at each AWA. On the top section, when sailing at AWA=120°, the *Cp* shows the unexplained and rather interesting trailing edge suction. It should be noted that the unexpected suction do not occur at AWA=80°, while in the previous test (Figure 4), when different trims were tested at AWA=80°, the unexpected suction occurred at the optimum trim.

Figure 8 shows that the sail can be trimmed at AWA=80° and AWA=120° to achieve a high suction on the entire leeward side of the sail. Conversely, when the AWA is increased further, the sail cannot be eased sufficiently and stall occurs. The integral of *Cp* along the curve length represents most of the aerodynamic force due to the sail. Figure 8 thus indicates that the aerodynamic force is decreased when stall occurs.

The *Cp* on the windward side is not presented here because it does not present any significant differences from the *Cp* trends shown in Figure 7.

FULL-SCALE AND WIND-TUNNEL COMPARISON

Figure 9 shows *Cps* on the leeward side of the 3 horizontal sections of the asymmetric spinnaker, measured on-the-water and in the wind tunnel respectively. *Cps* were measured on water for the optimum trim at AWA=80°. Wind-tunnel measurements were performed with a 1/15th model-scale flexible sail at the optimum trim at AWA=70°. A detailed description of the wind tunnel measurements can be found in Viola & Flay 2009 and Viola & Flay 2010. Figure 9 shows very good agreement and few differences between the *Cps* measured in full-scale and in the wind tunnel. The first difference is due to the unexplained trailing edge suction on the top section of the full-scale test, which has already been discussed. The second difference is the more positive pressure recovery related to the leading edge reattachment, which could be due to a tighter trim in the full-scale experiment. In fact, the higher the angle of attack, the higher the leading edge suction peak and the smoother the pressure recovery. A tighter trim is thought to have been used in the full-scale experiment due to trimming in the unstable conditions. Conversely, the stationary wind conditions and fixed yacht model attitude in the wind tunnel allowed a more eased trim to be used.

The different leading edge pressure distributions could also be due to a Reynolds number effect. The wind-tunnel tests were performed at Reynolds number about 1/10th lower than the full-scale Reynolds number. The higher Reynolds number in full-scale could affect the leading edge separation bubble and thus the leading edge pressure distribution. Finally, leading edge separation bubbles can be affected by different characteristics of wind turbulence. However, the authors consider that it is more likely that the differences are due to different sail trims, rather than to Reynolds number or to different wind turbulence characteristics.

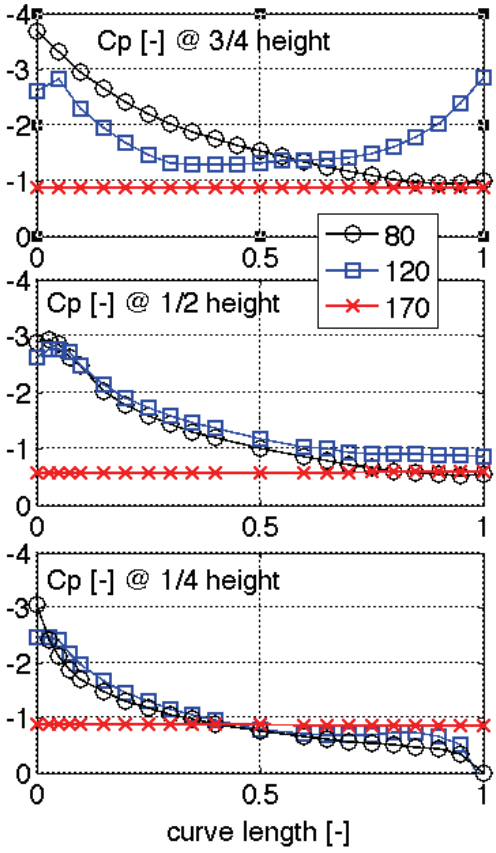

Figure 8: Leeward *Cp* on the 3 sail sections for 80°, 120° and 170° AWA.

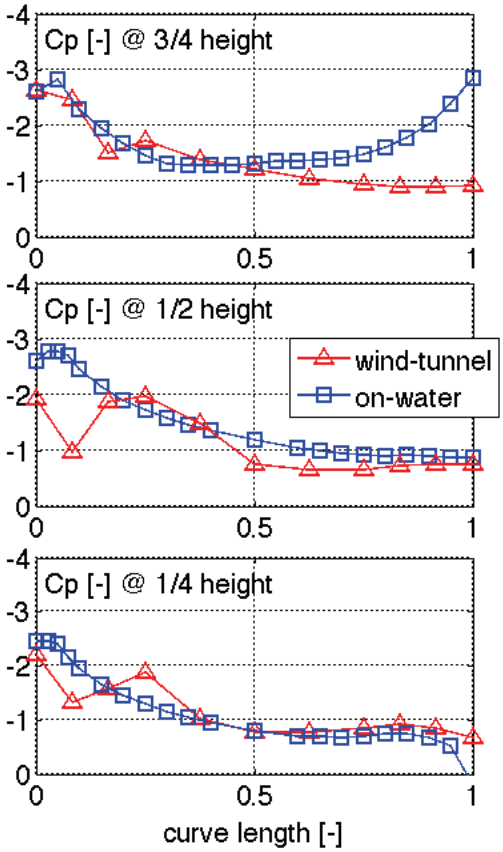

Figure 9: Wind-tunnel and on-water leeward *Cps* on the 3 sail sections.

5. Acknowledgments

The authors wish to acknowledge the support of staff and students in the Yacht Research Unit, and in particular, the authors are grateful to Mr. Baptiste Watier and Mr. Etienne Gauvain for the passion and the support in managing and performing the on-water and wind tunnel experiments. The authors also acknowledge the support of Dr Nick Velychko in building and supporting the multi-channel pressure system.

6. Conclusions

Pressure distributions on sails have been measured only rarely. In particular, on-water pressure measurements have been performed only in upwind sailing conditions. As far as known by the authors, the present paper presents the first pressure measurements on sails flown in downwind sailing conditions. While numerical modelling and wind tunnel experiments neglect or model relatively poorly the unsteadiness of the wind, the movement of the sails and the yacht, on-water sail tests automatically take them into account.

Pressures were measured using 63 pressure taps distributed along three horizontal sections at $1/4^{th}$, $1/2^{nd}$ and $3/4^{th}$ of the sail height, respectively, on an asymmetric spinnaker. The sail was designed for Emirates Team New Zealand, a possible challenger for the 34^{th} America's Cup, when it was expected to be sailed with AC33-class yachts. Pressure distributions were measured for several sail trims and 3 apparent wind angles (AWAs) on both the leeward and windward sides of the sail.

The main conclusions that can be drawn from the experiments are summarised below.

PRESSURE DISTRIBUTIONS FOR DIFFERENT TRIMS

- For the optimum sail trims, the *Cp* on the leeward side of the sail near the leading edge has a suction peak between *Cp* = -3 and *Cp* = -4, and downstream, *Cp* increases monotonically.
- On the leeward side, *Cp* is almost constant and is slightly less than 1. *Cp* decreases near the trailing edge to match the leeward-side trailing-edge suction.
- In some conditions, which were not well defined, on the top section only, an unexplained suction was measured near the trailing edge.
- Trimming-in the sail caused the leading edge suction to decrease due to trailing edge separation, until *Cp* becomes almost constant and equal to – 1 when stall occurs.

PRESSURE DISTRIBUTIONS FOR DIFFERENT AWAS

- Almost the same pressure distribution is achieved by re-trimming the sail for AWA=80° and AWA=120°. Conversely, at higher AWAs it was not possible to ease the sail enough and stall occurred. Therefore, *Cp* is almost constant and equal to – 1.
- On the leeward side, *Cp* is almost constant between 0 and 1, and it decreases near the trailing edge to match the leeward-side trailing-edge suction.

FULL-SCALE AND WIND-TUNNEL COMPARISON

- Full-scale and wind tunnel pressure measurements showed very good agreement and few differences on the leeward pressure distributions.
- The unexpected suction on the top section near the trailing edge has never been reported from wind tunnel test results.
- The pressure recovery is related to leading edge reattachment, which occurs around the first quarter of the curve length, and was visible in the wind tunnel-measurements but not in the full-scale measurements. Several possible reasons for this have been discussed.

7. References

Braun J.B. & Imas L., 2008. High Fidelity CFD Simulations in Racing Yacht Aerodynamic Analysis, *in the proceedings of The 3rd High Performance Sailing Yacht Conference (HPYDC3)*, 2nd-4th December, pp. 168-175, Auckland, New Zealand.

Flay R.G.J. & Millar S., 2006. Experimental Consideration Concerning Measurements in Sails: Wind Tunnel and Full Scale, *in the proceedings of The 2nd High Performance Yacht Design Conference (HPYDC2)*, February 14th-16th, Auckland, New Zealand.

Fluck M., Gerhardt F.C., Pilate J. and Flay R.G.J., in press. Comparison of Potential Flow Based and Measured Pressure Distributions Over Upwind Sails, *Journal of Aircraft*.

Gaves W., Barbera T., Broun J.B., Imas L. 2008. Measurements and Simulation of Pressure Distribution on Full Size Scales, *in the proceeding of The 3rd High Performance Yacht Design Conference (HPYDC3)*, December 2nd-4th, Auckland, New Zealand.

Hochkirch K. & Brandt H., 1999. Full-Scale Hydrodynamic Force Measurement on the Berlin Sailing Dynamometer, *in the proceedings of The 14th Chesapeake Sailing Yacht Symposium (14CSYS), SNAME,* pp. 33-44, 30th January, Annapolis, USA.

Masuyama Y. & Fukasawa T., 1997. Full-Scale Measurements of Sail force and Validation of Numerical Calculation Method, *in the proceedings of The 13th Chesapeake Sailing Yacht Symposium (13CSYS), SNAME*, pp. 23-36, 25th January, Annapolis, USA.

Milgram J.H., Peters D.B., Eckhouse D.N., 1993. Modeling IACC Sail Forces by Combining Measurements with CFD, *in the proceedings of The 11th Chesapeake Sailing Yacht Symposium (11CSYS), SNAME*, pp. 65-73, 29th-30th January, Annapolis, USA.

Puddu P., Erriu N., Nurzia F., Pistidda A., Mura A., 2006. Full Scale Investigation of One-Design Class Catamaran Sails, *in the proceeding of The 2nd High Performance Yacht Design Conference (HPYDC2),* February 14th-16th, Auckland, New Zealand.

Viola I.M., 2009. Downwind Sail Aerodynamics: a CFD Investigation with High Grid Resolution, *Ocean Engineering, vol. 36, issues 12-13,* pp. 974-984.

Viola I.M. & Flay R.G.J., 2009. Force and Pressure Investigation of Modern Asymmetric Spinnakers, *International Journal of Small Craft Technology, Trans. RINA*, vol. 151, part B2, pp. 31-40, 2009, DOI: 10.3940/rina.ijsct.2009.b2.98. Discussion in *Trans. RINA*, vol. 152, part B1, pp. 51-53.

Viola I.M. & Flay R.G.J., 2010. Pressure Distribution on Modern Asymmetric Spinnakers, *International Journal of Small Craft Technology, RINA,* Vol. 152, part B1, pp. 41-50.

Viola I.M. & Flay R.G.J., in press. Full-scale Pressure Measurements on a Sparkman & Stephens 24-foot Sailing Yacht, *Journal of Wind Engineering and Industrial Aerodynamics,* DOI:10.1016/j.jweia.2010.07.004

Viola I.M., Pilate J., Flay R.G.J., submitted. Upwind Sail Aerodynamics: a Pressure Distribution Database for the Validation of Numerical Codes, *International Journal of Small Craft Technology.*

Viola I.M. & Ponzini R., 2009. Sailing Past a Billion, *Ansys Advantage*, vol. 3, issue 2, pp. 47-48.

Warner E.P. & Ober S., 1925. The aerodynamics of Yacht Sails, *in the proceedings of The 3rd General Meeting of the Society of Naval Architects and Marine Engineers,* 12th-13th November, New York, USA.

Watier P.B., 2010. Comparison of Full-Scale and Model-Scale Measurements of the Aerodynamics of an Asymmetric Spinnaker, *MEng Thesis, DTU Mechanical Engineering, Technical University of Denmark*.

Wright A., Claughton A., Paton J., Lewis R., 2010. Offwind Sail Performance, Prediction and Optimisation, *in the proceedings of The 2nd International Conference on Innovation in High Performance Sailing Yachts (INNOV'SAIL)*, 30th June – 1st July, Lorient, France.

Fluid Structure Interaction Simulation of Spinnakers – Towards Simulation Driven Sail Design

H F Renzsch[1]
K U Graf[2]

NOMENCLATURE

a	scalar	$\mathbf{H}$	Hessian matrix
$\mathbf{a}$	vector	φ	rotation angle
$\mathbf{A}$	matrix	m_i	virtual mass of node i
$\hat{}$	material coordinate system	ν	Poisson number
$\bar{}$	element coordinate system	P_{Dyn}	dynamic pressure [N m^{-2}]
$\tilde{}$	wrinkled coordinate system	$\mathbf{R}_i$	total force on node i (residual)
xx, yy, xy	element axes	ρ_{Air}	density of air [kg m^{-3}]
11, 22, 12	material axes	σ	stress [N m^{-1}]
φ	in orientation of φ	σ_m	material stress [N m^{-1}]
AWA	apparent wind angle [deg]	t	at time t
AWS	apparent wind speed [m s^{-1}]	$\mathbf{V}_i$	velocity of node i
ε	strain	$\mathbf{x}_i$	displacement of node i
ε_1, ε_2, σ_1, σ_2	principal strains, stresses [N m^{-1}]	y^+	dimensionless wall distance
E	Young's modulus [N m^{-1}]		
G	shear modulus [N m^{-1}]		

1. INTRODUCTION

The flow around a spinnaker is characterized by partial separation, while large displacements of the flow body, the spinnaker, take place. Since both phenomena make flow simulation methods quite complex, spinnaker designs are commonly evaluated by wind tunnel testing. While the wind tunnel is rightfully accepted as a useful tool for the evaluation of a spinnaker, it has a few shortcomings. Due to the small scale of the models the laws of similarity are typically violated in several respects: Reynolds number, weight of cloth and structural properties of the cloth. As the remedies for these shortcomings are going in entirely different directions, usually the only one of these points that is observed is to keep the ratio of cloth weight to dynamic pressure of the wind the same in the model as in full scale. To observe Reynolds similarity, the wind speeds would have to be extremely high, requiring an impractically strong model. For structural similarity it is simply assumed that the strains are sufficiently small that the different stress-strain properties do not unduly affect the flying shapes of model and full scale sail. Furthermore, due to the violation of Reynolds similarity and a different Eigen frequency, instationary behaviour and associated stability issues are not captured correctly.

Numerical simulation methods promise to solve the problems of wind tunnel testing. They can be carried out at full scale Reynolds number and also the structural behaviour of sail fabric can be modelled at full scale.. Consequently they promise to be more accurate on flow force properties as well as on instationary phenomena and spinnaker stability.

Numerical simulations of the flow around sails, in particular spinnakers, have to cope with the problem of flow separation as well as for the large displacements of the sail under wind load, which obviously strongly interact with each other. Thus simulation methods based on the principle of fluid structure interaction are necessary.

For the simulation of sails structural codes have been successfully coupled with RANSE codes in the past, yet, due to the coupling paradigm, with both codes calculating until convergence for any single iteration, computation costs for the simulation were extremely high and practical solutions were limited to steady state.

FlexSail is a Fluid-Structure-Interaction program specifically designed to include a RANSE solver as flow code and still run in an efficient manner. To this end a different coupling paradigm, suited to the high computational costs of RANSE simulations, is used. This method is able to simulate steady state as well as fully instationary behaviour of spinnakers, capable to solve any instationarity or stability problems associated with downwind sail operation.

[1] External PhD-Student, Faculty Mechanical, Maritime and Materials Engineering, Delft University of Technology
[2] Professor for Ship Hydrodynamics, University of Applied Sciences Kiel

2. FLEXSAIL – BASIC IDEA

Like any other Fluid-Structure-Interaction program FlexSail iterates the flow and structural solver to find equilibrium in both solutions and a converged state in the coupling of both. Flow is computed using the commercial flow solver Ansys CFX 12.0, a program for the simulation of viscous turbulent flow by solving the steady or unsteady RANSE equations. The structural behaviour is simulated by a purpose-written membrane finite element code, capable of simulating large displacements and highly non-linear behaviour. It is embedded in the RANSE solver.

What sets FlexSail apart from other flow solvers is the coupling paradigm. The basic idea is to run the flow simulation in an unsteady mode, with each timestep considered to be a valid solution. Therefore the structural code can be called from within the flow code repeatedly at given timesteps of the flow solution. See Figure 1 for a flow chart of the process.

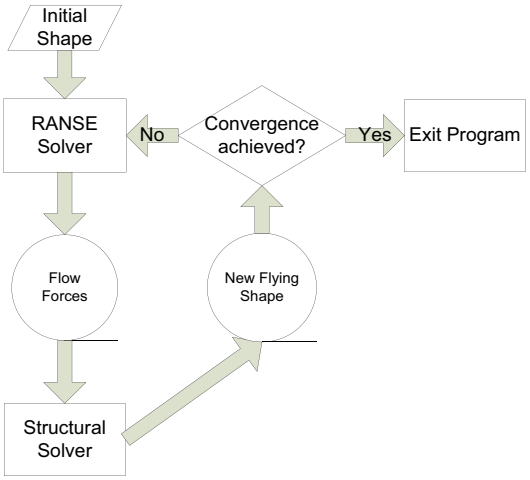

Figure 1: Flow Chart of FSI process

The coupling method results in a weak two-way coupling between flow and structural simulation. Therefore the timestep length has to be significantly smaller than any natural periods of dynamic occurrences considered in dynamic simulations. A typical application is shown in [1].

3. BASIC MEMBRANE THEORY

The structural method of FlexSail models the spinnaker as a membrane using a Finite Element solution approach.

3.1 GENERAL

Generally the stress – strain relationship is given by:

$$\boldsymbol{\sigma} = \mathbf{H} \cdot \boldsymbol{\varepsilon}$$

with $\boldsymbol{\varepsilon} = \{\varepsilon_{xx}; \varepsilon_{yy}; \sqrt{2}\varepsilon_{xy}\}^T$ and $\boldsymbol{\sigma} = \{\sigma_{xx}; \sigma_{yy}; \sqrt{2}\sigma_{xy}\}^T$. The factor √2 is included just for mathematical convenience later on.

To discretise the sail, Constant Stress Triangle (CST) elements as described in Figure 2 are used.

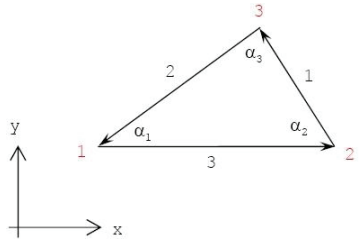

Figure 2: Description of triangle element

Note that edge 3 is parallel to the x-axis.

In FlexSail linear Hookean materials are assumed. The generalised stress-strain relationship, the Hessian matrix $\hat{\mathbf{H}}$, for the linear behaviour of an arbitrary material in material oriented coordinate system 1-2 (see Figure 3) is the partial derivative of stress by strain and can be written as:

$$\hat{\mathbf{H}} = \begin{bmatrix} \frac{\partial \sigma_{11}}{\partial \varepsilon_{11}} & \frac{\partial \sigma_{11}}{\partial \varepsilon_{22}} & \frac{\partial \sigma_{11}}{\partial \varepsilon_{12}} \\ \frac{\partial \sigma_{22}}{\partial \varepsilon_{11}} & \frac{\partial \sigma_{22}}{\partial \varepsilon_{22}} & \frac{\partial \sigma_{22}}{\partial \varepsilon_{12}} \\ \frac{\partial \sigma_{12}}{\partial \varepsilon_{11}} & \frac{\partial \sigma_{12}}{\partial \varepsilon_{22}} & \frac{\partial \sigma_{12}}{\partial \varepsilon_{12}} \end{bmatrix}$$

This approach only holds true under the assumption of small strains.

The stress strain relationship in the x-y coordinate system, with material directions rotated a positive angle φ from the x-axis (see Figure 3), can be written as follows:

$$\bar{\boldsymbol{\sigma}} = \mathbf{T}^{-1} \cdot \hat{\mathbf{H}} \cdot \mathbf{T} \cdot \bar{\boldsymbol{\varepsilon}}$$

With **T** being the transformation matrix from element to material coordinate system:

$$\mathbf{T} = \begin{bmatrix} c^2 & s^2 & \sqrt{2}cs \\ s^2 & c^2 & -\sqrt{2}cs \\ -\sqrt{2}cs & \sqrt{2}cs & c^2 - s^2 \end{bmatrix}$$

$$c = \cos(\varphi); s = \sin(\varphi).$$

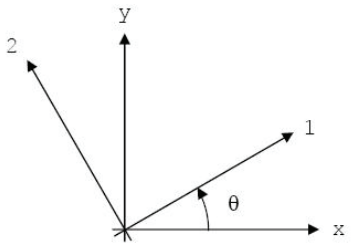

Figure 3: Element and material coordinate systems

A more detailed description of the structural method is given in [2] and [3].

4. ANISOTROPIC WRINKLING

A significant shortcoming of the basic membrane stress – strain formulation is its behaviour under compressive in-plane loads. “Real” sailcloth has a negligible bending stiffness and therefore negligible buckling strength, with compressive in-plane loads causing the cloth to wrinkle. Unfortunately, the basic membrane formulation has the same stress-strain gradient under compression as well as under tension.

This shortcoming is corrected by using a wrinkling model. Basic wrinkling models [4], [5] alter the stiffness matrix in case of wrinkling, yet until now this has only been described for isotropic materials and, in fact, doesn’t replicate the real behaviour of materials. Other wrinkling models [6], [7] modify the deformation vector under following observations:

- A wrinkled membrane is in a state of uniaxial tension.
- The wrinkles are aligned with this uniaxial tension.
- Material stresses are invariant to strain changes perpendicular to the wrinkles as long as the membrane is not coming under tension in this direction.
- In anisotropic materials principal stresses and strains are not aligned.
- If we assume the taut state as a starting point and reduce principle stress in direction two (σ_2), the basic membrane formulation holds up to - and including - the point where σ_2 is exactly zero but the material not yet wrinkled. From this point on material stress remains unchanged while element strain changes further (this assuming principle stress σ_1 being greater or equal than principle stress σ_2)

These observations lead to the mixed stress – strain wrinkling criterion

$$\sigma_2 > 0 \Rightarrow taut$$
$$\varepsilon_1 \le 0 \Rightarrow slack$$
$$\varepsilon_1 > 0 \; and \; \sigma_2 \le 0 \Rightarrow wrinkled$$

The last of above observations leads to the conclusion that it is possible to calculate the material stresses in the wrinkled state by calculating the material stresses in the state of *natural* uniaxial tension, respectively modifying the strains by the following:

$$\boldsymbol{\sigma}_m^{\varphi} = \mathbf{H}^{\varphi} \cdot \left(\boldsymbol{\varepsilon}^{\varphi} + \boldsymbol{\varepsilon}_w^{\varphi} \right)$$

with φ being the direction of uniaxial tension,

the material stress $\boldsymbol{\sigma}_m^{\varphi} = \begin{Bmatrix} \sigma_{m11}^{\varphi} \\ 0 \\ 0 \end{Bmatrix}$

and the wrinkling strain $\boldsymbol{\varepsilon}_w^{\varphi} = \begin{Bmatrix} 0 \\ \varepsilon_{w22}^{\varphi} \\ 0 \end{Bmatrix}$, where $\varepsilon_{w22}^{\varphi}$ is a measure for the amount of wrinkling.

Geometrically this modification can be described as shown in Figure 4:

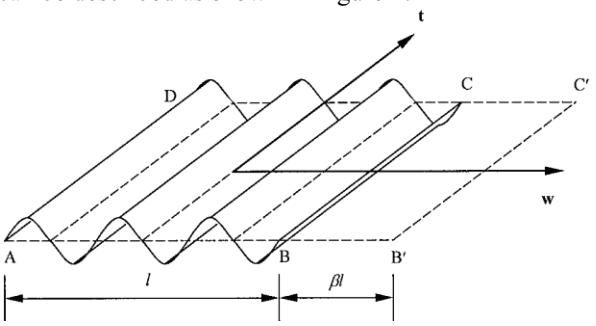

Figure 4: material under *natural* uniaxial tension (AB'C'D) and uniaxial tension (wrinkled, ABCD) [5]

ABCD are the corners of a wrinkled membrane element under uniaxial tension in direction **t**. Material stress in direction **w** is zero, yet strain in direction **w** is negative finite. If we extend the membrane direction **w** exactly up to the point where the wrinkles vanish but material stress is still zero (AB'C'D), we find the state of *natural* uniaxial tension. Up to this state material stress is invariant, yet from this state on the basic membrane formulation holds true.

In the state of *natural* uniaxial tension we can write:

$$\boldsymbol{\sigma}_m^{\varphi} = \mathbf{H}^{\varphi} \cdot \boldsymbol{\varepsilon}^{\varphi}$$

Defining $\boldsymbol{\sigma}_m^{\varphi} = \left\{ \sigma_{m11}^{\varphi}; 0; 0 \right\}^T$ we can rewrite:

$$\varepsilon_{22}^{\varphi} = \frac{H_{21}^{\varphi} H_{33}^{\varphi} - H_{23}^{\varphi} H_{31}^{\varphi}}{H_{23}^{\varphi} H_{32}^{\varphi} - H_{22}^{\varphi} H_{33}^{\varphi}} \cdot \varepsilon_{11}^{\varphi}$$

and

$$\varepsilon_{12}^{\varphi} = \frac{H_{22}^{\varphi} H_{31}^{\varphi} - H_{21}^{\varphi} H_{32}^{\varphi}}{H_{23}^{\varphi} H_{32}^{\varphi} - H_{22}^{\varphi} H_{33}^{\varphi}} \cdot \varepsilon_{11}^{\varphi}$$

Under the observations above we now can state that the formulation for $\varepsilon_{12}^{\varphi}$ holds true for general uniaxial tension, while $\varepsilon_{22}^{\varphi}$ is restricted to *natural* uniaxial tension.

Now we have two ways of calculating $\boldsymbol{\varepsilon}^{\varphi}$:

- transformation of $\boldsymbol{\varepsilon}$ into the coordinate system attached to φ using the transformation matrix $\mathbf{T}^{\varphi}$: $\breve{\boldsymbol{\varepsilon}}^{\varphi} = \mathbf{T}^{\varphi} \cdot \boldsymbol{\varepsilon}$
- $\hat{\boldsymbol{\varepsilon}}^{\varphi}$ for the conditions for *natural* uniaxial tension given above with $\hat{\varepsilon}_{11}^{\varphi} = \breve{\varepsilon}_{11}^{\varphi}$

Given the two methods to determine $\boldsymbol{\varepsilon}$, now we have to numerically find the angle φ where, under the condition of $\hat{\varepsilon}_{11}^{\varphi} = \breve{\varepsilon}_{11}^{\varphi}$, ε_{11} is positive definite, $\hat{\varepsilon}_{12}^{\varphi} = \breve{\varepsilon}_{12}^{\varphi}$ and $\hat{\varepsilon}_{22}^{\varphi} \geq \breve{\varepsilon}_{22}^{\varphi}$. $\varepsilon_{w22}^{\varphi}$ is given by $\varepsilon_{w22}^{\varphi} = \hat{\varepsilon}_{22}^{\varphi} - \breve{\varepsilon}_{22}^{\varphi}$ and is always positive finite. This is done by root-finding on the condition of $\hat{\varepsilon}_{12}^{\varphi} = \breve{\varepsilon}_{12}^{\varphi}$

5. Solver

The solver used so far for the structural part of FlexSail was based based on the minimization of total potential energy using a modified Newton approach [2]. However it was not able to treat the strong structural nonlinearities associated with wrinkling. Thus a new solver has been implemented.

Promising the necessary stability, a kinetically damped *Dynamic Relaxation* approach was chosen to solve the finite-element case [8]. In this approach separate equations for equilibrium and compatibility are used. The structure is described by a dampened vibrating system with virtual masses on the nodes and link forces to describe the elements. The solution then is based on a time strepping scheme.

Basically the motion of any node *i* at time *t* can be described by Newton's 2nd law of motion as

$$\dot{\mathbf{V}}_i^t = \frac{\mathbf{R}_i^t}{m_i}$$

with $\mathbf{R}_i^t$ being the vectorial sum of all forces (internal and external) acting on node *i* at time *t*.

In centred difference form this acceleration term can be approximated as:

$$\dot{\mathbf{V}}_i^t = \frac{\mathbf{V}_i^{t+\Delta t/2} - \mathbf{V}_i^{t+\Delta t/2}}{\Delta t} .$$

This yields the following term for nodal velocities at time $\left(t + \Delta t/2\right)$:

$$\mathbf{V}_i^{t+\Delta t/2} = \mathbf{V}_i^{t+\Delta t/2} + \Delta t \cdot \frac{\mathbf{R}_i^t}{m_i}$$

The updated geometry projected to time $\left(t + \Delta t\right)$ is therefore given by:

$$\mathbf{x}_i^{t+\Delta t} = \mathbf{x}_i^t + \Delta t \cdot \mathbf{V}_i^{t+\Delta t/2}$$

The virtual masses used above are calculated by

$$m_i = \frac{\Delta t^2}{2} \cdot S_i$$

with S_i being the largest direct stiffness that may occur during analysis.

To get the dynamic relaxation solver to converge some kind of damping method is necessary. Typically used is either viscous or kinetic damping. For FlexSail kinetic damping was chosen as it gives robust performance with little

computational overhead. In a kinetically damped system kinetic energy peaks of the whole vibrating system are detected and all nodal velocities set to zero before releasing the nodes again.

Due to the separation of equilibrium and compatibility giving a vectorial formulation of the problem, no global stiffness matrix has to be constructed, keeping computational overhead low. The vectorial formulation lends itself to parallelising using a SPMD paradigm on a multi-core machine. An initial, non-optimised, parallel implementation using OpenMP does not scale perfectly as yet but already gives a significant reduction in computational time.

6. IMPACT OF WRINKLING

Wrinkling has a dramatic impact on the shape of the sail. As shown in [9] for sails with little Gaussian deformation the amount of draft and its position is significantly changed. On sails with significant Gaussian deformation the impact is even more dramatic.

To show the effects flying shapes under constant pressure difference were calculated for a symmetric spinnaker with significant tack displacement and sheet length change. In Figure 5 the designed shape of the investigated spinnaker is shown. For discretization a triangular net of 7250 elements is used.

Figure 6 gives the flying shapes without and with wrinkling model.

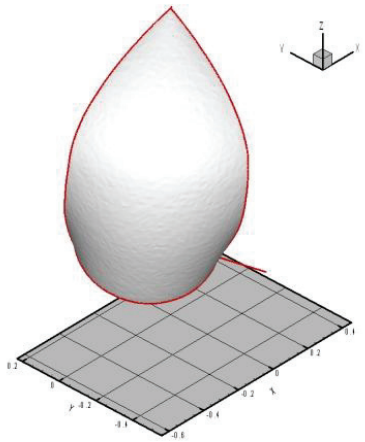

Figure 5: Mould of tested spinnaker (design shape)

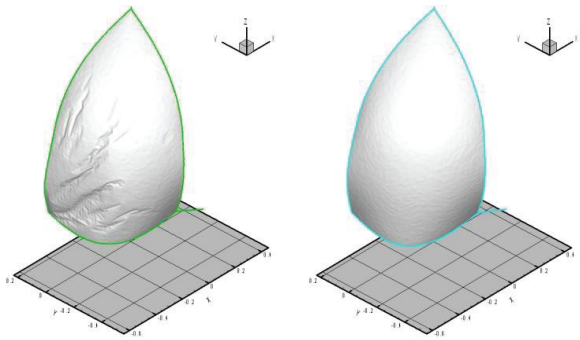

Figure 6: Flying shapes without (left) and with (right) wrinkling model

It can be seen that without accounting for wrinkling (Figure 6, left), significant folds radiate from the tack. Under strong Gaussian deformations the membrane without wrinkling model appears to behave like a thin sheet of plastic or metal under compression. Figure 6, right does not show this behaviour. Wrinkling is not visible as it occurs on a sub-element scale.

Figures 7 and 8 show principle stresses in direction 1 and 2. With wrinkling model the principal stresses 1 mostly radiate out from the corners and go up the side leeches, dissipating towards the centre of the sail. Principal stresses 2 are oriented perpendicular to them and equal or larger than zero. Without wrinkling model the principal stresses 1 are primarily oriented along the folds with significantly negative principal stresses 2 across the folds.

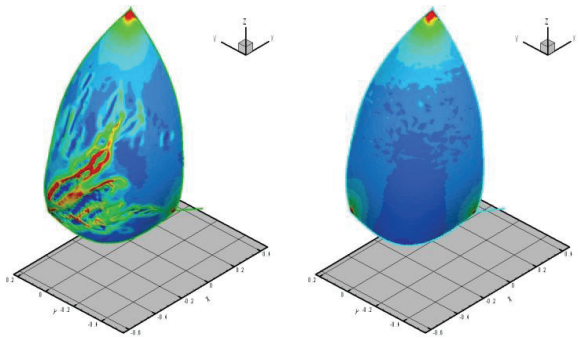

Figure 7: Principle stress 1 without and with wrinkling model

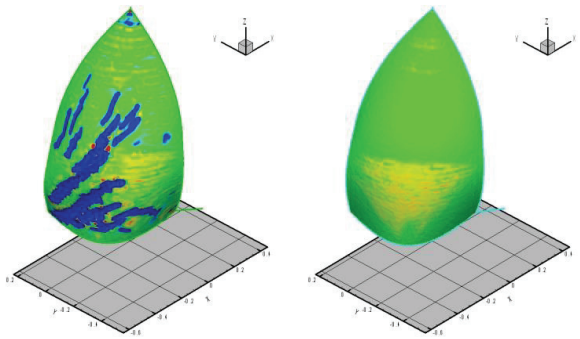

Figure 8: Principle stress 2 without and with wrinkling model

7. VALIDATION AND TESTCASES

For a simulation tool to be of meaningful use in a design environment it has to be validated against known quantities. For a FSI-program this validation can be broken down into three parts: flow, structural and interaction. Whilst data for the validation of the structural code can be calculated from first engineering principles, validation data for flow and FSI simulations has to be generated by experiments. In the following validation results for the flow simulation and the FSI simulation methods are given.

7.1 VALIDATION OF FLOW SIMULATION METHOD

In 1984 Stuart Wilkinson [10] published his PhD-Thesis about measurements of the flow around 2-dimensional setups of masts and mainsail sections at the University of Southampton wind tunnel. For these measurements a test objects consisting of a circular mast and a sail section conforming to the NACA a = 0.8 mean line was constructed and tested at various angles of attack and mast rotation (Figure 9).

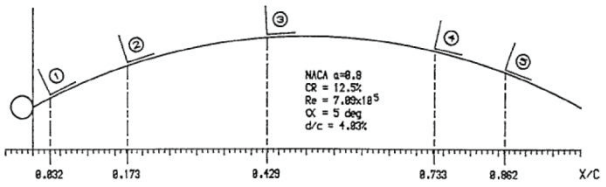

Figure 9: Two-dimensional setup for Wilkinson testcase with measurement locations

The pressure distribution along the sails section and the velocity profiles within the boundary layer at defined positions on the suction (leeward) side were measured.

In the chosen case the chord length was 0.7m, the ratio of mast diameter to chord length was 4.03%, the camber ratio 12.5%. The angle of the sails chord was 5 degrees to the boats centreline and 5 degrees to the incident flow. The test was conducted at a Reynolds number of 709000.

Qualitatively, Wilkinson described the flow around the mast-sail setup by 9 regions (see Figure 10).

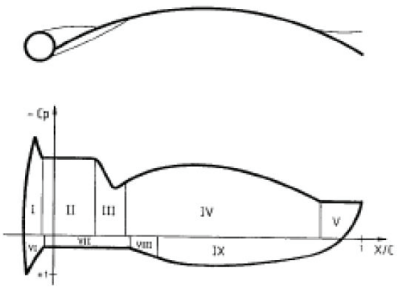

Figure 10: Wilkinson's regions of flow around mast and sail

He found three regions of separated (II, V and VII) and two regions of attached flow (IV and IX). Qualitatively the same regions can be found in the velocity contour from the CFD simulation shown in Figure 11: the separation areas behind the mast (II and VII) are clearly observable as is the area close to the trailing edge (V). On both sides the areas of attached flow (IV and IX) can be clearly seen as well. Of special interest (and a particular challenge) for the CFD simulations is the accurate prediction of the separation areas on the suction side (II and V).

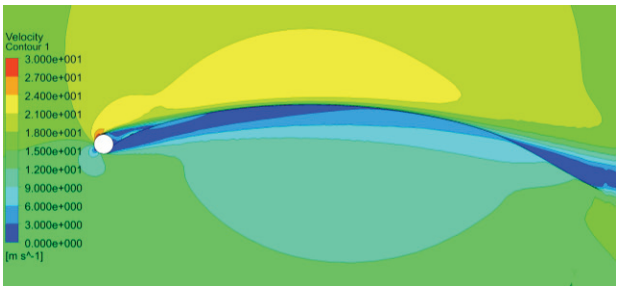

Figure 11: Velocity contours from CFD simulation

The CFD-simulations were conducted using the commercial RANSE-solver ANSYS CFX12.1®. The computational domain had the same height and length as the wind tunnel used for the measurements; it was discretised using fully three-dimensional tetraeder-prism grids to ensure full transferability of the results to sails. Various grid resolutions, turbulence models, time step lengths, incident turbulence levels and differencing schemes were tested.

Figure 12 shows a cut through a typical grid in the vicinity of the sail. As can be seen, the grid around the mast is highly refined. Typically around 15 prism layers are used to resolve the boundary layer, an effort was made to keep the precalculated y^+ value below 6, in the separation regions around and behind the mast to 1. Further, the development of cell volumes from the prism to the tetraeder layers was kept isotropic. These measures were deemed to be necessary to have the SST turbulence model working as intended and to prevent "jumps" in diffusivity form the prism to the tetraeder cells.

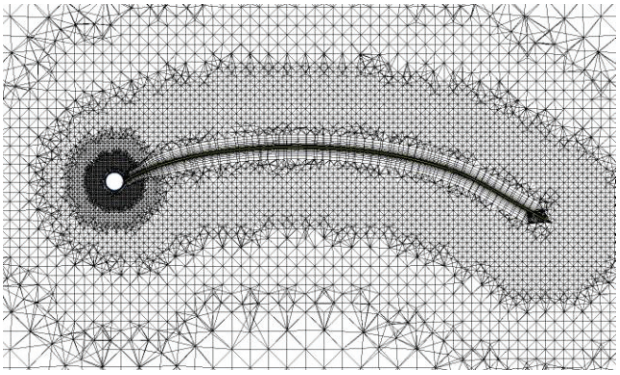
Figure 12: Grid around mast and sail

No force measurements are given by Wilkinson, however the quantitative data on pressure distribution on the sail and boundary layer velocity profiles allow a comparison to calculated results.

Comparing the pressure distributions given in Figure 13 generally a good agreement of measurement and simulation results can be observed. The largest deviations occur in the areas of separated flow behind the mast (II and VII) with

especially the suction peak on the leeward side being predicted too small. The trailing edge separation area (V) is predicted quite well, with the predicted pressure coefficient being just a little too small.

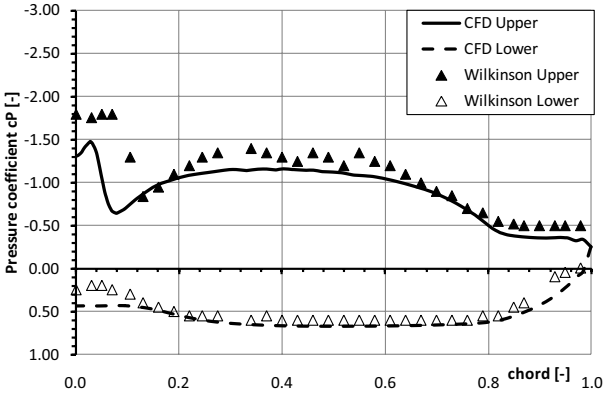

Figure 13: Pressure distributions on sail section from wind tunnel tests and RANSE simulation

The suction side boundary layer velocity profiles shown in figure 14 indicate the same discrepancies as the pressure distributions. A particularly good agreement between results in the area of attached flow is achieved, while significant deviation of results occurs at location 1, right behind the mast. At location 5 there is a small offset between measured and predicted flow velocity, yet the trend is captured quite good.

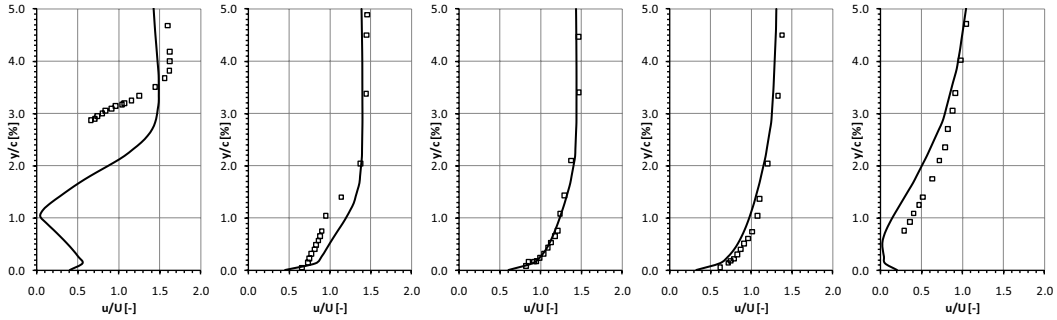

Figure 14: Velocity profile comparison in region with attached flow (location 1 to 5)

Flow separation is notoriously hard to predict correctly in flow simulations, while in experimental investigations it can be significantly influenced by factors such as onset flow turbulence, surface imperfections or even the measurement gear. Especially on quite bluff bodies, like a mast, the separation location may stabilise in different locations depending on the trigger, even after the trigger is removed.

Generally it can be said that the RANS-simulation with the described setup and grid parameters performed well in the prediction of the pressure distribution and flow separation of the flow around a mast – sail combination. All the important trends are well captured, yet the magnitude of the regions of separation is under predicted.

7.2 VALIDATION AND TESTING OF FSI SIMULATION METHOD

For the validation of the FSI simulation a symmetrical spinnaker was tested in the Yacht Research Unit Kiel's Twisted Flow Wind Tunnel (TFWT) [3]. This spinnaker's design was the result of a development for sailmakers *Holm Segel Schleswig/Germany.* The spinnaker design was developed as a generic mould based on a 40' cruiser/racer. During the tests it emerged to be beneficial to trade area for a more stable and controllable shape, maintaining more attached flow over a wider range of *AWA*s. Therefore the spinnaker has less than maximum surface area within the given design envelope. During wind tunnel tests the final design has proven to be quite stable and forgiving while having driving forces comparable to maximum sized spinnakers at significantly reduces sideforces. This was corroborated during testing this spinnaker at full scale.

The tested spinnaker had following dimensions:

SL = 1430 mm
SF = 808 mm
SMW = 820 mm

7.2(a) Wind tunnel testing and flying shape capturing

For validation purposes, the spinnaker was tested over an AWA-range of 90° to 180° at an AWS of 5 m s^{-1}. Trim settings were recorded during the tests for use in simulations. The resulting force areas are given in Figure 15, reproducibility of the results were confirmed during tests measurements using the recorded trim settings. For scaling and comparison purposes the forces are normalized by the dynamic pressure of the apparent wind ($P_{Dyn} = 1/2 \cdot \rho_{Air} \cdot AWS^2$), resulting in force areas. The trends of the measured forces appear to be quite peculiar with significant jumps between AWA = 120° and 127.5°. This appears to be caused by the flow being at least partially attached to the spinnaker at AWA ≤ 120° and fully separated at AWA ≥ 127.5°. At AWA = 120° the spinnaker trim for maximum driving force was quite unusual, especially compared to AWA = 112.5° & 127.5°. During the tests the spinnaker sheet lead was adjusted to prevent the sheet from being deflected by the main boom.

The general arrangement of the TFWT is shown in Figure 16.

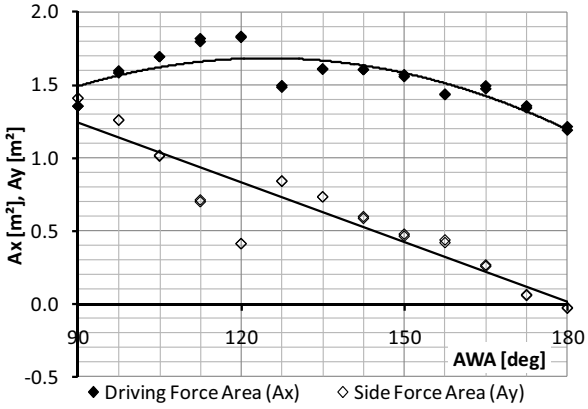

Figure 15: Driving and side force areas for spinnaker and main from TFWT-measurements

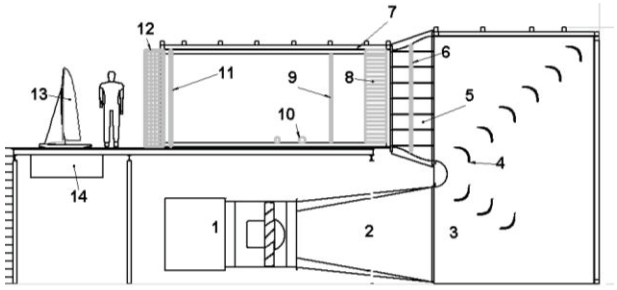

Figure 16: General arrangement of YRU-Kiel Twisted Flow Wind Tunnel

During the TFWT measurements the flying shape of main sail and spinnaker was recorded using photogrammetric techniques [11]. Figure 17 shows the relation between an exemplary picture used for the measurements and the resulting CAD model. The images were processed using *Photomodeller*®.

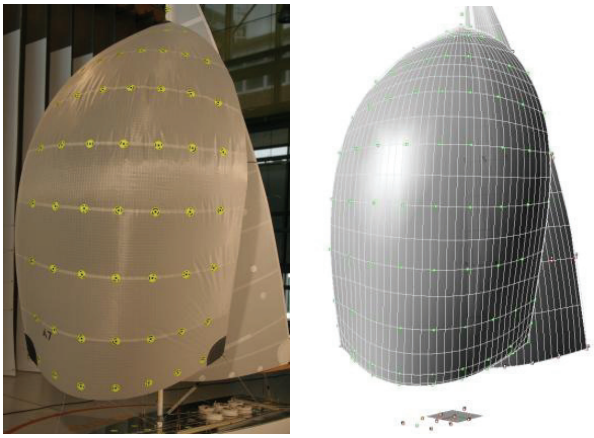

Figure 17: Exemplary photo from photogrammetric measurements and corresponding CAD model

7.2(b) Simulation using FlexSail

The flow around the main and spinnaker and the spinnakers structural behaviour were simulated using FlexSail. The simulations were carried out in model scale. For the simulations the main sail was assumed to be rigid with a flying shape as recorded during the wind tunnel tests, the spinnaker was trimmed according to the settings recorded during these measurements. To ensure comparability the incident flow was modelled based on measurements of the wind tunnel flow conditions. The structural properties of the spinnaker were the same as in the wind tunnel.

The discretisation mesh for the spinnaker consisted of 12479 triangular elements with local refinement near the three corners of the sail. Total control volumes in the domain numbered approx. $2.2*10^6$, this includes refinement by prism cells close to sails and hull to resolve the boundary layer as described in chapter 7.1. The same surface mesh is used for the structural computations and the flow simulation to prevent interpolation difficulties or errors. In all flow simulations the typical y^+ was between 1 and 4, the average Courant Number was around 30. Following the findings from the simulation of the Wilkinson case, the SST turbulence model was used with a free stream turbulence of 5%.

Figure 18 is a typical graphical result of the flow simulation part, showing streamlines and the chords used for pressure evaluation. Figure 19 gives a top view of the corresponding result of the structural part of the simulation. Figure 20 gives the driving and side forces resulting from the simulation, calculated the same way as above. The same peculiar jumps in driving and side force area as in the wind tunnel measurements can be observed.

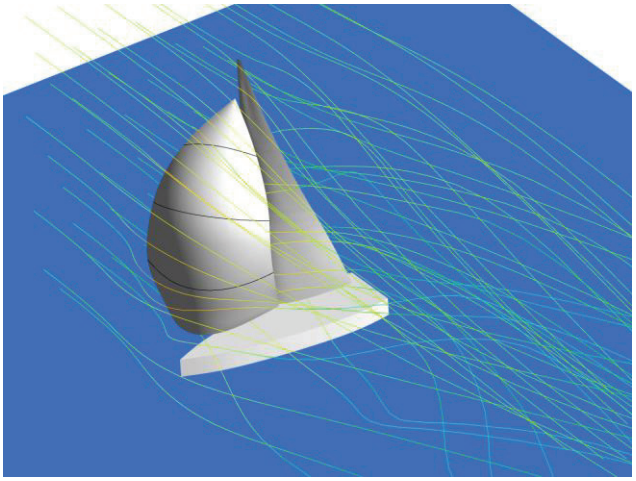

Figure 18: Streamlines from FlexSail simulation

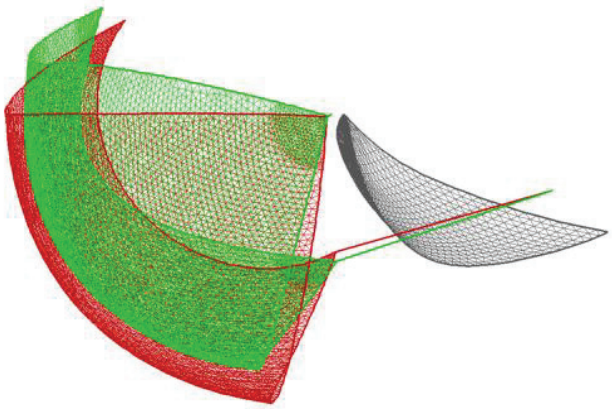

Figure 19: Initial (red) and deformed (green) spinnaker shape

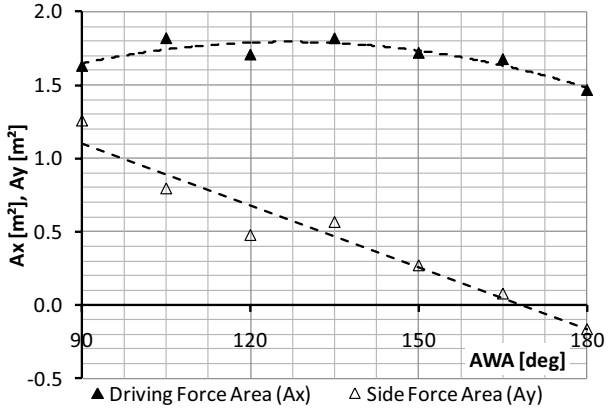

Figure 20: Driving and side force areas for spinnaker and main from FlexSail simulations

Figure 21 gives a typical pressure distribution along a girth line for both sides of the sail. While the pressure distribution on the suction (leeward) side is highly dependent on the actual flow conditions, it is always virtually the same on the pressure (windward) side. Figure 22 exemplarily gives the suction side pressure distributions on girths at different heights and AWAs. The pressure profiles indicate either leading edge separation with following reattachment and trailing edge stall (AWA 90° & 120°) or fully separated flow (AWA 150°). Comparison with measured pressure distributions on an asymmetric spinnaker, given by Viola [12], shows good qualitative agreement.

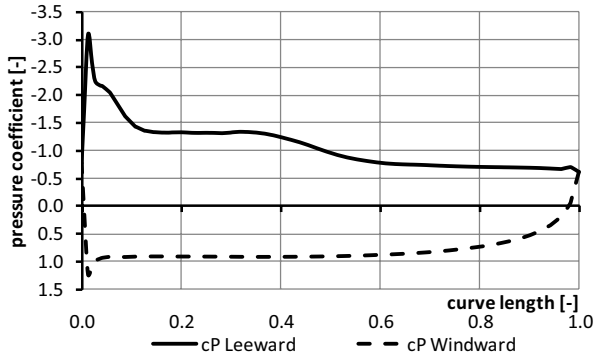

Figure 21: Typical pressure distribution on both sides of spinnaker with partially detached flow

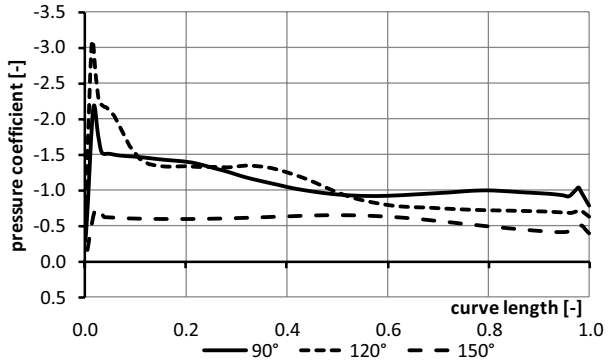

Figure 22: Pressure distributions along sail girth on ½ mitre height at different AWAs

7.2(c) Comparison of results

To validate the FSI simulation, flying shapes as well as forces have to be compared. Figure 23 gives a superposition of the measured and calculated flying shapes at AWAs 90° and 150°. As can be seen, the flying shapes agree well with respect to luff and leech positions and profile shapes. Table 1 gives the maximum deviations of luff, leech and clew positions as percentage of leech length. Obviously the largest deviations appear at the leech as this has the most freedom to move. The largest deviations per trim occur at AWAs 120° and 180°. As stated above, the trim at AWA 120° was quite peculiar, while at 180° the sail was a little unstable in the wind tunnel as well as during simulations.

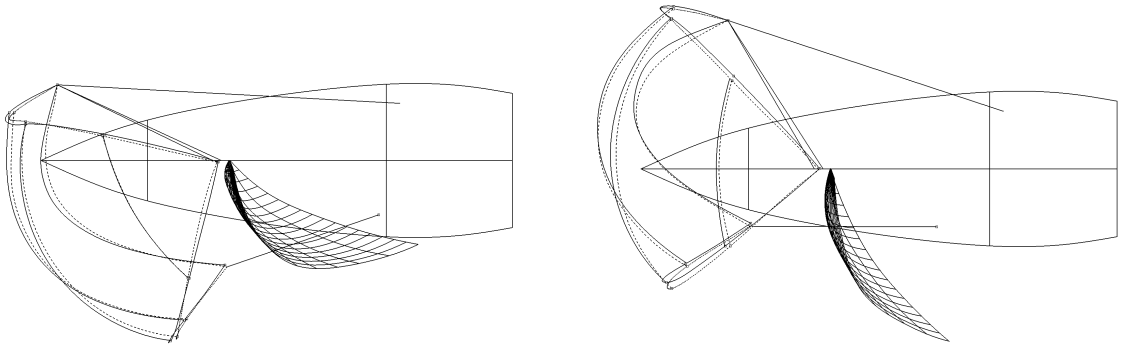

Figure 23: Comparison of flying shapes from wind tunnel (dashed) and FSI simulation (continuous) at AWA 90° (left) and 150° (right)

AWA	Luff	Leech	Clew
90°	0.90%	1.63%	0.49%
105°	1.39%	2.13%	0.58%
120°	1.57%	2.41%	2.40%
135°	2.17%	1.66%	1.58%
150°	1.15%	1.86%	0.83%
165°	1.11%	2.34%	1.53%
180°	1.95%	4.52%	2.20%
Avg.	1.46%	2.36%	1.37%

Table 1: Maximum deviation between measured and calculated leech and clew positions in percent of leech length

Figure 24 gives the resulting force areas from wind tunnel tests and FlexSail simulations in comparison. As can be seen the simulations correctly replicate the trends found by the wind tunnel measurements, yet driving as well as side force areas have almost constant offsets. It is as yet unclear whether this is due shortcomings in the wind tunnel measurements or flow simulations. A possible reason might be the omission of the mast in the simulations to improve meshing facility. According to Paton et al. [13], this can lead to a significant increase of lift and reduction of drag of the attached sail. Further investigations will be necessary to clarify this.

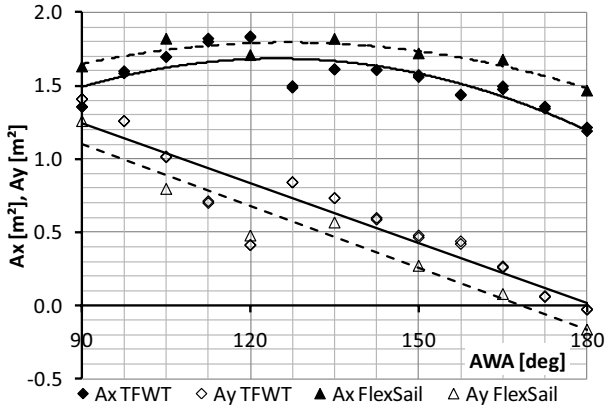

Figure 24: Driving and side forces from wind tunnel measurements and FlexSail simulations

8. CONCLUSIONS

In this paper an FSI solution for the simulation of spinnakers, based on ANSYS-CFX and a proprietary Finite Element code, is described. The capabilities of this program are shown, the necessity to use a RANS based flow solver is shown based on the Wilkinson validation case. The chosen gridding parameters and flow simulation setup have been shown to be well suited to the simulation of the partially detached flow occurring around sails.

The capabilities of the entire FSI method have been validated by comparison to a bespoke test case, based on measurements at the YRU-Kiel wind tunnel. Whilst the absolute forces are a bit off, the trends are accurately replicated. The flying shape is calculated quite accurately over the whole tested range of AWAs. Generally it can be said that the method presented is able to provide the sail designer with the information necessary to optimise the sail's design and construction.

9. REFERENCES

1. GRAF, K., BÖHM, C., RENZSCH, H., 'CFD- and VPP-Challenges in the Design of the New AC90 Americas Cup Yacht', *Proceedings 19th Chesapeake Sailing Yacht Symposium*, 2009

2. GRAF, K., RENZSCH, H., 'RANSE Investigations of Downwind Sails and Integration into Sailing Yacht Design Processes', *Proceedings 2nd High Performance Yacht Design Conference*, 2006

3. RENZSCH, H., MÜLLER, O., GRAF, K., 'FlexSail – A Fluid Structure Interaction Program for the Investigation of Spinnakers', *Proceedings International Conference on Innovation in High Performance Sailing Yachts*, 2008

4. MILLER, R. K., HEDGEPETH, J. M., 'An Algorithm for Finite Element Analysis of Partially Wrinkled Membranes', *AIAA Technical Note 82-4293*, 1982

5. ADLER, A. L., MIKULAS, M. M., HEDGEPETH, J. M., 'Static and Dynamic Analysis of Partially Wrinkled Membrane Structures', *AIAA-2000-1810*, 2000

6. KANG, S., IM, S., 'Finite Element Analysis of Wrinkling Membranes', *Journal of Applied Mechanics, Vol. 64*, 1997

7. LU, K., ACCORSI, M., LEONARD, J., 'Finite Element Analysis of Membrane Wrinkling', *International Journal for Numerical Methods in Engineering, 50*, 2001

8. BARNES, M. R., 'Form Finding and Analysis of Tension Structures by Dynamic Relaxation', *International Journal of Space Structures Vol. 14 No. 2*, 1999

9. HEPPEL, P., 'Accuracy in Sail Simulation: Wrinkling and growing fast sails', *Proceedings High Performance Yacht Design Conference*, 2002

10. WILKINSON, S., 'Partially Separated Flow Around Masts and Sails', *PhD-Thesis, University of Southampton*, 1984

11. GRAF, K., MÜLLER, O., 'Photogrammetric Investigation of the Flying Shape of Spinnakers in a Twisted Flow Wind Tunnel', *Proceedings 19th Chesapeake Sailing Yacht Symposium*, 2009

12. VIOLA, I. M., FLAY, R. G. J., 'Pressure Distributions on Modern Asymmetric Spinnakers', *Trans RINA, Vol. 151, Part B1*, 2009

13. PATON, J., MORVAN, H.P., HEPPEL, P., 'Fluid Structure Interaction of Yacht Sails', *Proceedings International Conference on Innovation in High Performance Sailing Yachts*, 2008

A simplified slamming analysis model for curved composite panels

Dr. Frederic Louarn (*)
Dr. Paolo Manganelli (**)

ABSTRACT

Hydrodynamic impact loads induced by motions in a seaway or due to waves breaking on the topsides are a critical and complex problem in the structural design of optimised racing yachts.

The traditional design approach consists of using a uniform pressure distribution over any given hull panel to simulate slamming loads in as far as it gives similar peak core shear stresses (critical for sandwich structures) and / or skin compressive stresses. Empirically derived pressure heads are often based on classification society guidelines. Curvature effects are only partially considered on the panel response, or, totally ignored as far as they affect the load itself.

At the other end of the spectrum, hydroelastic models have been developed attempting to address the interaction between fluid forces and the dynamic response of hull panels, in the time domain. To date, implementing such a complex approach tends to be impractical in a design situation.

A simplified in-house slamming model is presented relying on a 2 dimensional potential flow model to derive slamming pressures at different panel positions corresponding to as many time steps in the slam history. Finite Element Analysis (FEA) is used in order to study panel responses (deformation, stresses, “snap through” buckling) to the calculated pressure distributions.

The simplified model is intended to provide a practical design tool whilst accounting for the main parameters of the slamming problem, in particular, hull curvature effects.

Comparisons with the results obtained from the traditional constant pressure analysis and from a more detailed hydroelastic model are discussed in the paper.

(*) SP-High Modulus, the marine business of Gurit, frederic.louarn@gurit.com
(**) SP-High Modulus, the marine business of Gurit, paolo.manganelli@gurit.com

1. INTRODUCTION

It is common engineering practice to base the hull shell analysis for race boats on first principle panel calculations or on classification society guidelines such as, for example, the 1994 ABS Guide for Building and Classing Offshore Racing Yachts (including Notice 1).

Traditionally, such approaches rely on the analysis of a given panel subject to some design uniform pressure distribution with only limited account for the effect of panel curvature. For instance the pressure reduction factor “c”, in the ABS guide, only affects skin bending strength but not core shear which tends to be the critical failure mode for sandwich structures.

The objective of the work discussed in this paper is to investigate panel curvature effects further, particularly with regards to through thickness core shear in hull shell sandwich structures exposed to slamming loads.

A simplified slamming model is presented, aimed at providing a cost effective design and analysis tool for this complex problem. Methodologies are described for this model as well as for a more advanced hydroelastic analysis.

Comparative results obtained for a typical mono-hull bow section are discussed, highlighting the significance of curvature effects not only on panel response but also on hydrodynamic loads, as well as the implications of dynamic aspects.

2. SIMPLIFIED SLAMMING ANALYSIS

2.1 General Approach

Consideration of realistic slamming pressure loads acting on a curved shell involves two basic steps, namely, the calculation of slamming pressure distributions for the given panel geometry, e.g. curvature and width, and the analysis of the panel response to such load. The following assumptions have been made to simplify the problem:

1 the panel is considered to respond in a quasi-static fashion to the slamming load, that is, the amplitude of the response at any given instant is related only to the instantaneous loading and in no way to the previous condition of the panel
2 coupling effects between hydrodynamic loads and panel deformations are neglected, hence the model is not time dependent;
3 the slamming pressure field is two-dimensional so that it can be derived from a simple polynomial function considering a single reference section of the chosen panel.

The structural analysis of the panel is carried out with a standard FEA package.

Input of an impact velocity is required, corresponding to the normal component of fluid velocity, at the assumed point of impact. The panel is assumed to behave rigidly. Where the method is used to optimize shell laminates, the validity of this input is critical since, as shown in equation 1, pressure is a quadratic function of velocity. For comparison between various section shapes, the actual value of impact velocity becomes less important.

To date, the better way of estimating impact velocity is to derive it from onboard measurement of rigid body motions. Broadly speaking, it is possible to extrapolate wave data (frequency and amplitude) and derive impact velocity distributions from the measurement of the motion of the boat in its six degrees of freedom. In the past, Gurit has been able to obtain useful data of this type from measurement campaigns carried out on IMOCA 60’s (e.g. “Hugo Boss”) or maxi yachts (e.g. “Wild Oats XI”).

From the known or estimated impact velocity, slamming pressure distributions can be calculated for incremental wetted chords. These correspond to time steps along the slam history but, since the

simplified method is quasi-static, .i.e. not directly time dependent, they have to be chosen somewhat arbitrarily considering panel geometry.

Finite Element Analysis of the curved panel subjected to the slamming pressure distributions obtained above is carried out. The objectives are twofold, namely to assess curvature effects for a more realistic pressure distribution and, also, to check the panel for possible “snap-through” behaviour.

Snap-through is a non linear response whereby a curved panel undergoes local inversion of curvature from convex to concave. Core shear stresses induced in the vicinity of this inversion can exceed those that would be observed in a flat panel. Results published by Hildebrand (ref 1) suggest that this type of non linear responses is generally exhibited by slightly curved panels (e.g. for a panel camber less than 0.05). As shown in figure 1, the effective camber in way of the loaded section of the panel can be much reduced for a concentrated slamming pressure distribution (non circular section) compared to the camber measured across the whole panel chord.

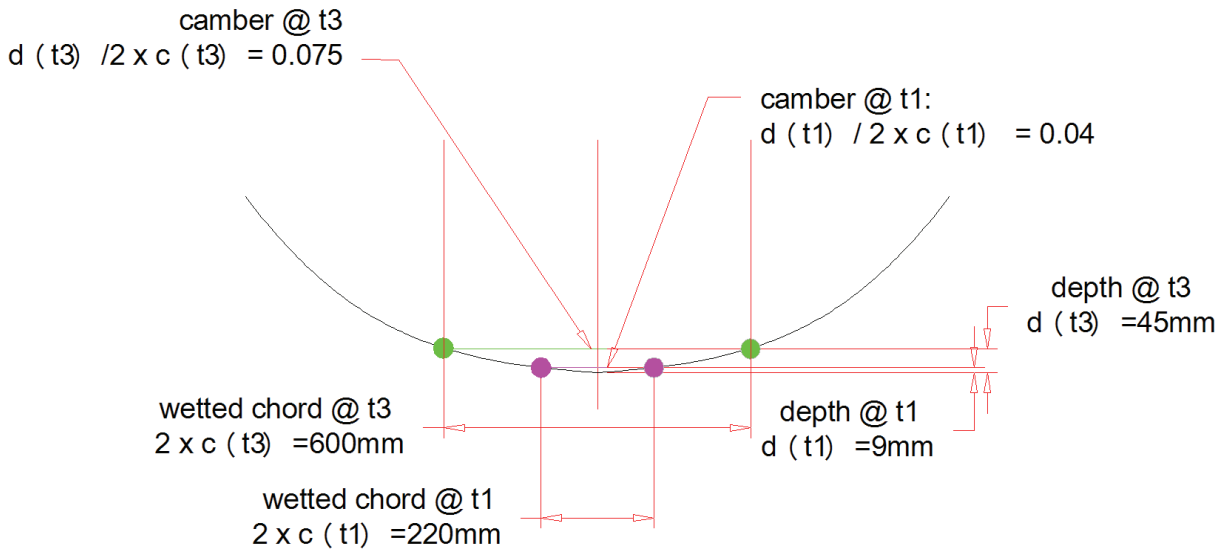

Figure 1: **Effective Panel Camber on Hull Bottom Panel for half wetted chords c(t1) and c(t3)**

2.2 Slamming Pressure Calculation

The evaluation of slamming pressure distributions relies on a Wagner type potential flow method discussed in reference 2 which, provided pressure peaks are “clipped” at the acoustic pressure, P_{ac} as defined in equation 2, has been shown to produce very good results for impact loads on curved sections,.

The pressure distribution function is of the following form:

$$P(y,t) = \frac{\rho U^2 c(t)}{\sqrt{(c(t)^2 - y^2)} \times \left(\frac{2}{\pi} p_1 + p_2 c(t) + \frac{4}{\pi} p_3 c(t)^2 + \frac{3}{2} p_4 c(t)^3 \right)} \qquad \textbf{eqn.1}$$

$$P(y,t)_{\max} = P_{ac} = \rho \times c_e \times U \qquad \textbf{eqn.2}$$

where:

- $\rho = 1025 kg/m^3$ is the salt water density
- U is the water impact velocity
- $c(t)$ is the “wetted chord” at time t, e.g. the instantaneous wetted panel breadth

- y is the transverse coordinate
- p_i is the ith coefficient of a polynomial fit to the hull section,
- P_{ac} is the acoustic pressure
- C_e is the speed of sound in water (C_e = 1400 m/s)

Note that the pressure distribution is assumed to be cylindrical (independent from global coordinate x) and symmetric about the panel centre-line.

Figure 2 shows the results of the regression analysis performed on the reference section: p_0 =0, p_1 =-0.0626, p_2 =0.389, p_3 =-0.5962, p_4 =0.6423. A fourth order polynomial appears to provide a good fit to the section shape.

Figure 3 presents plots of slamming pressure distribution at chosen half wetted chords C(t1), C(t2), C(t3) and C(t4), across the reference panel and for an impact velocity of 3.0 m/s.

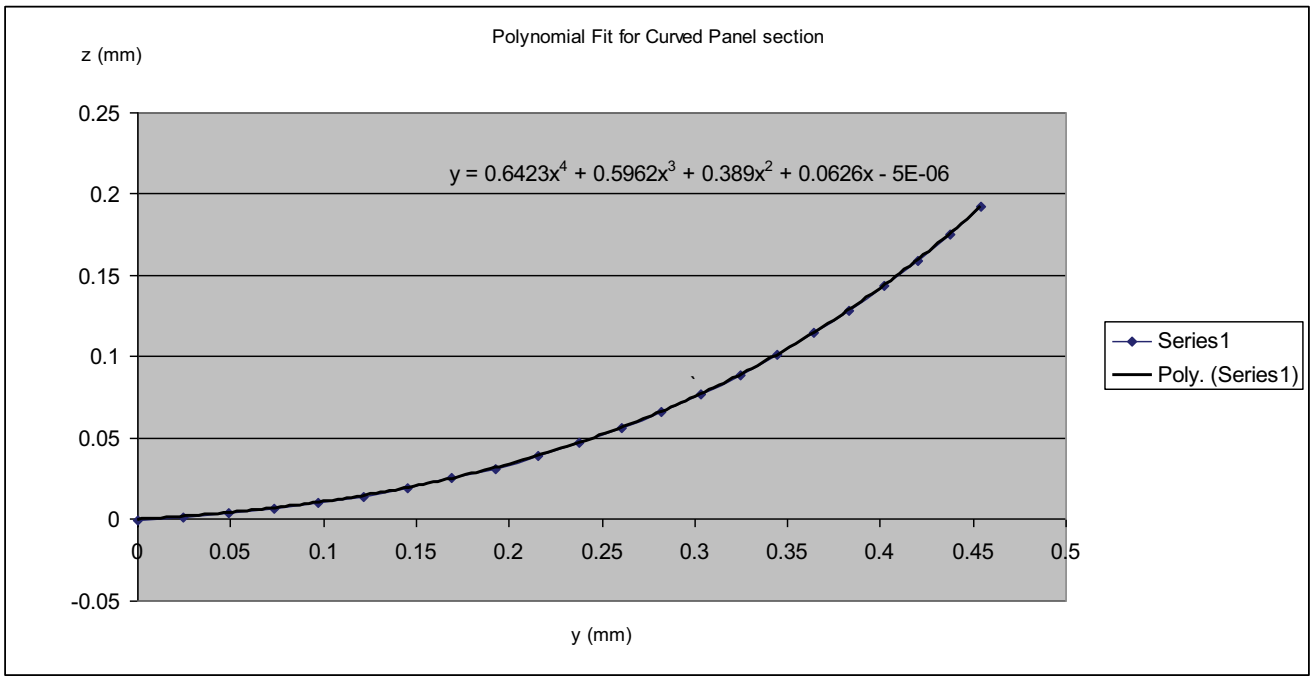

Figure 2: Regression Analysis for Reference Section – Polynomial Coefficients

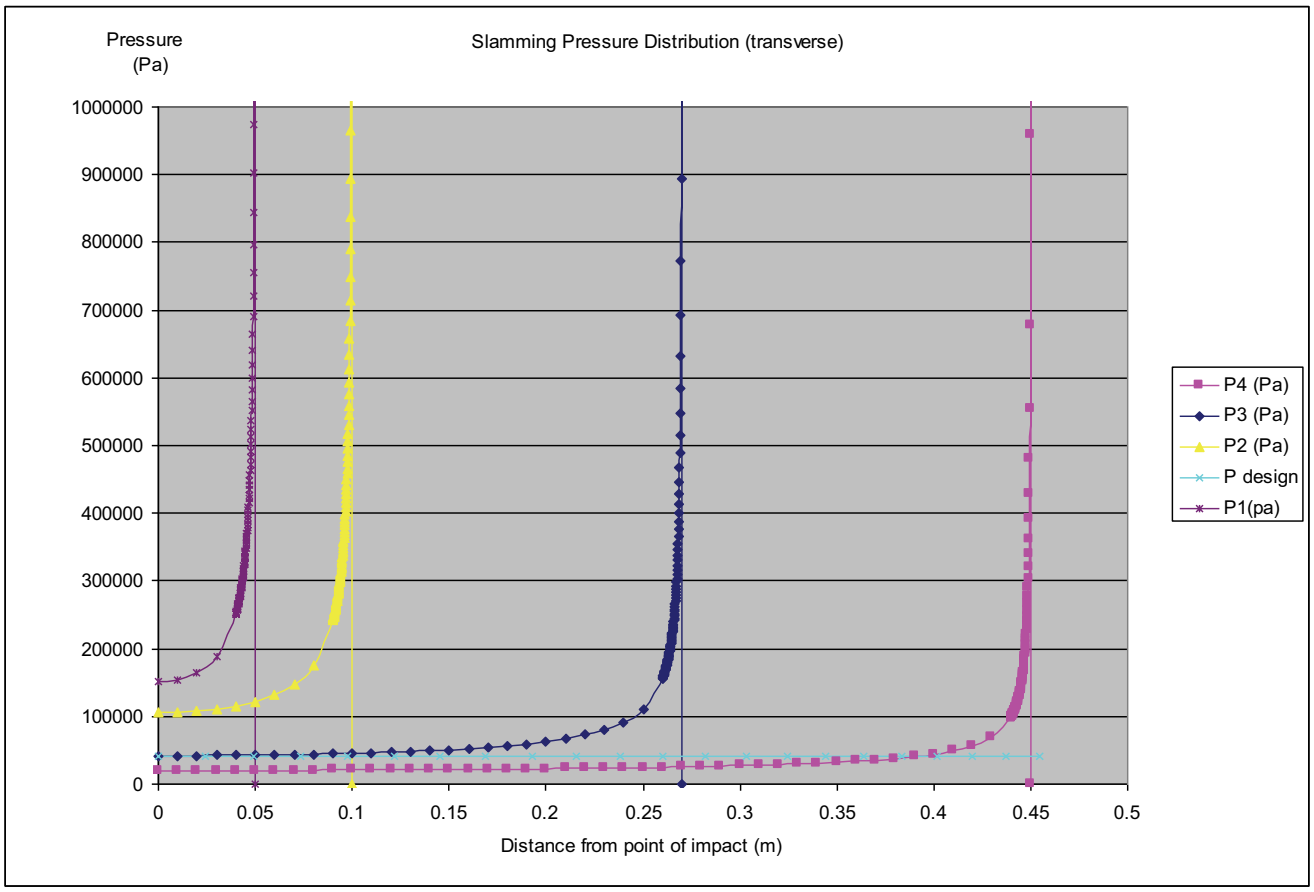

Figure 3: Slamming Pressure Distributions at c(t1), c(t2), c(t3) and c(t4) (symmetric about centreline)

Note: pressure peaks clipped at Pac = 4305000 Pa, not shown for clarity

2.3 Finite Element Analysis

Linear and non linear static analyses can be performed in order to assess the direction and magnitude of core shear and skin bending stresses or strains resulting from the various slamming pressure distributions.

Hildebrand (ref 1) suggests that non linear effects only develop for a panel deflection to skin thickness ratio larger than 2.

Convergence of the non linear analysis also indicates whether snap-through instability is likely to be the critical mode of failure.

FE models are, in this work, based on linear shell elements although there is no restriction in this respect. Typical model boundary conditions and element edge length are shown in Figure 4. In this case, the model extent has been restricted to an isolated panel and edge restraints have been chosen for consistency with boundary conditions assumed within the ABS guide, e.g. full fixity. Note that assuming Uy=0 along the long edges implies that displacements are restrained by the surrounding shell in the tangential direction.

Sufficient mesh refinement is required in order to capture the features of slamming pressure distributions, e.g. sharp pressure peaks as shown in Figure 3. Even so, the calculated pressure field may not be directly transposable into the FEM and may need to be modified according to element size. This is to ensure that the load applied over an element matches the integral of the theoretical pressure field over the same elemental area. Figure 5 illustrates the pressure load applied to the finite element model at half wetted chord c(t2).

Shell laminates considered are typical racing yacht sandwich high strength carbon laminates.

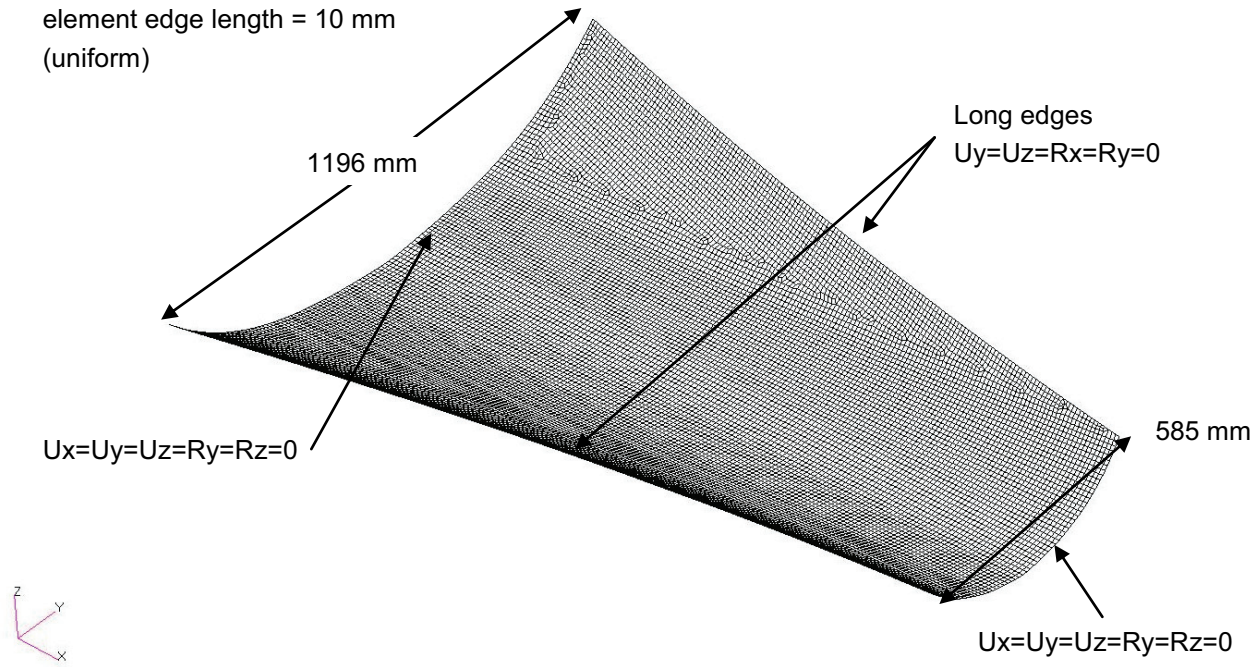

Figure 4: View of Typical Finite Element Mesh and Boundary Conditions

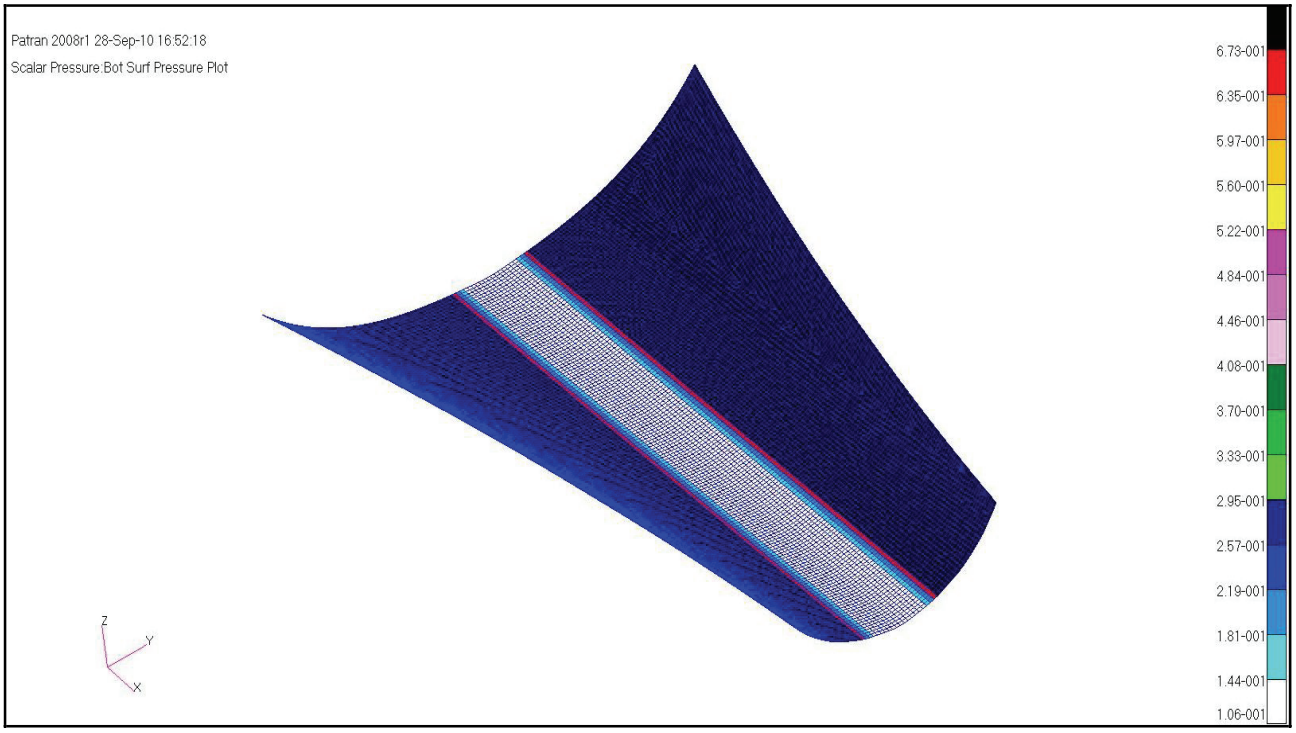

Figure 5: FE pressure field at wetted chord c(t2)

3. HYDROELASTIC MODEL

3.1 Model Description

The hydro-elastic response of a hull panel subject to slamming is the result of the combination of the following phenomena:

1. the panel is subject to a transient hydrodynamic impulsive loading
2. the panel responds to the transient load in a dynamic fashion: it is effectively set into vibration by the impulsive loading, the instantaneous magnitude of the response is not directly proportional to the magnitude of the instantaneous excitation, and the maximum response can typically lag or precede the peak of the loading impulse
3. as the panel responds to the hydrodynamic pressure by deflecting (and vibrating), the velocity of its surface relative to the water changes, which affects the instantaneous loading, which, in turn, influences the subsequent mechanical response. In other words, the structural response and the hydrodynamic loading are coupled.

In order to account for all the physical parameters involved in the response of panels subject to slamming, a full hydro-elastic model has been developed and implemented by the authors through the recent years (ref.2). This remains a linear model, yet it is believed to provide accurate predictions in most cases and has undergone substantial validation as discussed in ref. 2.

Since the evolution of the hydrodynamic slamming pressure and of the hull panel response are mutually dependent, the method simulates both within a single coupled model. The inputs to the model are the initial impact velocity (as described in section 2.1), the panel three-dimensional geometry and the weight and stiffness of the laminates. The result is a full time history of pressures, panel deflections and internal forces.

The actual method is outlined in Figure 6. In the terms of the inputs, the velocity of the panel relative to the free surface is derived typically from full-scale measurements or from sea-keeping models. The surface of the panel is discretised into a large number of transverse strips with constant cross-section, each described by a polynomial equation as shown in section 2.2.

The simulation of the dynamic structural response is based on a modal approach, therefore normal mode shapes, natural frequencies and generalised stresses across the panel are required as an input to the time-stepping routine. For the present study, they have been calculated through the same finite element model that has been described in section 2.3, with all of the same boundary conditions and element properties.

The initial time in the simulation corresponds to the instant when the panel first touches the water. At each subsequent time step, the instantaneous vertical velocity of the panel (the "effective impact velocity") is obtained by adding the initial impact velocity ("U" as described in section 2.2) to the vertical velocity component associated with the dynamic response of the panel. The wetted chord (2 x c(t)) and the pressure distribution across each strip are then calculated on the basis of the instantaneous effective velocity and of the strip geometry using the same "Wagner-type" approach outlined in section 2.2. For example, Figure 7 shows the instantaneous wetted chords along the length of the panel for different times and Figure 8 represents the three-dimensional pressure distribution corresponding to 't=6ms'. Both of these graphs demonstrate how the variation of the section shape can affect the size of the wetted chord and magnitude of the slamming pressures.

Generalised forces for each time step are derived by projecting the instantaneous pressure distributions in modal space. The modal response at the following time step is obtained through step-by-step integration (ref.4). The actual panel deflection and velocities are then calculated by converting back from modal to physical coordinates. Similarly, stresses across the panel can be evaluated at each time step through multiplying the generalised stresses by their corresponding modal coordinate and then adding them all up.

The velocity component associated with the vibratory response of the panel is finally added to the rigid-body impact velocity to obtain the 'effective impact velocity' for the subsequent time step.

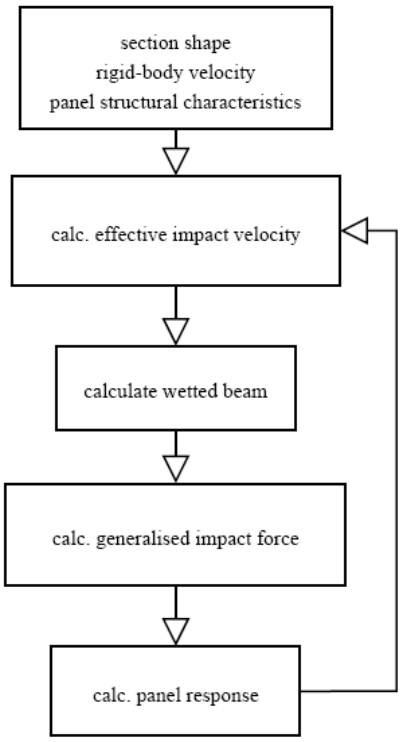

Figure 6 – Flow-chart of the numerical hydro-elastic model.

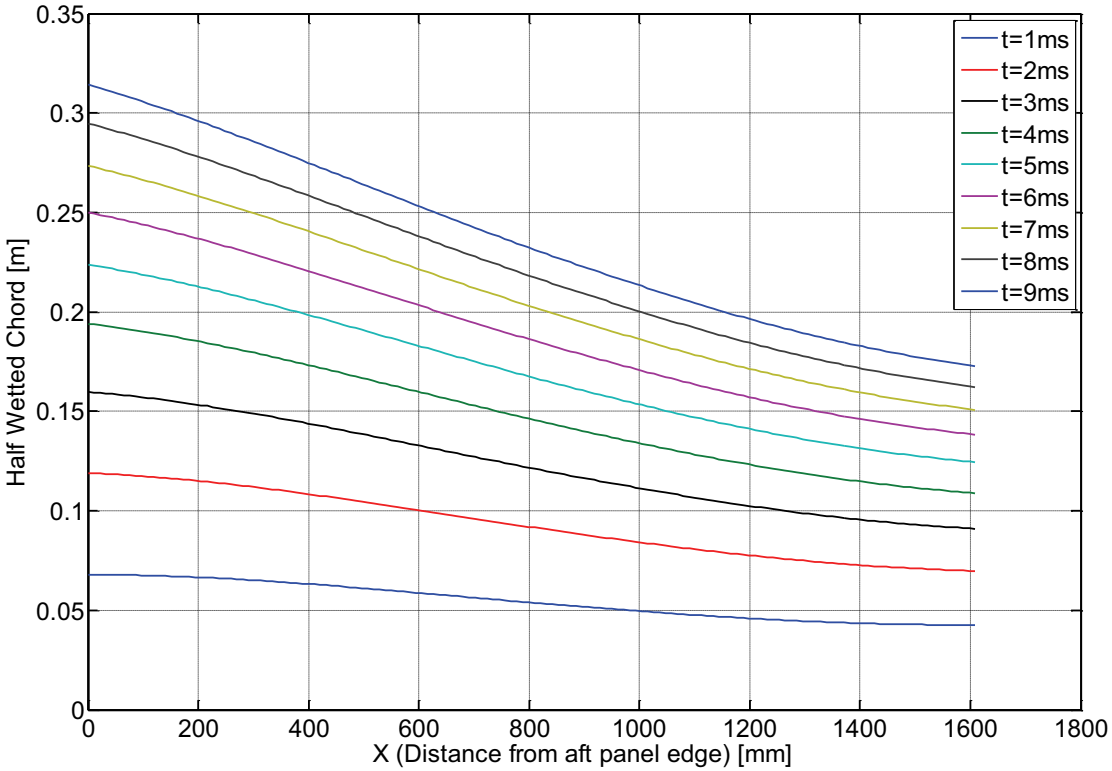

Figure 7: Half-wetted chords at 1ms time intervals

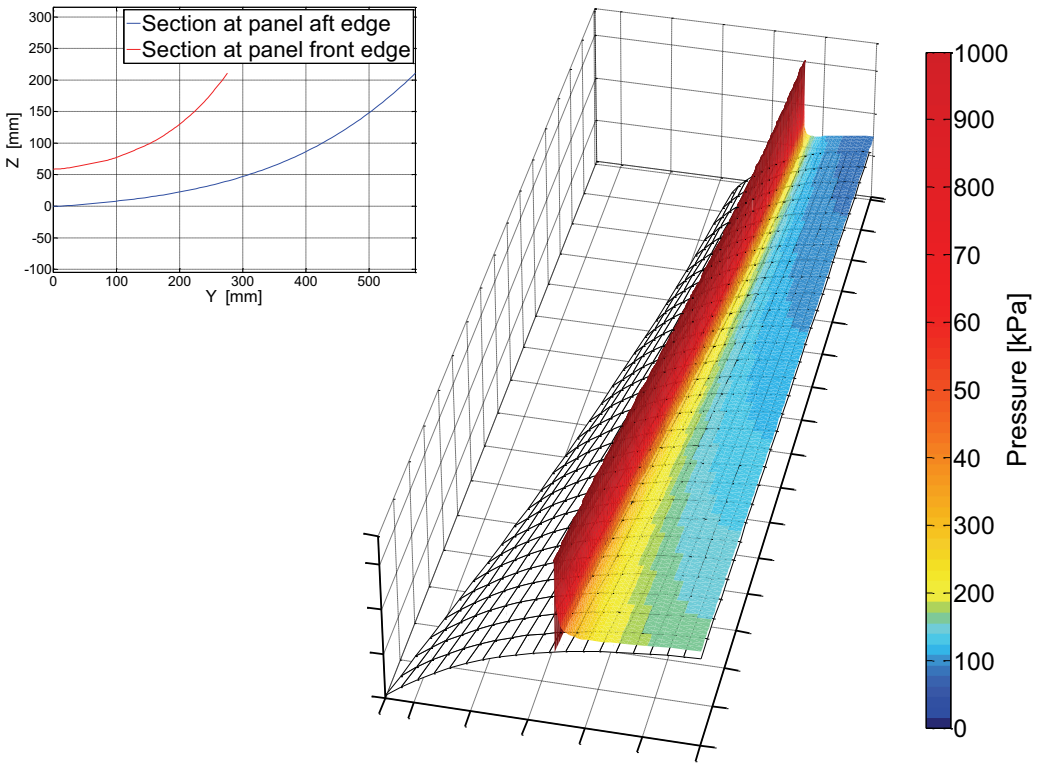

Figure 8: '3d' Pressure Distribution over half hull panel (U=3m/s, t=6ms)
Note: pressures have been 'clipped' at 1MPa for clarity; pressure distribution is assumed to symmetric about centre line.

4. RESULTS AND DISCUSSION

4.1 Simplified Slamming Model vs. ABS Guide

Main results forming the basis for ensuing discussions are summarised in Table 1.

Case	Analysis Type	Pressure	wmax (mm)	ε_{min} (%) Skin strain	ε_{max} (%) Skin strain	τ_{yz} (MPa) Long edge Core shear stress	τ_{zx} (MPa) Short edge Core shear stress
1 ABS	Linear static FEA	0.0414 MPa Uniform (see note 1)	3.17 (hog)	-0.077	+0.077	0.565	0.35
2 uniform	Linear static FEA	0.0414 MPa Uniform (see note 1)	0.41	-0.033	0.003	0.047	0.15
3 FEA slamming	Linear static FEA	Slamming @ t2 c(t2)=0.1 m U=3.0 m/s	1.85	-0.009	0.004	0.414	0.59
4 FEA slamming	Non Linear static FEA	Slamming @ t2 c(t2)=0.1 m U=3.0 m/s	1.93	-0.01	0.004	0.426	0.59

Table 1: Summary of skin bending stains and core shear stresses for ABS calculations and simplified slamming model

Notes:

1- Ultimate uniform design pressure does not include pressure reduction factor ("c, k") related to panel curvature and aspect ratio respectively and pertaining to the strip beam analysis method.

Case 1 corresponds to the analysis of an idealised flat rectangular panel against ABS requirements. The panel is assumed to be flat, rectangular and fully fixed around its perimeter. Therefore, according to classical theory of plates and shells, the location of peak skin bending strains and core shear stresses coincides with the middle of the long edge. In this case, the panel is 1.6m long by 0.89m wide, considering the average chord, so the short span is transverse, giving the critical direction of the bending and shear loads.

In **Case 2**, the ABS pressure has been applied uniformly to the finite element model of the panel which accounts for the true panel plan-form geometry and for its curvature.

It can be observed that core shear stress in the transverse direction, τ_{yz}, is an order of magnitude lower than in case 1. This is due to the well known "arch effect" which is effective in the plane of curvature of the panel and whereby some of the applied transverse pressure load is carried in membrane rather than shear and bending. Comparison of minimum and maximum principal strains also shows how compressive membrane effects in the transverse direction reduce the bending response of the panel. The average strain of - 0.015% corresponds to the compressive membrane strain whose magnitude is about half of the minimum principal strain. Hence, in this case, membrane and bending strains have similar magnitude.

It should be noted that membrane response is promoted by tangential restraints along the long edges (see section 2.3). The chosen boundary conditions may be somewhat optimistic in this respect but they reflect the fact that surrounding shell would indeed provide some degree of tangential restraint. Modelling of edge restraints could be improved by inclusion of the shell surrounding the loaded panel within the FE model.

The peak core shear stress in the longitudinal direction is reduced by 57% compared to **Case 1** Curvature in this direction is insignificant so this reduction is mostly due to a change in load distribution along the short edges. As can be seen from Figure 9 and Figure 11 the panel deflection has a complex double concave shape which results in more spread of the load along the short edges, hence the reduction in peak τ_{zx}, compared to a flat panel as in Case 1. This behaviour was not depicted by Hildebrand for semi circular sections (ref 1), i.e. sections featuring constant curvature. The panel considered has variable curvature in the chordwise direction as well as a slight hard edge on centreline (e.g. polynomial coefficient p1 is not 0). This more complex geometry produces more complex deformation patterns.

The location of stress peaks toward the aft end of the panel, where the transverse span is larger is coherent with the trapezoidal plan form of the panel considered.

With **Case 3**, results are presented for the worst slamming pressure load case which has been found to coincide with a half wetted chord of 0.1m, for an impact velocity of 3 m/s. The finite element model is otherwise identical to that used for case 2.

The deformed shape illustrated in Figure 9 is essentially similar to that obtained for Case 2 except for the extent of the deformation being more localised. This is consistent with the more concentrated pressure load distribution (see figure 5). Accordingly, through thickness core shear stresses are also more localised resulting in an increase in magnitude compared with Case 2.

Figure 10 shows peak transverse shear stresses to coincide with the position of the pressure wave front, and, indeed, core shear failures in hull panels are not always seen at the supports. The magnitude of this peak is an order of magnitude higher compared to the uniform pressure load case 2 but remains approximately 27% less than in the flat plate **Case 1**. Thus, membrane effects are still effective as far as relieving shear loads in the core.

Figure 11 indicates that through thickness core shear stresses are up not only compared to Case 2, by a factor of 3, but also by about 70% compared to the flat plate calculations. In fact, contrary to Cases 1 and 2, results for Case 3 indicate that the fore and aft direction is critical as far as core shear strength is concerned.

Unlike what had been observed for flat hull bottom plating by Allen and Jones (Ref. 3), maximum shear stresses in curved panels do not necessarily arise when the front of the slamming pressure wave reaches the edges of the panel. Depending on local curvature, peaks are found to correspond to more concentrated slamming pressure distributions, i.e. nearer the point and time of impact. Furthermore, whereas a uniform pressure distribution maximizes reduction in stresses due to membrane effects, peak stresses arising with a more realistic slamming pressure load can exceed those obtained for a flat plate: in this example, τ_{xz} in case 3 exceeds τ_{yz} in case 1 by 4.4%. <u>These results show that not accounting for curvature effects on core shear stresses is not necessarily conservative.</u>

As discussed by Hildebrand (ref. 1), yet higher stress magnitudes can arise locally in the event of snap through. Non linear results given for case 4 show that convergence has been obtained for the panel considered indicating that this type of instability is not critical. Similarity of results compared to the linear analysis in Case 3 show that panel behaviour is essentially linear in this particular case.

The results obtained from the simplified slamming model could be used to optimize core specification in this bottom panel. Taking into account that, in real life situations, the point of impact is not necessarily on centreline, these results would suggest that, compared to what could be concluded from the standard flat plate model, a stronger core may be needed along the aft edge of the panel whereas a lighter core may be used elsewhere. Furthermore, the information on load direction would be helpful when selecting the grade and orientation of <u>orthotropic core materials such as honeycomb cores for example: where the flat plate analysis would show maximum core shear stresses in the transverse y direction, the slamming model predicts higher stresses in the for and aft x panel direction.</u>

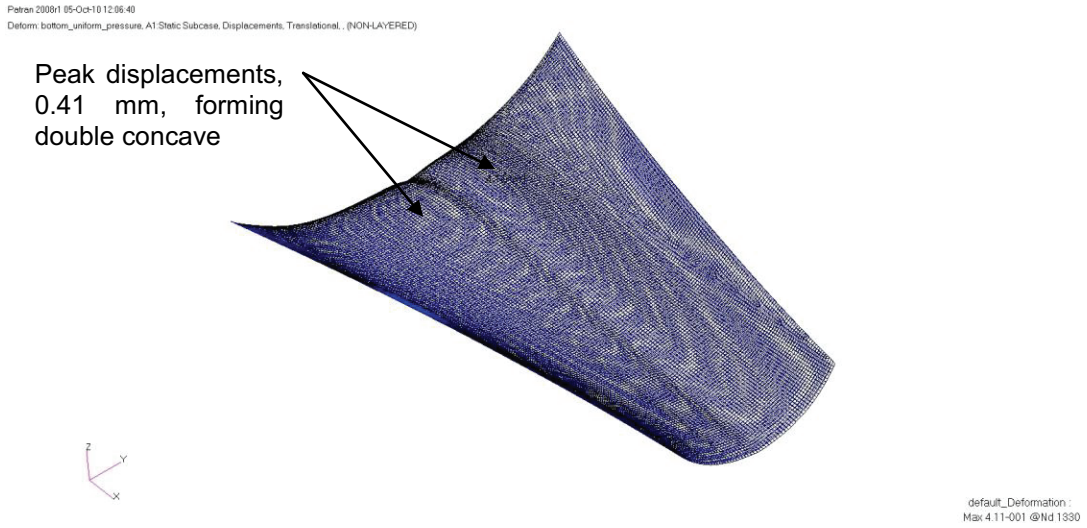

Figure 9: Case 2 – Uniform pressure – Displacements

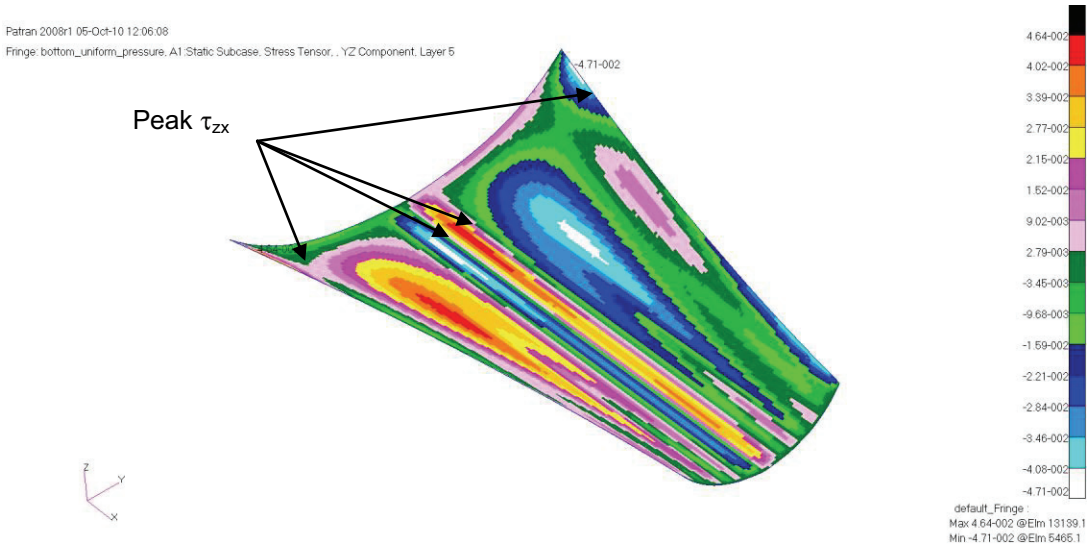

Figure 10: Case 2 – Uniform pressure – Shear stress (τ_{yz}) contour plot (MPa)

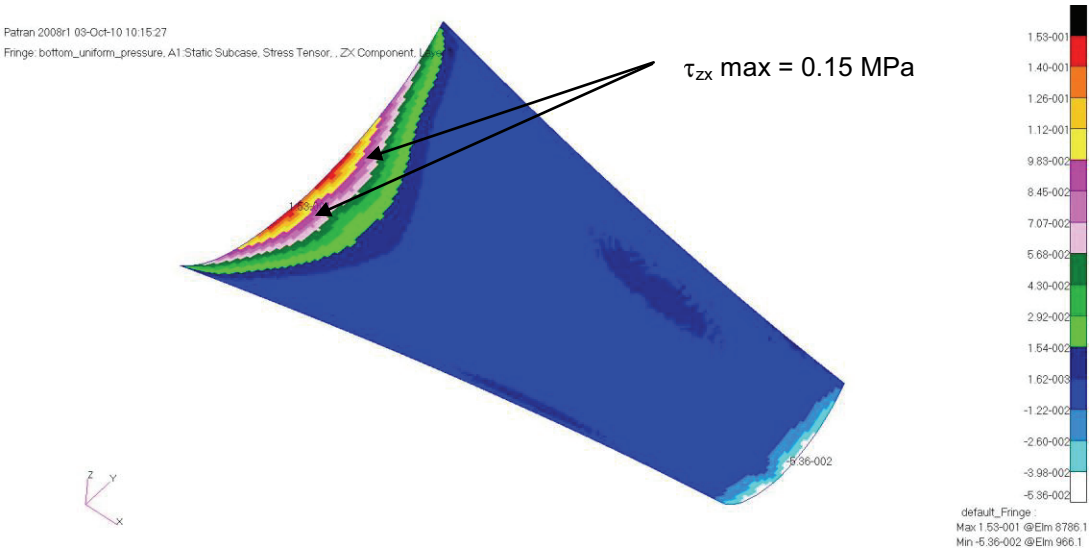

Figure 11: Case 2 – Uniform pressure – Shear stress (τ_{zx}) contour plot (MPa)

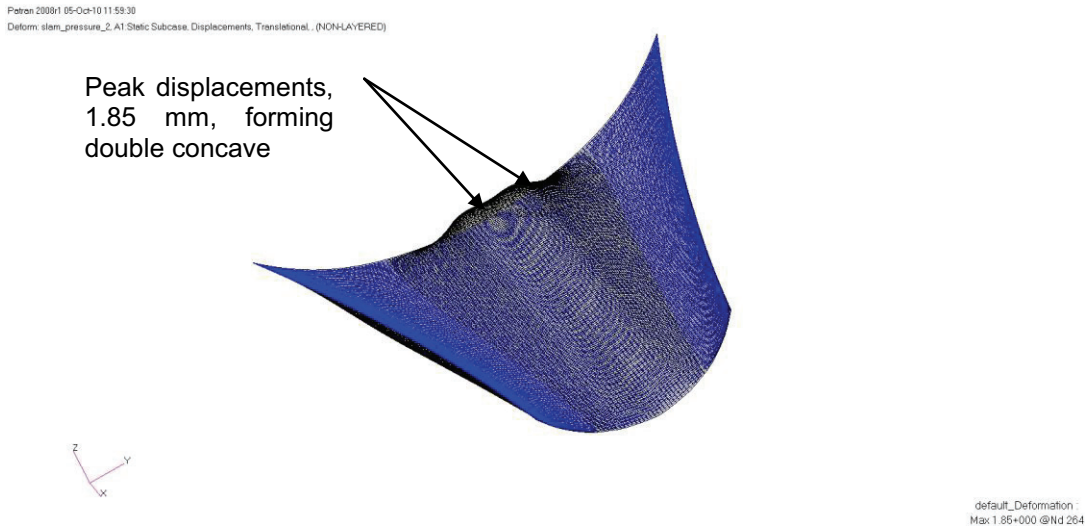

Figure 12: Case 3 – Slamming pressure @ c(t2) – Displacements

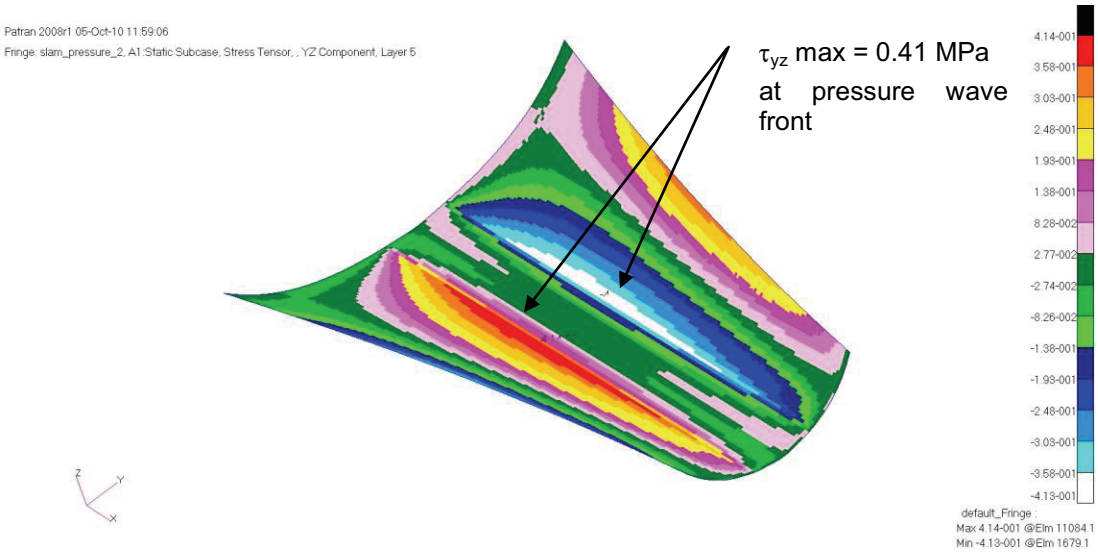

Figure 13: Case 3 – Slamming pressure @ c(t2) – Shear stress (τ_{yz}) contour plot (MPa)

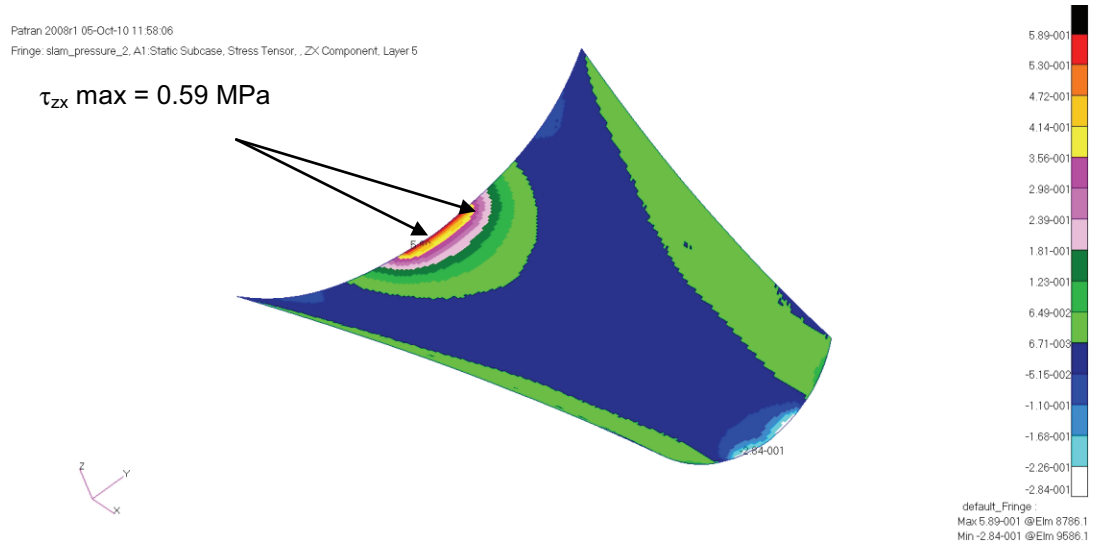

Figure 14: Case 3 – Slamming pressure @ c(t2) – Shear stress (τ_{zx}) contour plot (MPa)

4.2 Simplified slamming model Vs Hydroelastic analysis

In order to validate the results obtained with the simplified approach and verify its general applicability, the same panel impact described in the previous sections has been modelled with the full hydro-elastic model.

In the hydro-elastic model, dynamic and hydro-elastic effects can be numerically 'switched on and off", independently. By turning both 'off', the model produces the same results of a quasi-static analysis with no hydro-elastic effects, which is the same as the simplified model. This is particularly useful since, by its own nature, the simplified method gives results only for a few time instants, corresponding to arbitrarily chosen wetted chords, and by looking at the continuous time histories output by the more advanced method, one can verify whether such wetted chords give representative values of maximum stresses and deflections.

4.2.1 Comparison of maximum deflection and shear stresses

The main results from the comparison of the simplified model with the hydroelastic model are summarised in Table 2. The hydro-elastic model has been run with both the same distribution as the simplified model (labelled "2D") and with a more realistic "3D" distribution of the kind shown in Figure 8.

The magnitudes of deflections predicted by the hydro-elastic model and by the simplified model are in very good agreement. The "3D" pressure distribution appears to produce larger displacements than the "2D" case, however only by 8.5%. Figure 15 (a) shows that, in terms of the magnitude of maximum deflection, the panel dynamic response is close to the quasi-static one, however the maximum deflections occur at larger wetted chords when hydro-elastic effects are considered. Figure 15 (b) illustrates how the hydro-elastic model predicts the maximum deflection to be found on the panel centre-line. In fact, it can be shown that double concave patterns like the one show in Figure 12, only appear at the earliest stages of the impact, when peak deflections have not yet reached the maximum value.

Case	**Analysis Type**	**Pressure**	**wmax (mm)**	τ_{yz} **(MPa)** Long edge Core shear stress	τ_{zx} **(MPa)** Short edge Core shear stress
3 FEA slamming	Linear static FEA	Slamming @ t2 c(t2)=0.1 m U=3.0 m/s	1.85	0.414	0.59
5 Hydro-Elastic Model,	Hydro-Elastic, "2D" Pressure	Slamming 0< c(t) < 0.26m Ui=3.0m/s	1.84	0.423	0.61
6 Hydro-Elastic Model,	Hydro-Elastic, "3D" Pressure	Slamming 0< c(t) < 0.33m Ui=3.0m/s	2.00	0.433	0.71

Table 2: Comparison of Simplified and Hydro-Elastic model Results

Peak values of shear stress are also in good agreement. The 'long edge' core shear stress predicted by the simplified method is within 4.5% of the hydro-elastic model. A more significant difference is found on 'short edge' core shear values, but comparing the results of the "2D" and "3D" hydro-elastic models, shows that this difference is mainly due to the actual “3D” 'shape' of the pressure distribution.

From Figure 7 and Figure 8 we can see that "3D" pressures are not just higher in way of the flatter aft sections, but also act over a wider wetted chord. From Figure 17 we can conclude that the "3D" pressure distribution has a force resultant that is even slightly smaller than the "2D" case, but acts further aft, producing much higher shear in way of the panel aft edge.

It is worth noting that this feature of larger shear stresses along the aft edge of the panels is likely to be amplified in real life by the fact that bottom panels often impact the water with a slight "bow-up" trim, which reduces pressures in way of the panel front end and moves the highest force resultants even closer to the aft edge.

Figure 18 and Figure 19 show the maximum values of respectively 'longitudinal' (τ_{zx}) and 'transverse' (τ_{yz}) shear found at each point of the panel through the duration of the slam. In line with Figure 14, the peak value of shear stress is found in way the panel aft edge, with large values concentrated within 250mm from the centre-line. The panel front edge is comparatively lightly loaded, and approximately half as much as the simplified method predicts.

Figure 19 shows that the maximum value of transverse core shear is found on the panel outboard edges, and while the simplified model appears slightly to over-predict stresses close to the pressure front, shear stresses of up to 85% of the absolute peak are still found mid way between centre-line and the edge of the panel. Figure 20 represents how the point of maximum transverse shear 'travels' across the panel: at the very first stage of the impact (t<1ms) the pressure front has only moved over less than 50mm from centre-line, the peak transverse shear stress is relatively small (<0.15MPa) and still located in the vicinity of the front. As time progresses, the amplitude of response of the lower natural modes increases, and the peak transverse shear moves to the panel outboard edge.

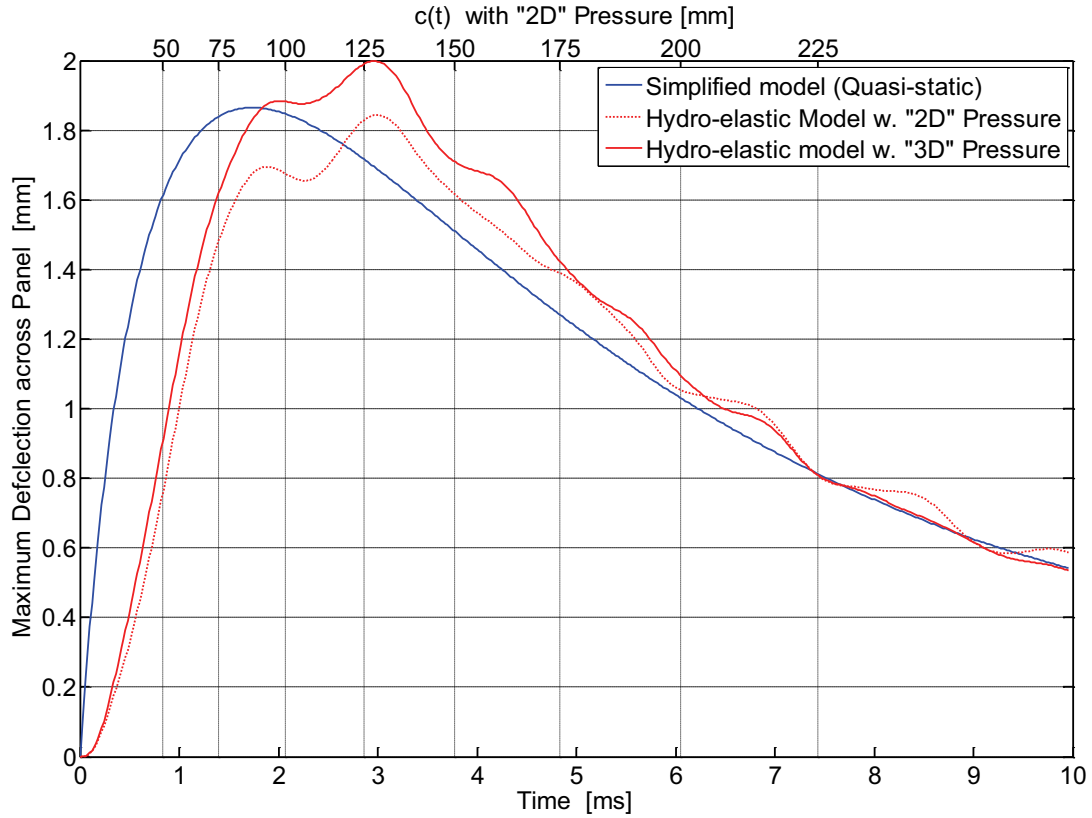

(a)

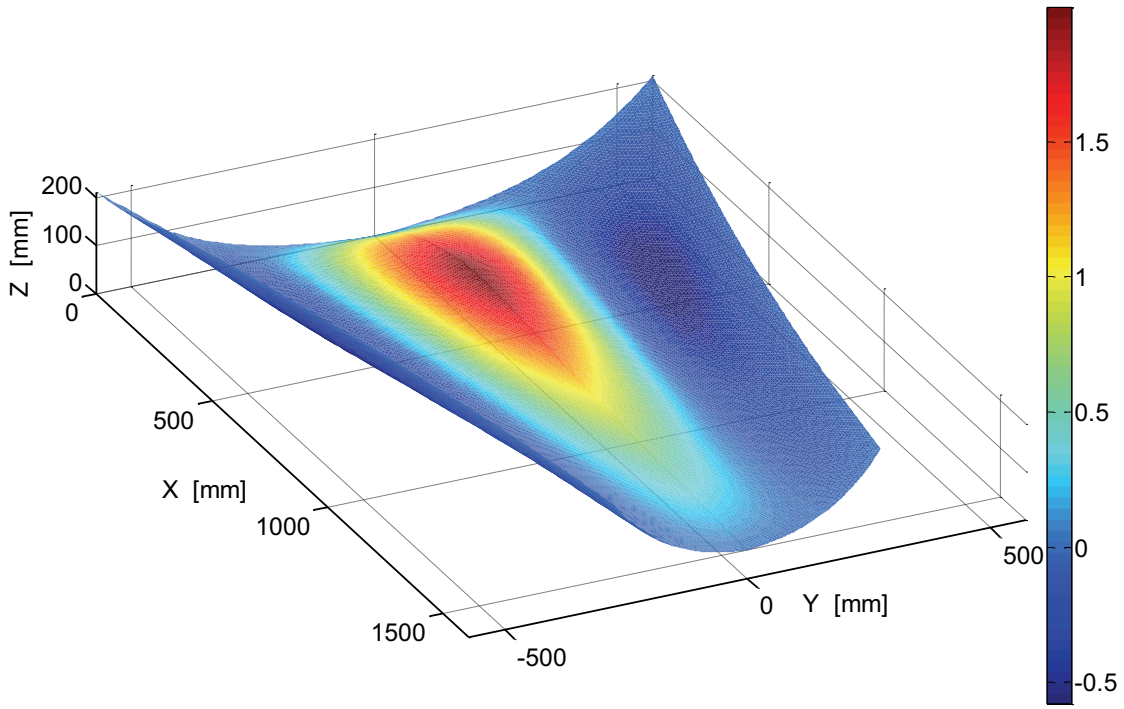

(b)

Figure 15: Case 6 – (a) Time History of Panel Deflection and (b) Deflection at time of maximum deflection for "3D" Pressure Distribution [mm]

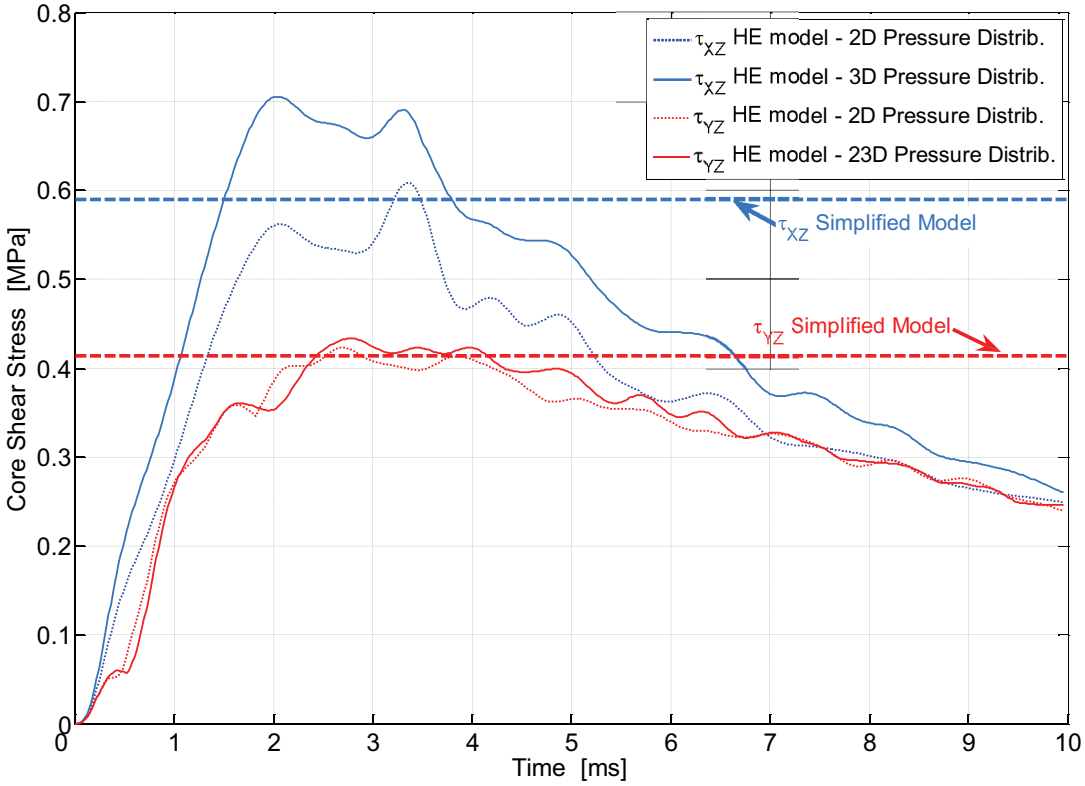

Figure 16: Core Shear Stress - Hydro-elastic Model with "2D" (Case 5) and "3D" (Case 6) Pressure Distributions vs Simplified model (Case 3)

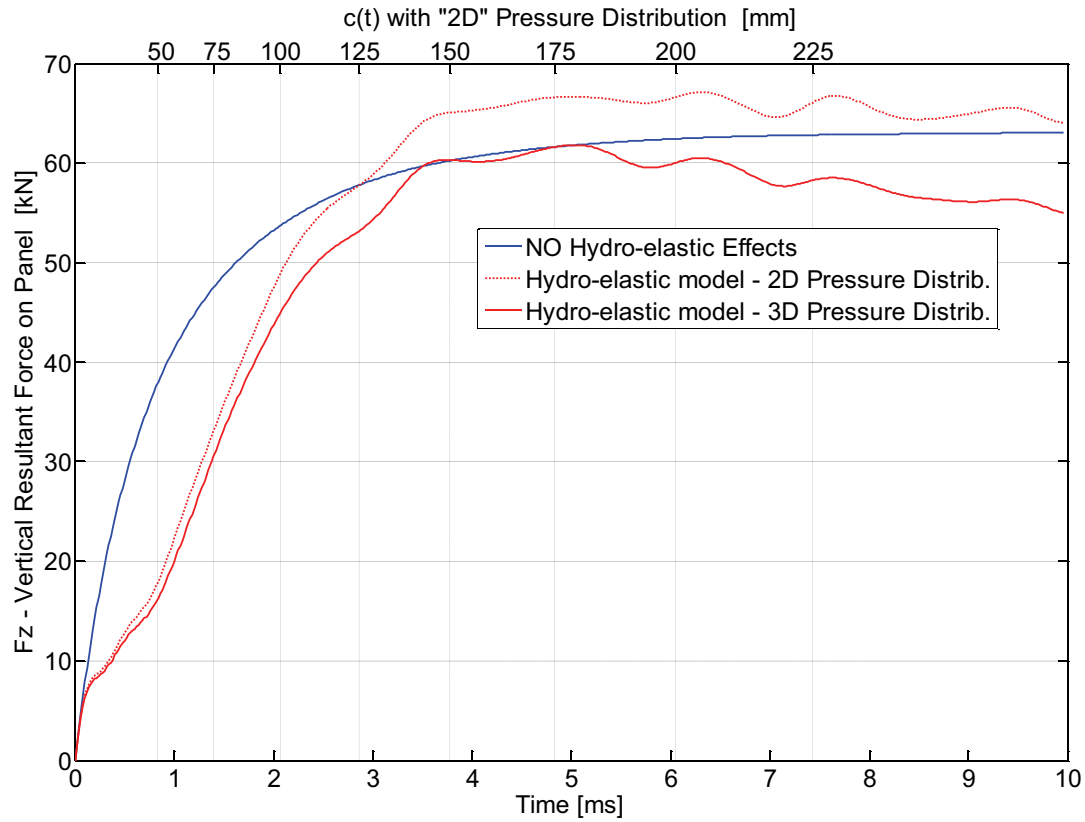

Figure 17: Case 5 and 6 Vs Case 3 - Vertical Resultant Force on Panel

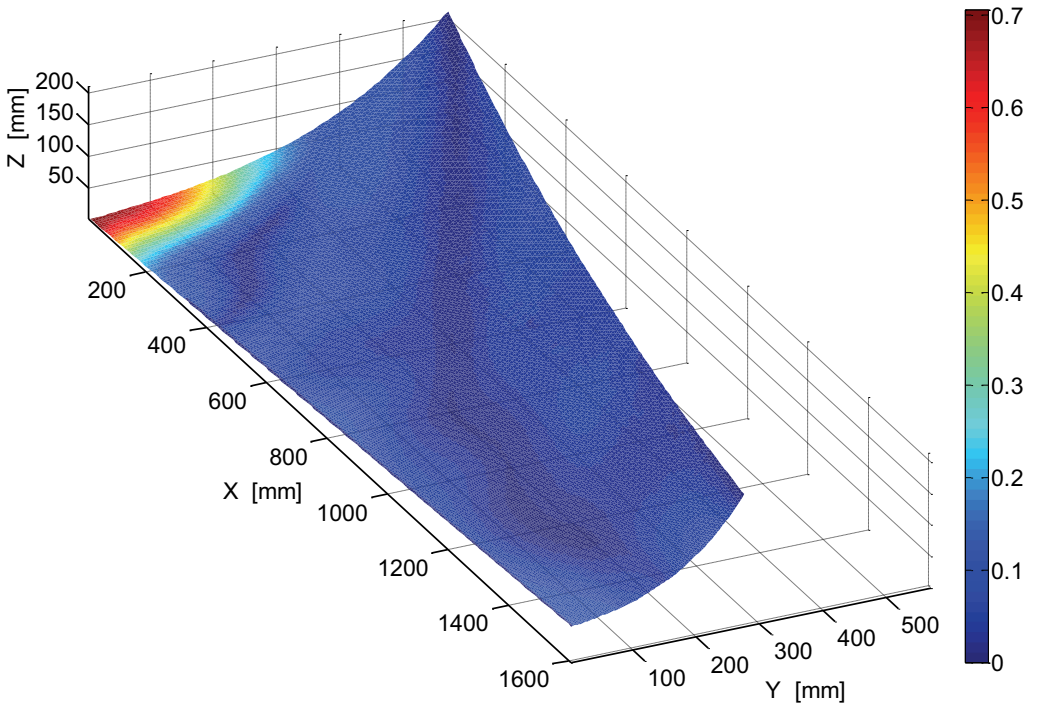

Figure 18: Case 6 - Maximum Shear Stress τ_{xz} at any time through slam [MPa]

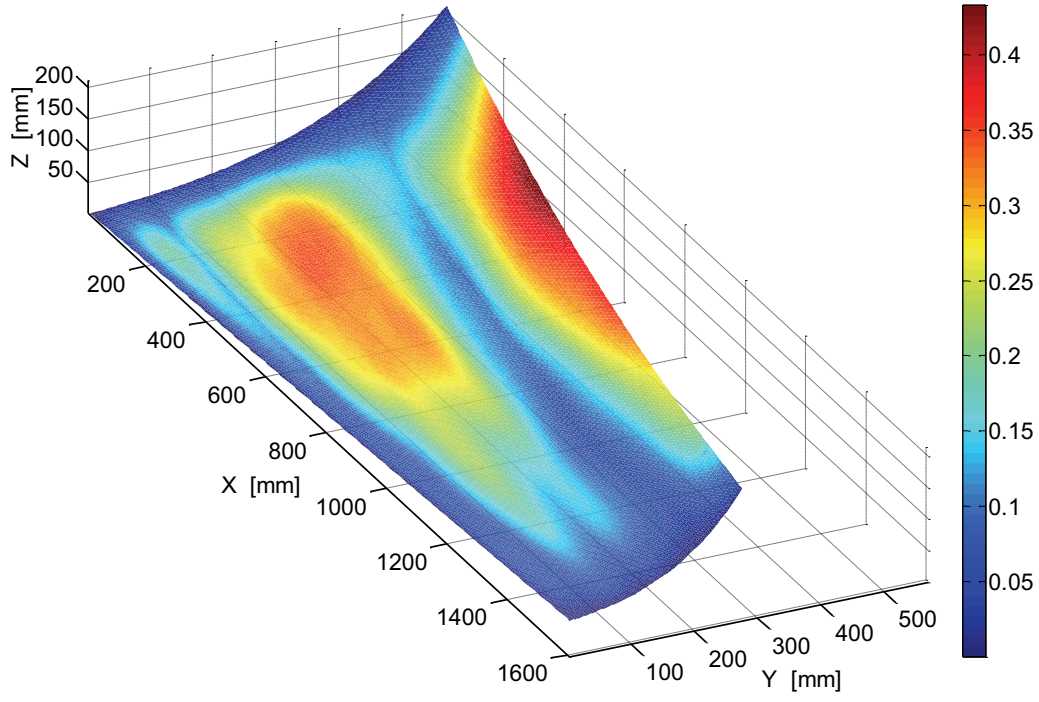

Figure 19: Case 6 - Maximum Shear Stress τ_{yz} at any time through slam [MPa]

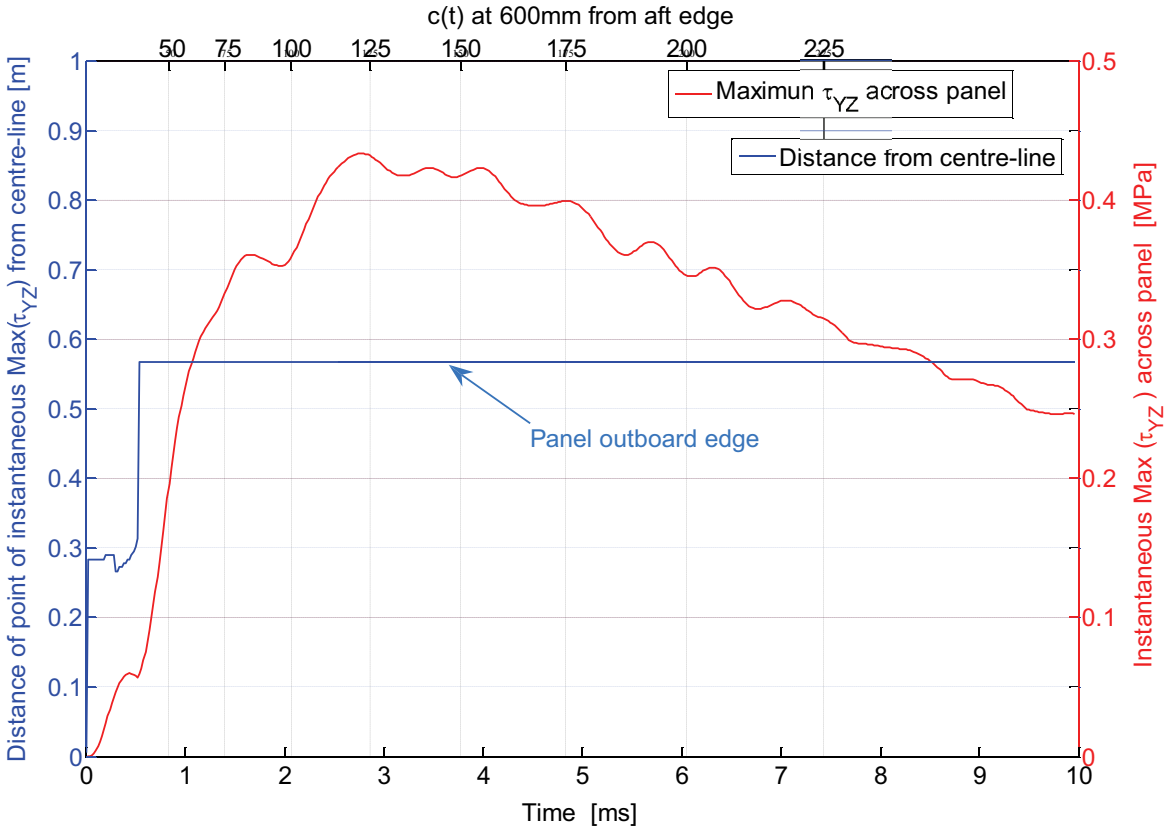

Figure 20: Distance of maximum transverse shear τ_{YZ} from centre-line

4.2.2 Validity of the "quasi-static" and "rigid body" assumptions

In the previous section we have seen how the simplified model appears to predict fairly accurately the maximum deflections and stresses, with minor discrepancies being due mainly to the "2D" idealisation of the slamming pressure distribution.

However, it would be wrong to conclude from this that the panel responds in a quasi-static fashion or even that hydro-elastic effects are negligible. In fact, looking at Figure 21, one can see that, if we were to neglect the hydro-elastic effects, the panel would exhibit a clearly impulsive response with large amplitude oscillations, and, for the case of the longitudinal shear τ_{XZ}, stress amplification factors of the order of 1.35. Furthermore, it can be seen from Figure 22 that the effective impact velocity drops significantly below the initial value of 3m/s through the first stage of the impact: when the wetted chord is of the order of 50mm, the effective impact velocity is actually only 2m/s which will produce instantaneous hydrodynamic loads that are 55% lower than those that would be experienced by a rigid-body with a constant effective impact velocity of 3m/s.

In practice, for the case examined in the present study, one may consider that the attenuation of the hydrodynamic loads due to hydro-elasticity has the almost the same effect as a critical damping, whereby the system reaches the quasi-static response amplitude with neither over-shooting, nor significant residual oscillations. Alternatively, as illustrated by Figure 23, we may argue that the attenuation of the loads due to the fast and early response of the higher natural modes of the panel is capable of "smoothing" the otherwise very steep and sudden initial pressure rise to a level where the lower modes can respond in an almost quasi-static way.

It is expected that, as impact velocities are increased, the simplified approach will tend to give more and more conservative estimates of maximum stresses and deflections as the relative effect of hydro-elasticity becomes more significant.

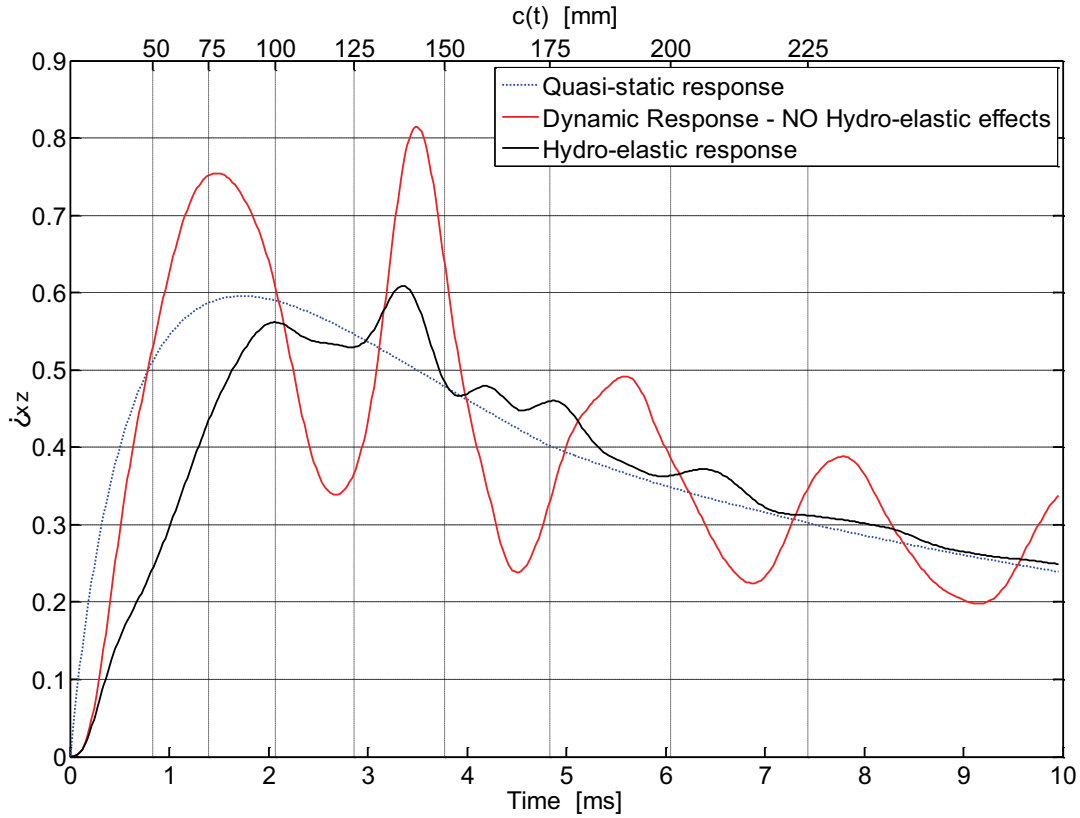

Figure 21: Dynamic and hydro-elastic response vs. quasi-static ("2D" pressure distribution)

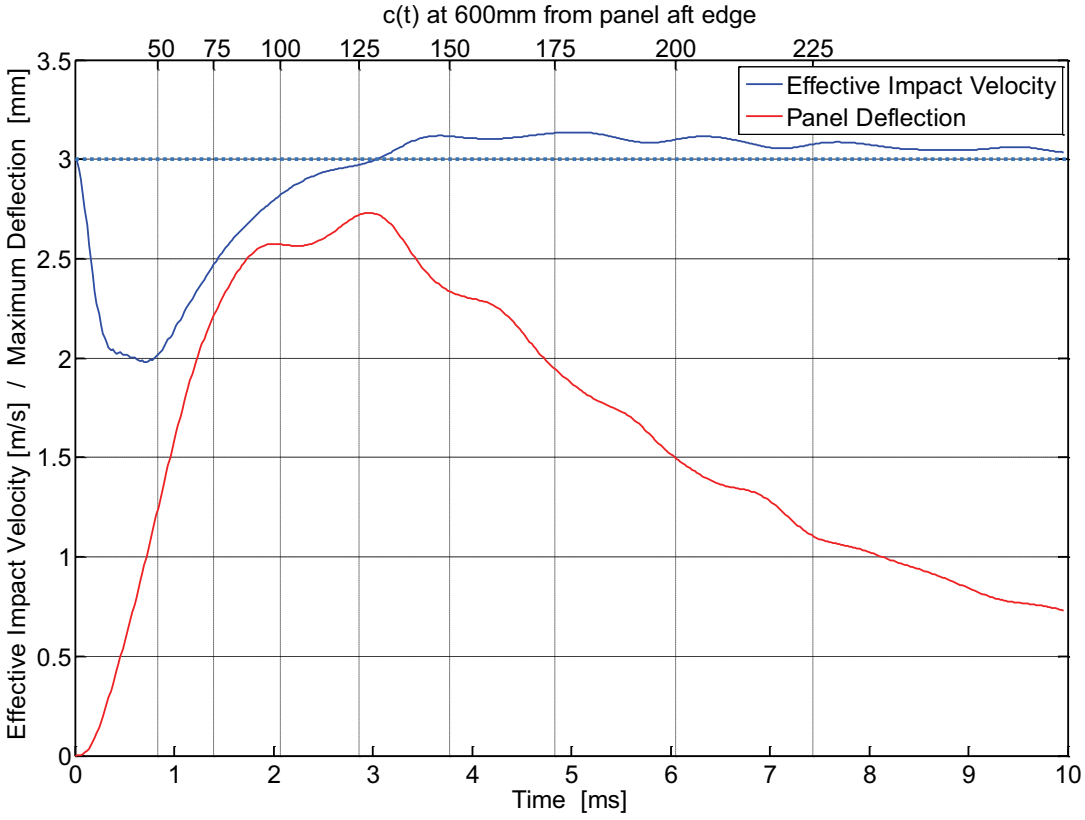

Figure 22: Effective Impact Velocity Vs Time

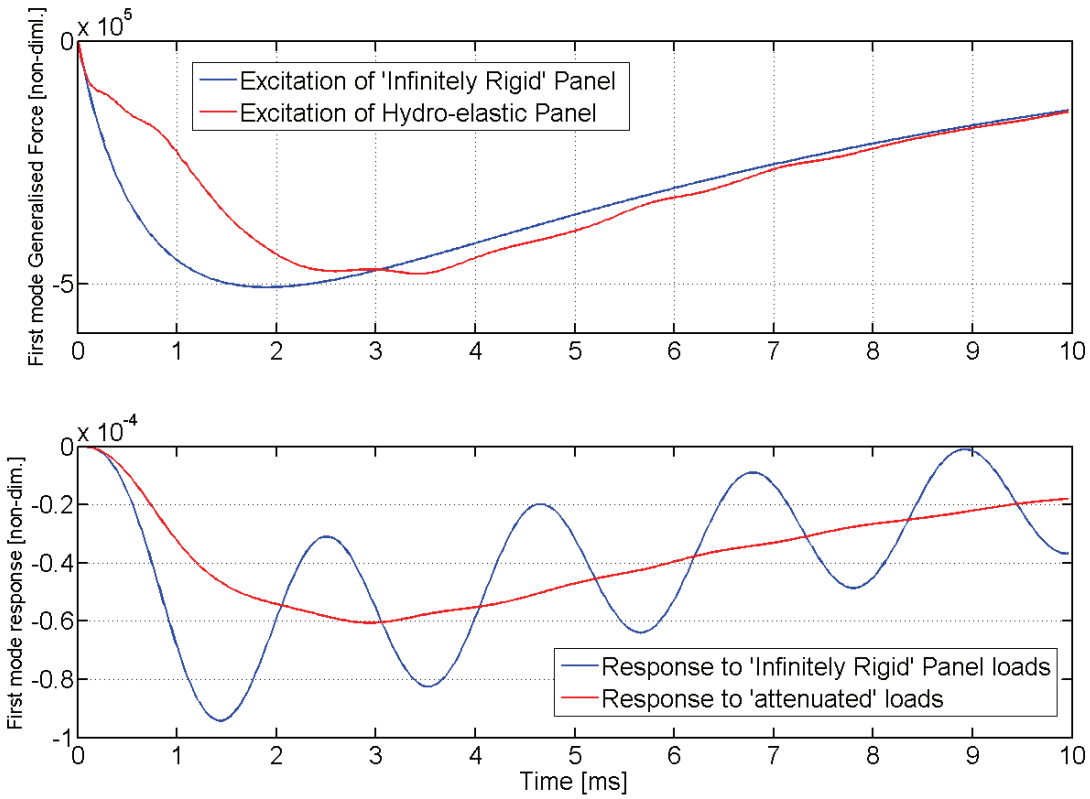

Figure 23: First natural mode excitation and response

5. CONCLUSIONS

A development project has been carried out with the aim of producing a simplified method for the analysis of hull panels subject to slamming without the use of specialised software.

Compared with standard approaches, the simplified method is based on a more realistic description of the pressure distribution and more correct modelling of the effects of panel curvature on core shear stress in particular (membrane response).
Detailed stress and strain distributions can be obtained and used to optimise panel laminates in terms of performance and reliability. Where membrane effects are significant in relieving core shear stresses, structural weight can be saved. Where, on the other hand, neglecting the influence of curvature on core shear appears to be non-conservative (e.g. along aft edge of panel), using of such analysis techniques, reliability can be improved by selection of an adequately stronger core material.

Since the simplified method neglects dynamic and hydro-elastic effects to minimise the computational effort, the validity of such simplifications had to be tested by comparing results against a full hydro-elastic model.

Initial benchmarking has revealed that the method can indeed provide accurate indications of panel deflections and shear stresses, as well as identifying critical load areas and patterns. However, limitations of the 2D quasi-static assumptions have also been highlighted as follows:

- core shear stress distribution influenced by three-dimensional nature of pressure distribution, thus the accuracy of the simplified model applied to a non rectangular panel depends on the choice of reference section geometry;
- prediction of peak responses depends on arbitrary selection of wetted chords: actual response peaks can be missed if they do not coincide with the chosen wetted chords;
- the method is not applicable where hydro-elastic phenomena are pre-dominant, i.e. near the time of impact or at very short wetted chords; it is expected that the range of applicability will decrease for higher impact velocities.

Further development work is currently focusing on establishing a suitable set of criteria that can define the range within which the simplified method can be trusted to give accurate or, at worse, conservative results. Such criteria should remain relatively simple to calculate to fit within the scope of the simplified method.

References:

1- “On the bending and transverse shearing behaviour of curved sandwich panels”, Espoo 1991, Hildebrand Martin

2- “Experimental Investigation of Dynamic Loads on Offshore Racing Yachts”, Paolo Manganelli, PhD Thesis, University of Southampton

3- “A simplified method for determining structural design-limit pressures on high performance marine vehicles”, R.G. Allen, R.R. Jones

4- "Dynamics of Structures", R.W.Clough and J.Penzien, McGraw-Hill, 1993

HISWA SYMPOSIUM - AMSTERDAM RAI - METS 2010

HYBRID POWER SYSTEMS FOR LARGE RECREATIONAL YACHTS AND SMALL COMMERCIAL CRAFT – by Roel ter Heide and Martijn Favot, WhisperPower BV, the Netherlands. (With contribution of Bas Isselman)

1. INTRODUCTION

Whisper Power is an internationally leader in the development, production and sales of modern diesel based power systems. As a spinoff of Mastervolt, the company was founded in 2007 by Mastervolt's co-founder, Roel ter Heide. One of the objectives of the company is to encourage a world in which energy is produced in a smarter, cleaner and greener way.

In 2008, WhisperPower was approached by leading superyacht builder Holland Jachtbouw to co-develop the next generation of hybrid power systems. Being active in the power generation field with lots of experience in battery systems and power electronics, WhisperPower quickly accepted the challenge and started work. A new division was founded, Hybrid Power Systems, controlled and financed by WhisperPower, with the purpose to develop high power systems for yachts from 15 to 60 metres.

We recruited eight new engineers, some with over 15 years of experience in this field. Our international network of specialist engineering, product development and manufacturing companies was also engaged in order to enlarge our think-tank and development capacity.
The core competencies we have now united in our Hybrid Power division are shown below.

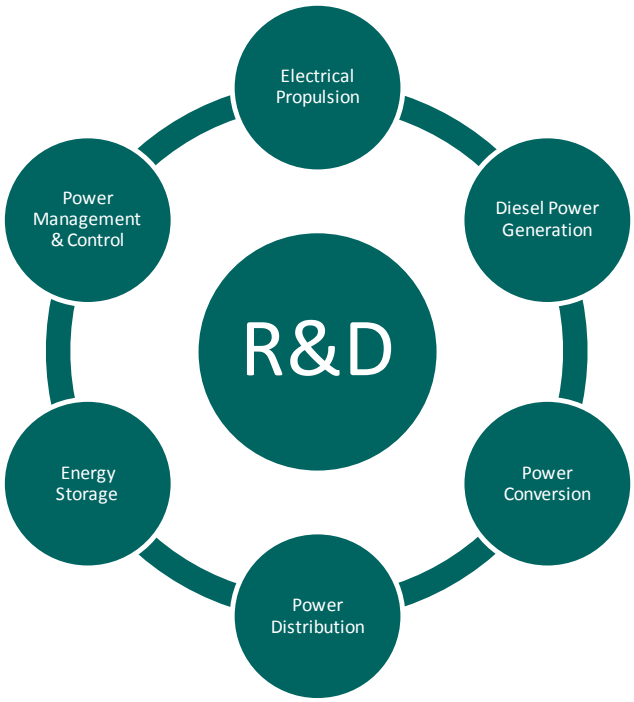

Developing hybrid-type products that combine electronic, electrical and mechanical technologies is a complicated matter. For example, it took ten years for an extended team of hard working engineers to develop the Toyota Prius. However, power storage, power conversion and power generation technologies have evolved a lot since then. More ready-to-use components are available so that the development process is easier to oversee and financially feasible.


WhisperPower premises in Drachten (NL)

2. MARKET TRENDS

Owner representatives and owners are far more critical about their ecological footprint than in the past. While the yachting sector is not stimulating new technologies in a very intensive way, owners are much more progressive with their demands. They are pushing stakeholders in the branch to develop better ways to propel their yacht and provide onboard comfort: More efficiently, cleaner and quieter.

Around 15 to 20 years ago we worked on large power systems for 30-40 metre sailing yachts such as *Cyclos III* from Royal Huisman, *Conny Fever* from Jongert and many other projects. Our role at that time was to engineer and supply large battery systems and inverter systems with battery charging capacities allowing a recharge of the banks (which could go size wise up to 7000 Ah) within hours. Owners at that time required extended silent periods without generator running and no gensets switched on during sailing.

As yachts became ever larger and AC and DC power consumption increased exponentially, the industry started to install 24-hr running generator systems. Inverter technology remained limited in output power rating (15 kVA) and as high DC voltage systems were not implemented at the time they had to operate on 24 VDC. The systems were heavy, voluminous, expensive and maintenance intensive.

But things have changed. New power storage technologies such as lithium–ion batteries have become available, offering more compressed power, lower weight and a much longer life cycle. New inverter technologies have also been introduced, offering smaller sizes and lower weight with powerful sine wave outputs. Combined with the experience WhisperPower has built up working with solar systems that operate on high DC voltages (up to 1000 VDC), we were positive the company could create an excellent new system to meet the demands of a new era.

Cyclos III

3. THE PROJECT

In September 2008 we were asked to work out a system for a traditional sailing yacht - a brand-new replica of an aluminium J-Class yacht with a length of 40 metres. An experienced sailor, the owner's brief was for a performance yacht which would also combine comfort and luxury.

A key aspect of comfort on such a yacht is the audible noise levels. Situated next to the engine room, the owner's suite is most vulnerable to sound contamination. The use of relatively quiet machinery components and outstanding insulation will contribute to reducing sound levels to an acceptably low level.

Another major owner demand was to reduce engine running hours without affecting the operational profile. This automatically leads to generating 'silent periods' onboard the yacht. When in port, the owner expects the yacht to make it through the night without needing to use power from the main engine or generator set. The same should apply when anchored at sea.

The owner also required that emissions be reduced. Propelling the yacht using batteries makes it possible to manoeuvre in and out of port without the use of the main engine, reducing exhaust fumes as well as sound levels. E-propulsion for up to four hours at a limited speed (4-5 knts) needed to be made possible.

A sailing yacht is constantly exposed to the forces of nature. The wind and sun can be seen as 'free' sources of power, providing yachts with their own energy source. The use of solar panels and wind generators, heat recovery and (fresh)water management contribute to a more balanced 'green' energy housekeeping. Crucially, the owner wanted the yacht to generate power during sailing by smartly combining the CPP propeller and shaft generator.

During discussions with the owner and yard we tried to collect as much information as possible about the power consumption in order to gain a clear idea about the size of the system. The most important factor was to be able to calculate a realistic load balance.

4. THE LOAD BALANCE

In order to reach a realistic load balance, we first determined which electric components would be installed. Wherever possible, low energy consumers such as LED lights have been selected. This has resulted in relatively low total installed electric power of all electric components.

A day to day simulation of the expected load behaviour of the yacht was then generated. This makes it possible to determine from minute to minute which components are being used or not and at which operational setting. This enabled us to determine a realistic load balance. Figure A shows an example of a typical day: 24 hours of port load behaviour in Mediterranean conditions, without guests on board.

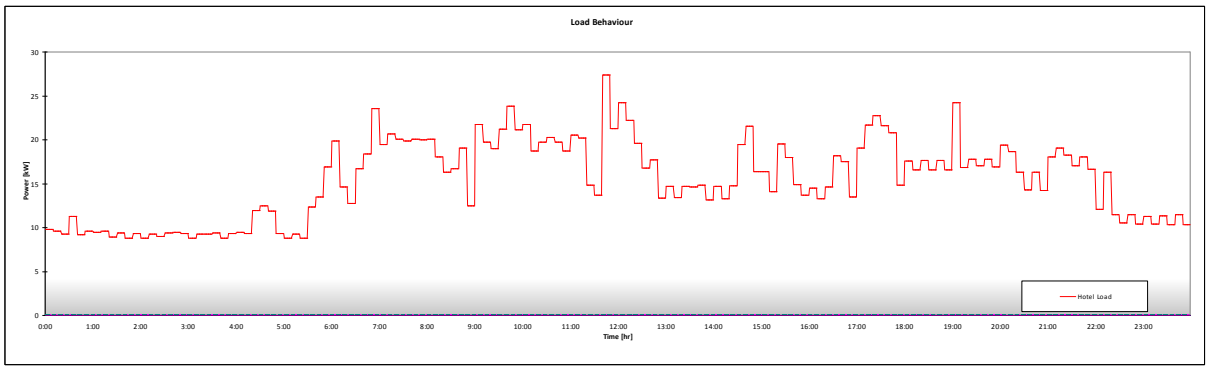

Figure A

By creating different load behaviour overviews for other modes the yacht will encounter, a detailed minute to minute overview can be made, simulating anything from a typical day to a week of chartering. Combining all overviews, a summary can be made displaying the amount of time a specific amount of power is required.

Figure B shows an overview of the different operational modes the yacht will encounter during a two-week charter in the Caribbean. The amount of time a specific load will be required during this charter is shown in figure C.

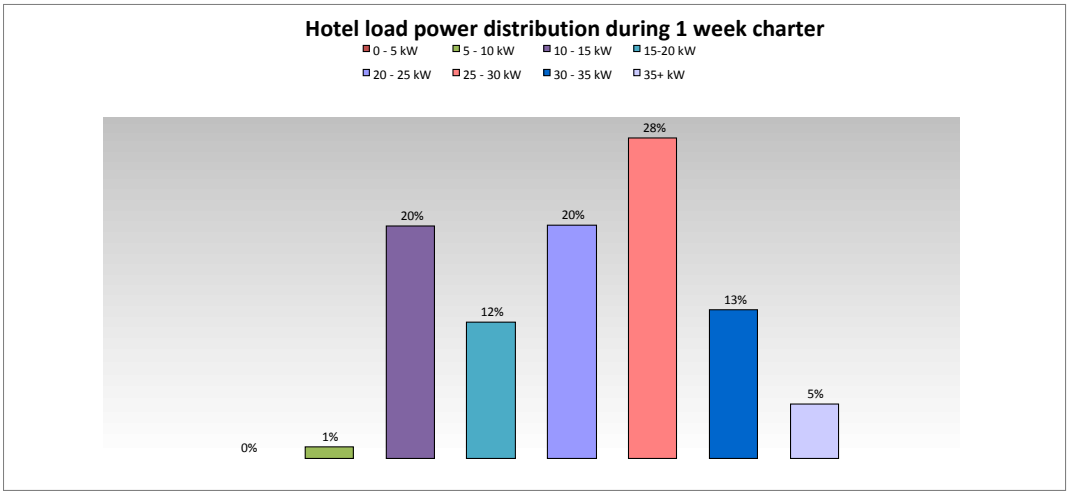

Figure B

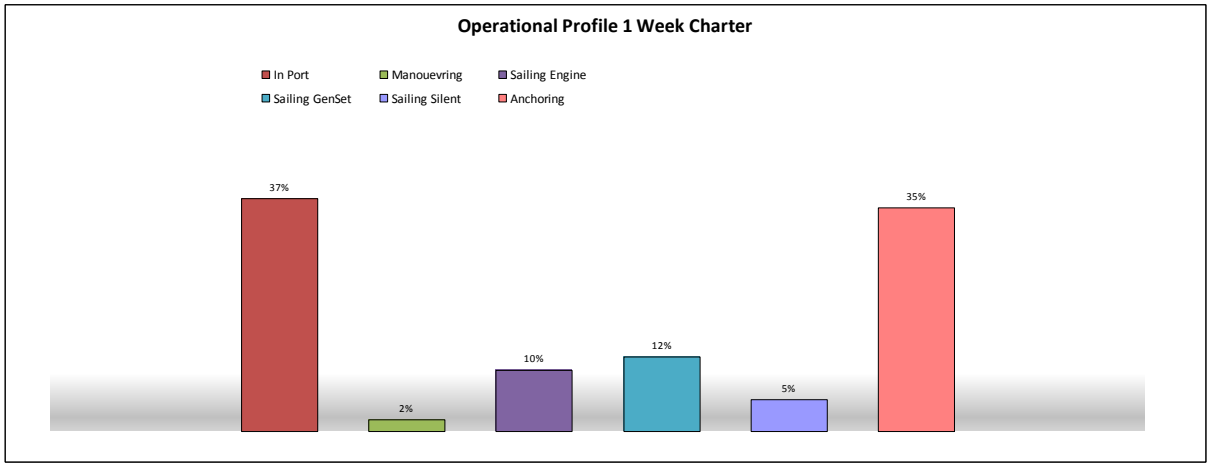

Figure C

5. OUR FIRST SYSTEM PROPOSAL

Our first proposal was for a true diesel electric, fully hybrid system based on a high DC power bus of 750 VDC, which we called the Hy-Grid. The power supply came from two WhisperPower variable speed diesel generators (VST) of max 200 kW, connected to the DC Power Bus by means of AC/DC power converters through automatic switches. All this would be built into two DC main switchboards (see figure D).

A 350 kW permanent magnet based electrical motor (DC) provides propulsion, driving the propeller shaft through a gearbox. This electric drive is connected to the DC power bus by means of DC/DC power converters and automatic switches. A lithium-ion battery pack feeds the DC Power Bus. Both generators operate on variable speed to achieve the optimum balance between fuel consumption, cost of ownership and the power provided. During operation of the yacht, the Hybrid Power Management System (HPMS) serves as the heart of the system, constantly sensing the electric power demand.

This system had our preference, offering the most flexible solution as far as the location and layout of the engine room was concerned with maximum freedom of design.

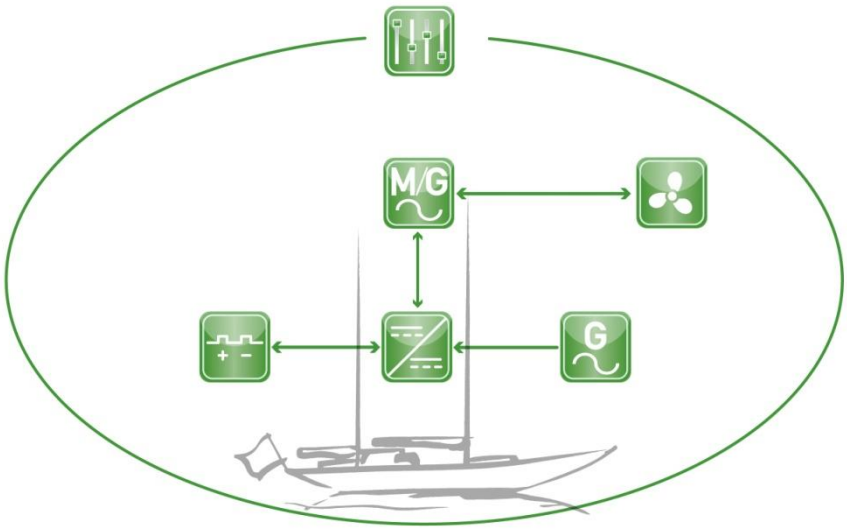

Figure D

In a serial hybrid system (fully hybrid) the conventional diesel engine is replaced by an electrical motor. A battery bank is connected to the common high voltage electric power bus, which is connected to the motor.
The electrical energy is either provided by variable speed power generators or by the battery bank. With large batteries you can have long periods of electric propulsion (and/or driving onboard electrical appliances) without resorting to the generator. Energy can also be produced by the propeller when sailing.

6. THE FINAL CHOICE

After some months of discussing the pros and cons of the proposed serial hybrid system, the customer asked us to propose an alternative system. This parallel hybrid system would have a similar set-up but with a combined traditional propulsion engine/generator instead of the electrical propulsion engine (see figure E).

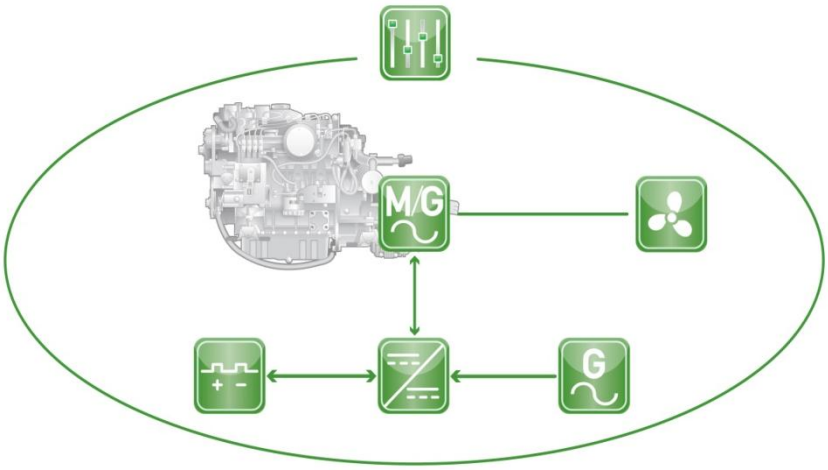

Figure E

In this parallel hybrid system the mechanical connection between the engine and propeller shaft is maintained, with the electric motor acting on the drive shaft in parallel with the engine. The power split is a mechanical device that allows transfer of power between its connections. The propeller can be driven directly from the engine, the electric motor or both. The propeller can also be disconnected to let the propulsion engine operate a stand-alone generator function.

An additional WhisperPower variable speed generator (VST) of 50 kW is installed as the main generator during peak energy consumption periods, running low rpm at low demand (1200 rpm) and high rpm (up to 3600 rpm) during high power demands. We choose this kW size to realise an optimum balance between P-out and rpm. As the 400 VAC 3 phase load is indirectly connected to a WhisperPower generator via the inverter and main battery, peak power loads will be handled by the combination of both. This peak shaving effect means that the generator kW size can be kept smaller.

All key system components projected in the yacht are described below.

Hy-Gen power generator
Variable speed generators (1200-3600 V) based on intelligent, permanent magnet, water-cooled alternator technology, utilising an ultra-compact diesel engine (4 cil Steyr), fitted in a sound shield. This power pack feeds a high DC power bus, connected to the propulsion systems and the DC-AC power conversion system (30 kW inverter) for the hotel load. Power rating: 50 kW.

Hy-Store power storage
Deep cycle, long-life lithium-Ion LiFeYPO4 battery banks (port and starboard) provides emission-free power for propulsion and/or power generation, without operating the auxiliary generators (Hy-Gen) or using the engines. Capacity of each bank: 288 VDC nom/ 160 Ah, 35 kWh power available effective. WhisperPower Battery Management System (BMS) ensures accurate cell balancing.

Hy-Charge battery charging
Sophisticated system for recharging the Lithium-Ion battery bank from the Hy-Gen power packs or shore power. DC- DC converters connected to the 650 VDC bus system and the 288 VDC (nom voltage) battery.

Hy-Grid distribution system
The DC power distribution system that supplies electric power on demand from the power sources to the power consumers. An isolated and laminated copper bus bar rail system with various switches, built into modular cabinets.

Hy-Invert AC power supply
The highly efficient DC to AC inverters smoothly convert power from the various DC sources into a sine wave one and three phase 230/400 VAC/ 50 Hz. The power rating of 30 kVA is sufficient to operate all domestic appliances including airco.

Hy-Control
All system components are connected to the overall power management system, which controls and monitors the entire system. This advanced automation system is configured according to the yacht's requirements and fitted with a manual override to ensure redundancy. In this project, a PLC-based system is embedded in the total ship's electrical system.

Hy-Prop propulsion
E-propulsion is taken care of by a 50 kW permanent magnet electric motor, driving the propeller shaft through a gearbox. This PM motor is placed between the main engine and the gearbox and shaft. The electric drive is powered by either the Hy-Store or Hy-Gen module. Bow and stern thrusters are operated in a similar way.

7. THE 40-METRE J-CLASS SYSTEM DIAGRAM

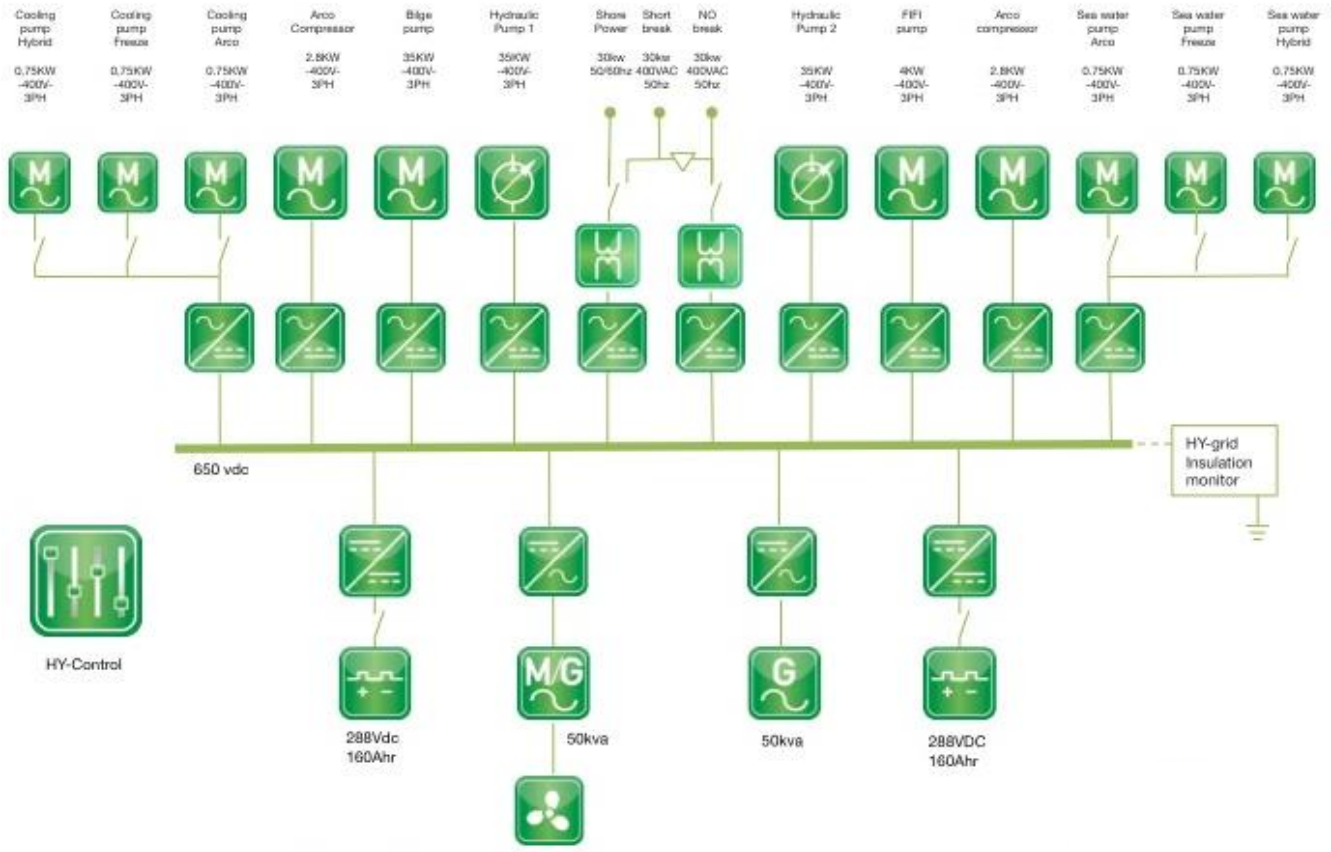

8. ESSENTIAL SYSTEM FEATURES: POWER GENERATION DURING SAILING

In the system we integrated the possibility to generate substantial electrical power (10 kW) when sailing by using the 50 kW electrical motor as a shaft alternator, fitted to the main engine. This way of generating power will result in a speed reduction. Because a controllable pitch propeller is installed, the amount of power to be generated with accompanying speed reduction can be regulated, depending on the available wind speed. For the owner it is important to be able to select between speed and power.

To calculate the possible amount of power generated by the chosen CPP propeller, a four quadrant diagram must be used. While open water diagrams only represent the condition for stationary forward sailing, four quadrant diagrams show the torque and thrust behaviour of a propeller over all four quadrants, as shown in the table below.

Quadrant		Ship Speed V_s	Propeller Speed n_s
1st	0 – 90	+	+
2nd	90 – 180	-	+
3rd	180 – 270	+	-
4th	270 – 360	-	-

Open water diagrams do not provide enough information. The region for instance where the propeller speed approaches zero, torque and thrust coefficients rise to infinity. For this reason, the MARIN research institute developed four quadrant diagrams for various Wageningen B-series propellers. These diagrams depict thrust and torque coefficients, C_T*, C_Q*, for different hydro mechanical pitch angles (β [-]).

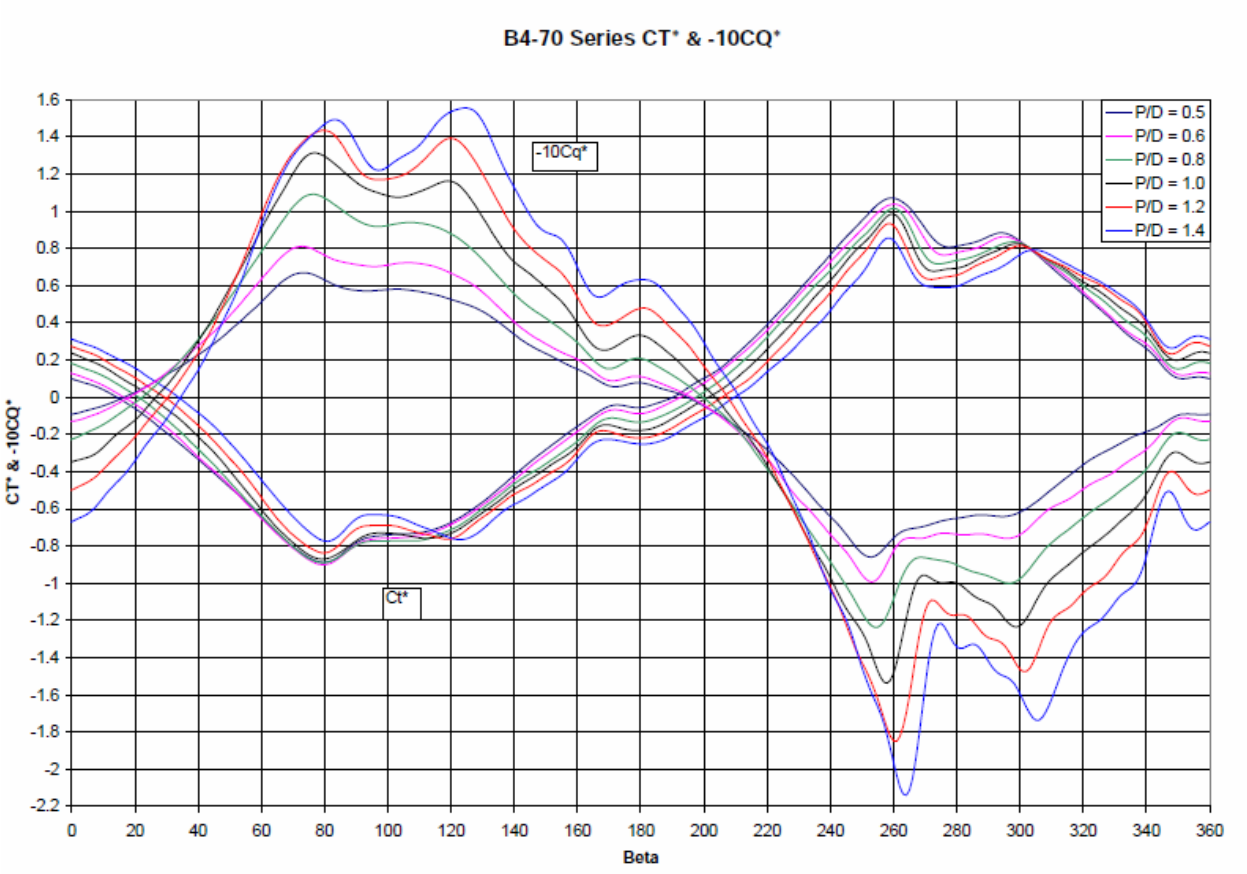

Figure F

To calculate the power generated by the CPP propeller, the torque and propeller speed need to be calculated. These will vary with changing pitch settings, ship speed and allowed speed reduction. The Wageningen B4-70 series four quadrant diagram (figure F) is used because it contains data for most pitch ratios.

D	Propeller diameter	[m]
V_A	Advance velocity	[m/s]
V_S	Intended ship speed	[m/s]
B	Hydro-mechanical pitch angle	[-]
J	Advance ratio	[-]
n_P	Propeller speed	[1/s]
w	Wake fraction	[-]
C_T*	Thrust Coefficient (four Quadrant)	[-]
C_Q*	Torque Coefficient (four Quadrant)	[-]
K_T	Thrust Coefficient (open water)	[-]
K_Q	Torque Coefficient (open water	[-]
R	Resistance	[N]
ρ	Water density	[kg/m^3]

P	Power	[W]
η	Efficiency	[-]

As the ship sails at a certain speed it encounters resistance, R_{int}. When the propeller is trailing it slows the ship down, adding resistance, R_{trail}. At this new speed the ship encounters the new resistance R_{red}, so;

$$R_{trail} = R_{\text{int}} - R_{red} \quad [1.1]$$

At this new ship speed, V_S, the open water diagram intersects with the pitch ratio curves by;

$$K_T = \frac{K_T}{J^2} J^2 \quad [1.2]$$

Combining this with $R_{trail} = -T$, assuming the thrust factor is 0,

$$J = \frac{V_A}{n_p \cdot D} \ , \quad [1.3]$$

$$V_A = V_s \cdot (1-w) \text{ and} \quad [1.4]$$

$$K_T = \frac{T}{\rho \cdot n_p{}^2 \cdot D^4} \text{ this leads to,} \quad [1.5]$$

$$K_T = \frac{-R_{trail} \cdot n_p^2 \cdot D^2}{\rho \cdot n_p{}^2 \cdot D^4 \cdot V_s{}^2 \cdot (1-w)^2} J^2 = \frac{-R_{trail}}{\rho \cdot D^2 \cdot V_s{}^2 \cdot (1-w)^2} J^2 \quad [1.6]$$

Kt relates to CT* through,

$$K_{T,Q} = C_{T,Q}{}^* \cdot \frac{\pi}{8} \cdot [illegible]^2 + 0.7 \cdot \pi^2 \quad [1.7]$$

Combining equations [1.6] and [1.7] with

$$\beta = \arctan\left(\frac{V_A}{0.7 \cdot \pi \cdot n_p \cdot D}\right), \ \beta = \tan^{-1}\left(\frac{J}{0.7 \cdot \pi}\right) \quad (1.8)$$

This leads to

$$C_T{}^* = -\frac{8}{\pi} \cdot \frac{R_{trail}}{\rho \cdot D^2 \cdot V_s^2 \cdot [illegible](1-w)^2} \cdot \frac{J^2}{[illegible]J^2 + 0.7 \cdot \pi^2} = -\frac{8}{\pi} \cdot \frac{R_{trail}}{\rho \cdot D^2 \cdot V_s^2 \cdot [illegible](1-w)^2} \cdot \frac{\tan^2 \beta}{[illegible]\tan^2 \beta + 1} \quad (1.9)$$

Equation [1.9] is plotted in the four quadrant diagram for different ship speeds at different trailing resistances. These curves intersect with the different pitch ratio propeller curves in the four quadrant diagram, at which *CT**, *CQ** and accompanying *B* were determined.

Combining equation [1.7] with [1.8] and [1.3] results in values for K_Q and n_p.
Now P_{prop} can be calculated, with

$$K_Q = \frac{Q}{\rho \cdot n_p^{\ 2} \cdot D^5}$$, resulting in [2.0]

$$P_{prop} = 2\pi \cdot K_Q \cdot \rho \cdot n_p^3 \cdot D^5$$ [2.1]

The power generated by the trailing propeller can now be calculated by taking the shaft, gearbox and generator efficiency into account.

$$P_{gen} = P_{prop} \cdot \eta_s \cdot \eta_{GB} \cdot \eta_{gen}$$ [2.2]

Sailing at an intended speed of 10 kn, and allowing several reductions up to a maximum of 2 kn, the power at the propeller (generated by the trailing propeller) and accompanying shaft speed is shown for varying pitch ratios in figure G. In the same way this is shown for an initial speed of 13 kn in figure H.

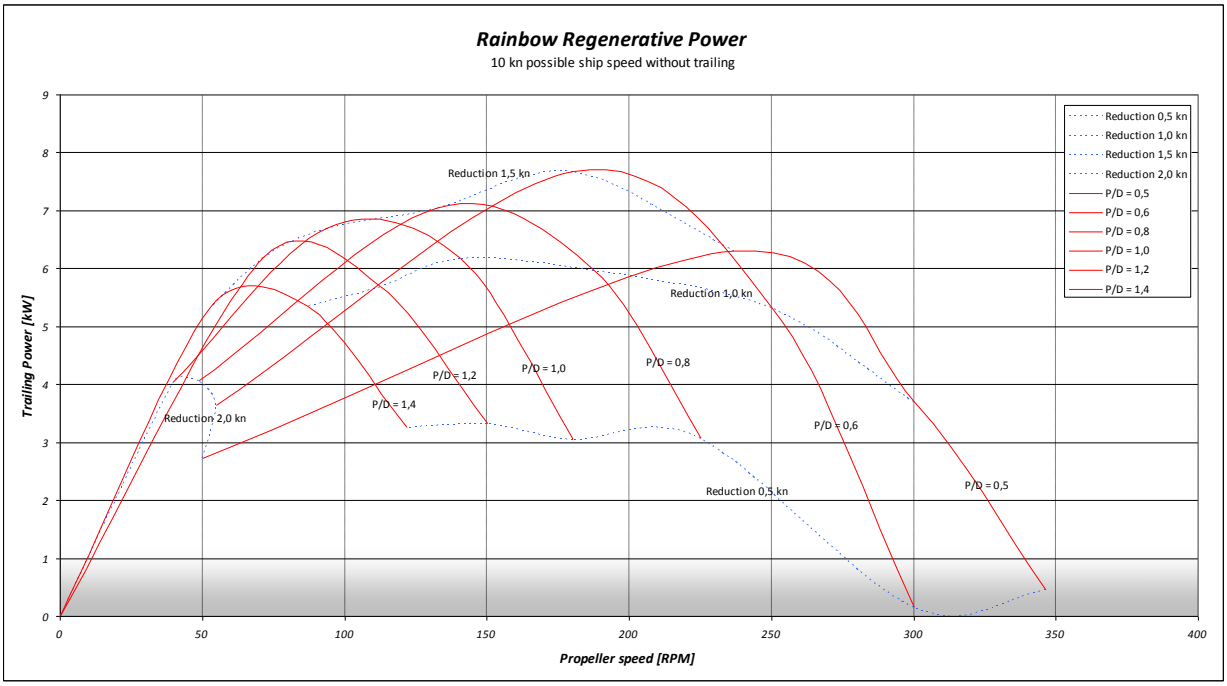

Figure G

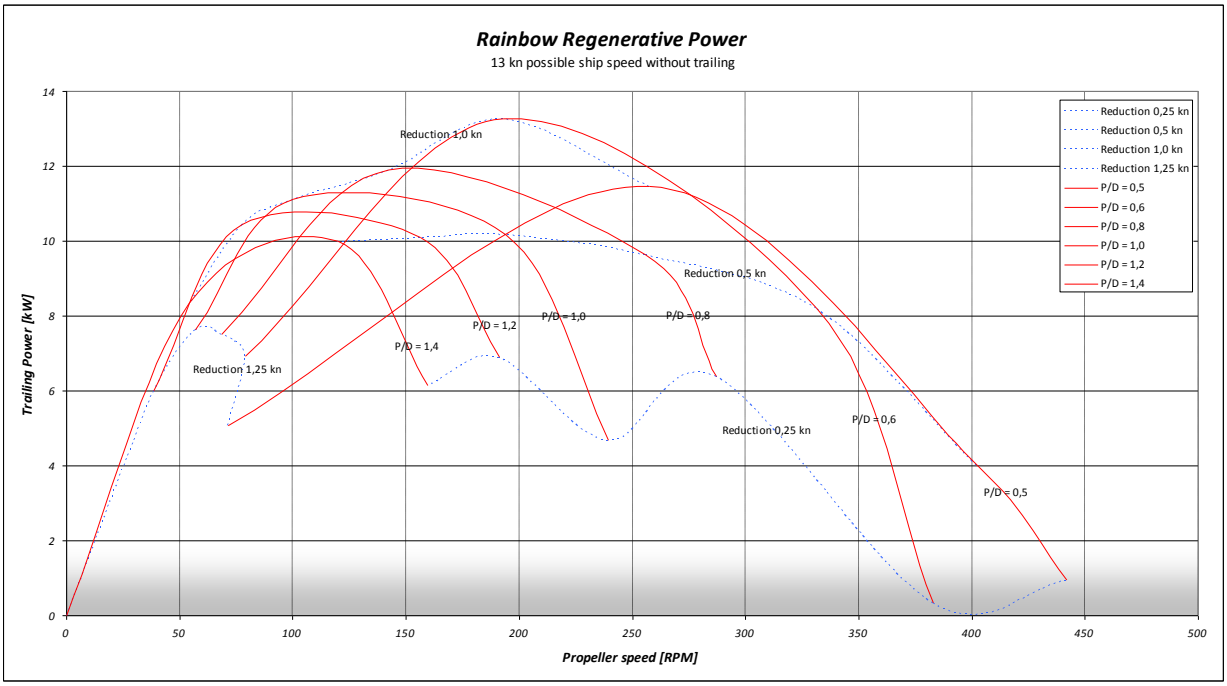

Figure H

When sailing at an intended speed of 10 kn, and allowing for a 1.5 kn reduction, the maximum power can be generated at a pitch ratio of P/D = 0.6. This results in P_{gen} = 7.1 [kW], at a shaft speed of 180 [RPM]. For an intended speed of 13 kn, the maximum power to be generated is at a pitch ratio of about P/D = 0.6 and a speed reduction of about 1.0 kn. This will generate about P_{gen} = *12.2* [kW] at a shaft speed of 193 [rpm].

9. ESSENTIAL SYSTEM FEATURES: THE BATTERIES

In battery-based systems such as our hybrid system, the specifications of the selected batteries are crucial for the performance of both power and propulsion. Traditional lead acid batteries are not good enough for such systems, which is why we use lithium-ion batteries. Common in consumer electronics, they are one of the most popular types of rechargeable battery for portable electronics, with one of the best energy-to-weight ratios, no memory effect, and a slow loss of charge when not in use. Lithium-ion batteries are also growing in popularity for military electric vehicles and aerospace applications due to their high energy density. They are three times smaller, three times lighter and three times more durable than conventional semi-traction lead-acid batteries.

As lithium-ion batteries vary in materials and construction, the type selected depends on the target application. For our hybrid systems we use lithium-ion phosphate type batteries. These are the best choice for frequent high deep discharge and charge cycles, and can handle the heat which comes into the battery the best way. Stacks are engineered in such a way that cooling is optimised.

Our LiFeYPO4 batteries can be charged and discharged by 1/C. To prevent damage and complete malfunction of the batteries, a sophisticated Battery Management System is added which ensures proper cell balancing at charge and discharge. Safety requirements are given a high priority during the engineering process of the system as overcharging and discharging can short circuit the cell, potentially making recharging unsafe.

10. SYSTEM COSTS

We can roughly estimate the price difference between conventional systems and our new hybrid systems. Installing a hybrid system offers a range of benefits: 1/ extended silent time, with no generator running, 2/ peak shaving, and 3/ electrical navigation and manoeuvring. These features cannot be realised with traditional systems. As a rule of thumb we calculate the price of a hybrid system to be at least twice that of conventional system. Orders for large systems in general take 40 to 50 weeks, with smaller systems being available in around 25 weeks.

HISWA SYMPOSIUM - AMSTERDAM RAI - METS 2010

HYBRID POWER SYSTEMS FOR LARGE RECREATIONAL YACHTS AND SMALL COMMERCIAL CRAFT – by Roel ter Heide and Martijn Favot, WhisperPower BV, the Netherlands. (With contribution of Bas Isselman)

1. INTRODUCTION

Whisper Power is an internationally leader in the development, production and sales of modern diesel based power systems. As a spinoff of Mastervolt, the company was founded in 2007 by Mastervolt's co-founder, Roel ter Heide. One of the objectives of the company is to encourage a world in which energy is produced in a smarter, cleaner and greener way.

In 2008, WhisperPower was approached by leading superyacht builder Holland Jachtbouw to co-develop the next generation of hybrid power systems. Being active in the power generation field with lots of experience in battery systems and power electronics, WhisperPower quickly accepted the challenge and started work. A new division was founded, Hybrid Power Systems, controlled and financed by WhisperPower, with the purpose to develop high power systems for yachts from 15 to 60 metres.

We recruited eight new engineers, some with over 15 years of experience in this field. Our international network of specialist engineering, product development and manufacturing companies was also engaged in order to enlarge our think-tank and development capacity.
The core competencies we have now united in our Hybrid Power division are shown below.

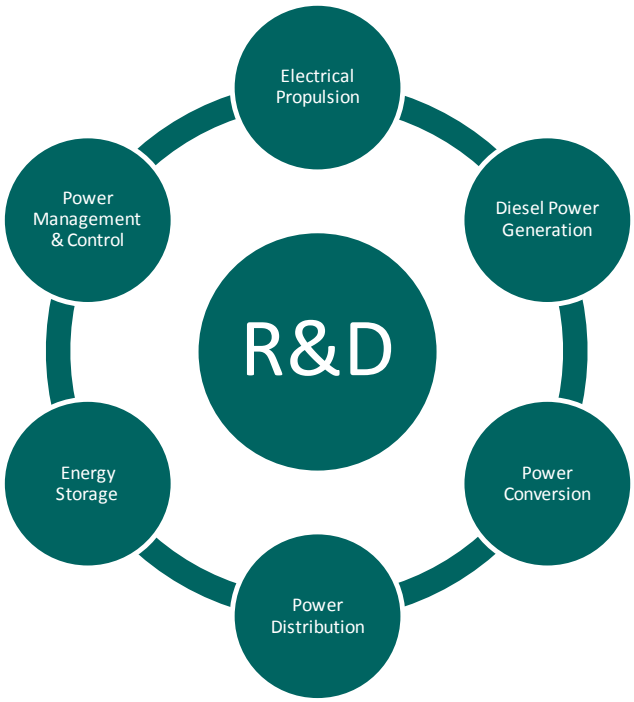

Developing hybrid-type products that combine electronic, electrical and mechanical technologies is a complicated matter. For example, it took ten years for an extended team of hard working engineers to develop the Toyota Prius. However, power storage, power conversion and power generation technologies have evolved a lot since then. More ready-to-use components are available so that the development process is easier to oversee and financially feasible.


WhisperPower premises in Drachten (NL)

2. MARKET TRENDS

Owner representatives and owners are far more critical about their ecological footprint than in the past. While the yachting sector is not stimulating new technologies in a very intensive way, owners are much more progressive with their demands. They are pushing stakeholders in the branch to develop better ways to propel their yacht and provide onboard comfort: More efficiently, cleaner and quieter.

Around 15 to 20 years ago we worked on large power systems for 30-40 metre sailing yachts such as *Cyclos III* from Royal Huisman, *Conny Fever* from Jongert and many other projects. Our role at that time was to engineer and supply large battery systems and inverter systems with battery charging capacities allowing a recharge of the banks (which could go size wise up to 7000 Ah) within hours. Owners at that time required extended silent periods without generator running and no gensets switched on during sailing.

As yachts became ever larger and AC and DC power consumption increased exponentially, the industry started to install 24-hr running generator systems. Inverter technology remained limited in output power rating (15 kVA) and as high DC voltage systems were not implemented at the time they had to operate on 24 VDC. The systems were heavy, voluminous, expensive and maintenance intensive.

But things have changed. New power storage technologies such as lithium–ion batteries have become available, offering more compressed power, lower weight and a much longer life cycle. New inverter technologies have also been introduced, offering smaller sizes and lower weight with powerful sine wave outputs. Combined with the experience WhisperPower has built up working with solar systems that operate on high DC voltages (up to 1000 VDC), we were positive the company could create an excellent new system to meet the demands of a new era.

Cyclos III

3. THE PROJECT

In September 2008 we were asked to work out a system for a traditional sailing yacht - a brand-new replica of an aluminium J-Class yacht with a length of 40 metres. An experienced sailor, the owner's brief was for a performance yacht which would also combine comfort and luxury.

A key aspect of comfort on such a yacht is the audible noise levels. Situated next to the engine room, the owner's suite is most vulnerable to sound contamination. The use of relatively quiet machinery components and outstanding insulation will contribute to reducing sound levels to an acceptably low level.

Another major owner demand was to reduce engine running hours without affecting the operational profile. This automatically leads to generating 'silent periods' onboard the yacht. When in port, the owner expects the yacht to make it through the night without needing to use power from the main engine or generator set. The same should apply when anchored at sea.

The owner also required that emissions be reduced. Propelling the yacht using batteries makes it possible to manoeuvre in and out of port without the use of the main engine, reducing exhaust fumes as well as sound levels. E-propulsion for up to four hours at a limited speed (4-5 knts) needed to be made possible.

A sailing yacht is constantly exposed to the forces of nature. The wind and sun can be seen as 'free' sources of power, providing yachts with their own energy source. The use of solar panels and wind generators, heat recovery and (fresh)water management contribute to a more balanced 'green' energy housekeeping. Crucially, the owner wanted the yacht to generate power during sailing by smartly combining the CPP propeller and shaft generator.

During discussions with the owner and yard we tried to collect as much information as possible about the power consumption in order to gain a clear idea about the size of the system. The most important factor was to be able to calculate a realistic load balance.

4. THE LOAD BALANCE

In order to reach a realistic load balance, we first determined which electric components would be installed. Wherever possible, low energy consumers such as LED lights have been selected. This has resulted in relatively low total installed electric power of all electric components.

A day to day simulation of the expected load behaviour of the yacht was then generated. This makes it possible to determine from minute to minute which components are being used or not and at which operational setting. This enabled us to determine a realistic load balance. Figure A shows an example of a typical day: 24 hours of port load behaviour in Mediterranean conditions, without guests on board.

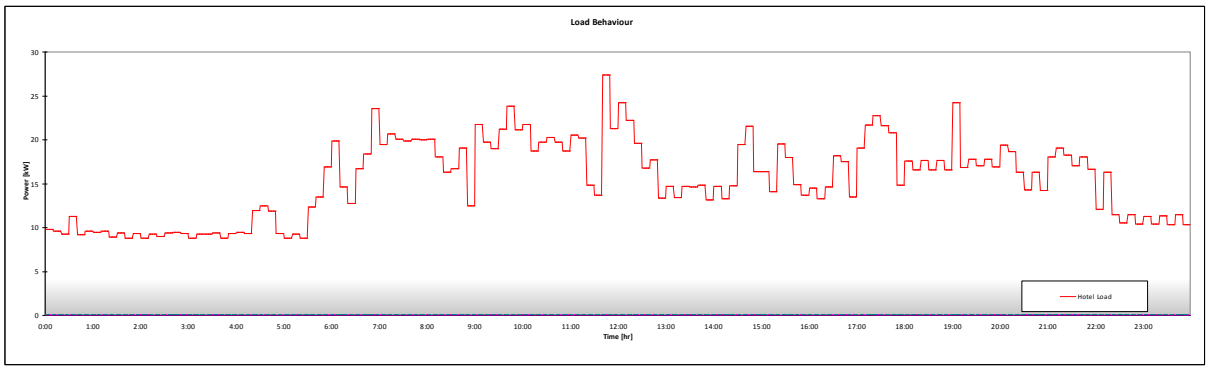

Figure A

By creating different load behaviour overviews for other modes the yacht will encounter, a detailed minute to minute overview can be made, simulating anything from a typical day to a week of chartering. Combining all overviews, a summary can be made displaying the amount of time a specific amount of power is required.

Figure B shows an overview of the different operational modes the yacht will encounter during a two-week charter in the Caribbean. The amount of time a specific load will be required during this charter is shown in figure C.

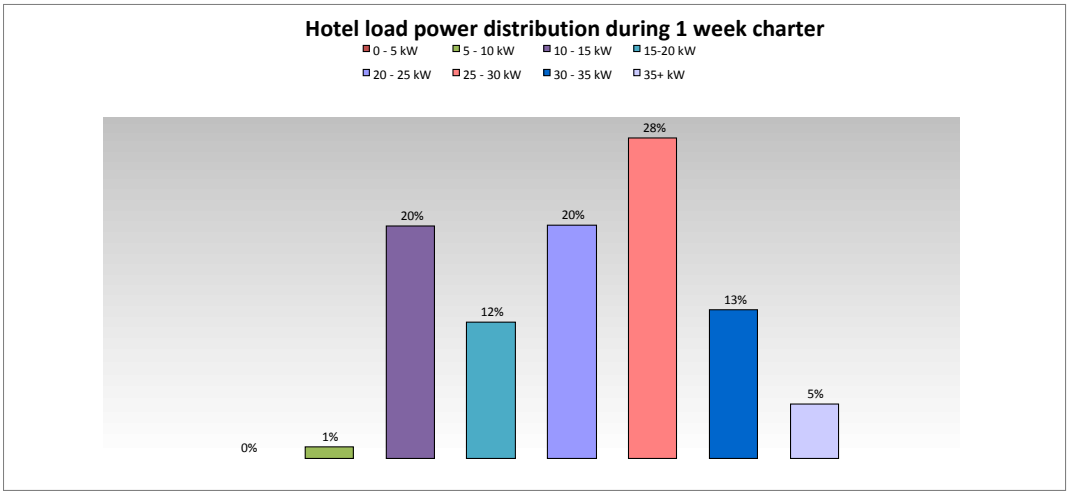

Figure B

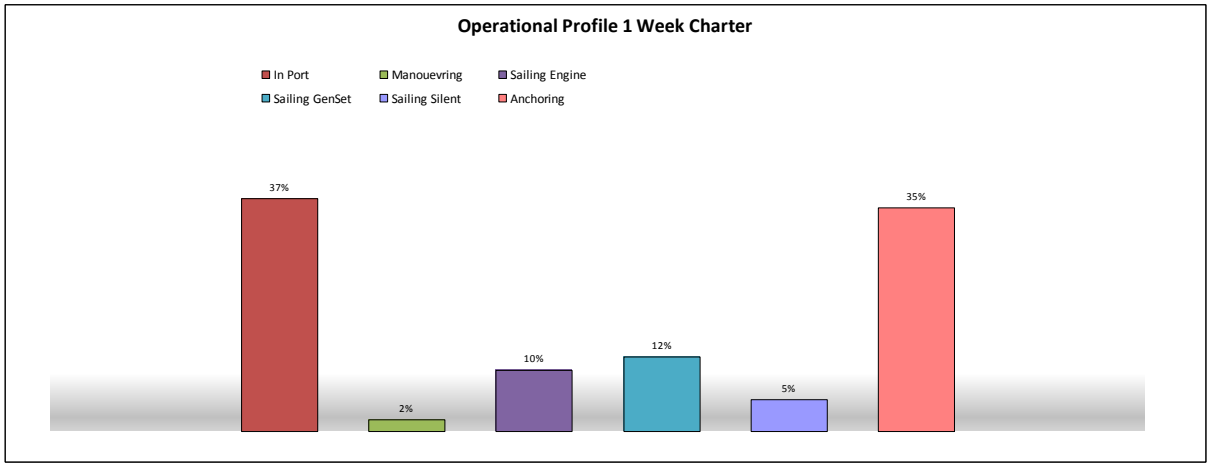

Figure C

5. OUR FIRST SYSTEM PROPOSAL

Our first proposal was for a true diesel electric, fully hybrid system based on a high DC power bus of 750 VDC, which we called the Hy-Grid. The power supply came from two WhisperPower variable speed diesel generators (VST) of max 200 kW, connected to the DC Power Bus by means of AC/DC power converters through automatic switches. All this would be built into two DC main switchboards (see figure D).

A 350 kW permanent magnet based electrical motor (DC) provides propulsion, driving the propeller shaft through a gearbox. This electric drive is connected to the DC power bus by means of DC/DC power converters and automatic switches. A lithium-ion battery pack feeds the DC Power Bus. Both generators operate on variable speed to achieve the optimum balance between fuel consumption, cost of ownership and the power provided. During operation of the yacht, the Hybrid Power Management System (HPMS) serves as the heart of the system, constantly sensing the electric power demand.

This system had our preference, offering the most flexible solution as far as the location and layout of the engine room was concerned with maximum freedom of design.

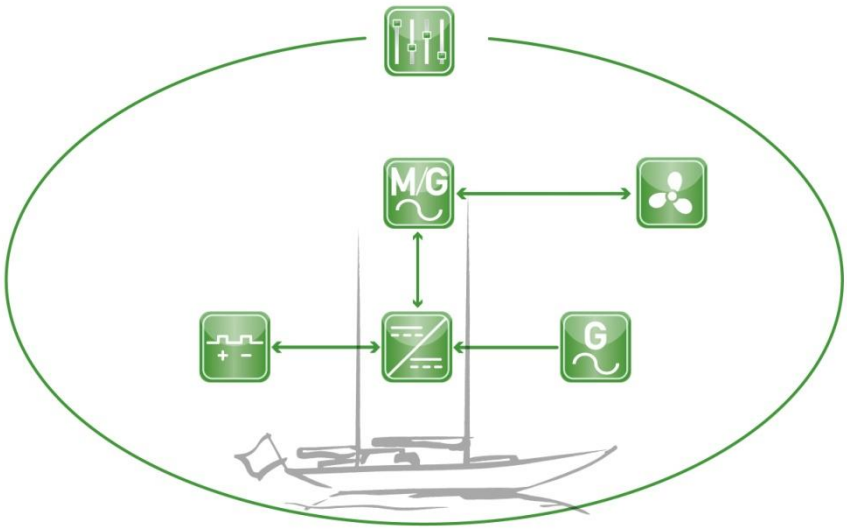

Figure D

In a serial hybrid system (fully hybrid) the conventional diesel engine is replaced by an electrical motor. A battery bank is connected to the common high voltage electric power bus, which is connected to the motor.
The electrical energy is either provided by variable speed power generators or by the battery bank. With large batteries you can have long periods of electric propulsion (and/or driving onboard electrical appliances) without resorting to the generator. Energy can also be produced by the propeller when sailing.

6. THE FINAL CHOICE

After some months of discussing the pros and cons of the proposed serial hybrid system, the customer asked us to propose an alternative system. This parallel hybrid system would have a similar set-up but with a combined traditional propulsion engine/generator instead of the electrical propulsion engine (see figure E).

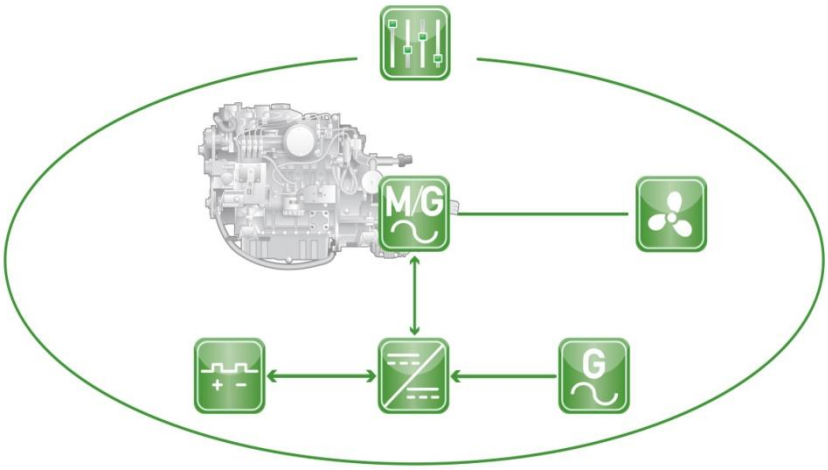

Figure E

In this parallel hybrid system the mechanical connection between the engine and propeller shaft is maintained, with the electric motor acting on the drive shaft in parallel with the engine. The power split is a mechanical device that allows transfer of power between its connections. The propeller can be driven directly from the engine, the electric motor or both. The propeller can also be disconnected to let the propulsion engine operate a stand-alone generator function.

An additional WhisperPower variable speed generator (VST) of 50 kW is installed as the main generator during peak energy consumption periods, running low rpm at low demand (1200 rpm) and high rpm (up to 3600 rpm) during high power demands. We choose this kW size to realise an optimum balance between P-out and rpm. As the 400 VAC 3 phase load is indirectly connected to a WhisperPower generator via the inverter and main battery, peak power loads will be handled by the combination of both. This peak shaving effect means that the generator kW size can be kept smaller.

All key system components projected in the yacht are described below.

Hy-Gen power generator
Variable speed generators (1200-3600 V) based on intelligent, permanent magnet, water-cooled alternator technology, utilising an ultra-compact diesel engine (4 cil Steyr), fitted in a sound shield. This power pack feeds a high DC power bus, connected to the propulsion systems and the DC-AC power conversion system (30 kW inverter) for the hotel load. Power rating: 50 kW.

Hy-Store power storage
Deep cycle, long-life lithium-Ion LiFeYPO4 battery banks (port and starboard) provides emission-free power for propulsion and/or power generation, without operating the auxiliary generators (Hy-Gen) or using the engines. Capacity of each bank: 288 VDC nom/ 160 Ah, 35 kWh power available effective. WhisperPower Battery Management System (BMS) ensures accurate cell balancing.

Hy-Charge battery charging
Sophisticated system for recharging the Lithium-Ion battery bank from the Hy-Gen power packs or shore power. DC- DC converters connected to the 650 VDC bus system and the 288 VDC (nom voltage) battery.

Hy-Grid distribution system
The DC power distribution system that supplies electric power on demand from the power sources to the power consumers. An isolated and laminated copper bus bar rail system with various switches, built into modular cabinets.

Hy-Invert AC power supply
The highly efficient DC to AC inverters smoothly convert power from the various DC sources into a sine wave one and three phase 230/400 VAC/ 50 Hz. The power rating of 30 kVA is sufficient to operate all domestic appliances including airco.

Hy-Control
All system components are connected to the overall power management system, which controls and monitors the entire system. This advanced automation system is configured according to the yacht's requirements and fitted with a manual override to ensure redundancy. In this project, a PLC-based system is embedded in the total ship's electrical system.

Hy-Prop propulsion
E-propulsion is taken care of by a 50 kW permanent magnet electric motor, driving the propeller shaft through a gearbox. This PM motor is placed between the main engine and the gearbox and shaft. The electric drive is powered by either the Hy-Store or Hy-Gen module. Bow and stern thrusters are operated in a similar way.

7. THE 40-METRE J-CLASS SYSTEM DIAGRAM

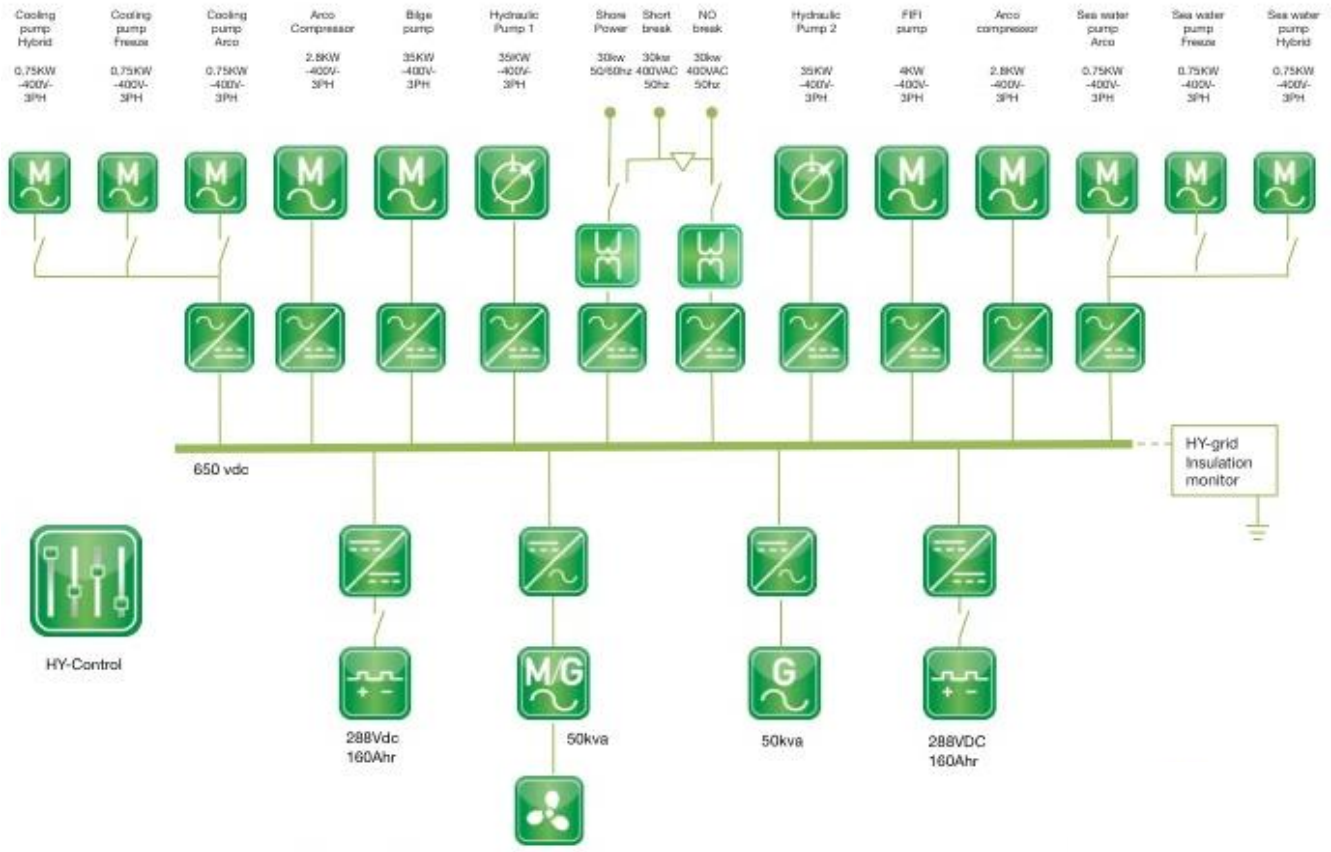

8. ESSENTIAL SYSTEM FEATURES: POWER GENERATION DURING SAILING

In the system we integrated the possibility to generate substantial electrical power (10 kW) when sailing by using the 50 kW electrical motor as a shaft alternator, fitted to the main engine. This way of generating power will result in a speed reduction. Because a controllable pitch propeller is installed, the amount of power to be generated with accompanying speed reduction can be regulated, depending on the available wind speed. For the owner it is important to be able to select between speed and power.

To calculate the possible amount of power generated by the chosen CPP propeller, a four quadrant diagram must be used. While open water diagrams only represent the condition for stationary forward sailing, four quadrant diagrams show the torque and thrust behaviour of a propeller over all four quadrants, as shown in the table below.

Quadrant		Ship Speed V_s	Propeller Speed n_s
1st	0 – 90	+	+
2nd	90 – 180	-	+
3rd	180 – 270	+	-
4th	270 – 360	-	-

Open water diagrams do not provide enough information. The region for instance where the propeller speed approaches zero, torque and thrust coefficients rise to infinity. For this reason, the MARIN research institute developed four quadrant diagrams for various Wageningen B-series propellers. These diagrams depict thrust and torque coefficients, C_T*, C_Q*, for different hydro mechanical pitch angles (β [-]).

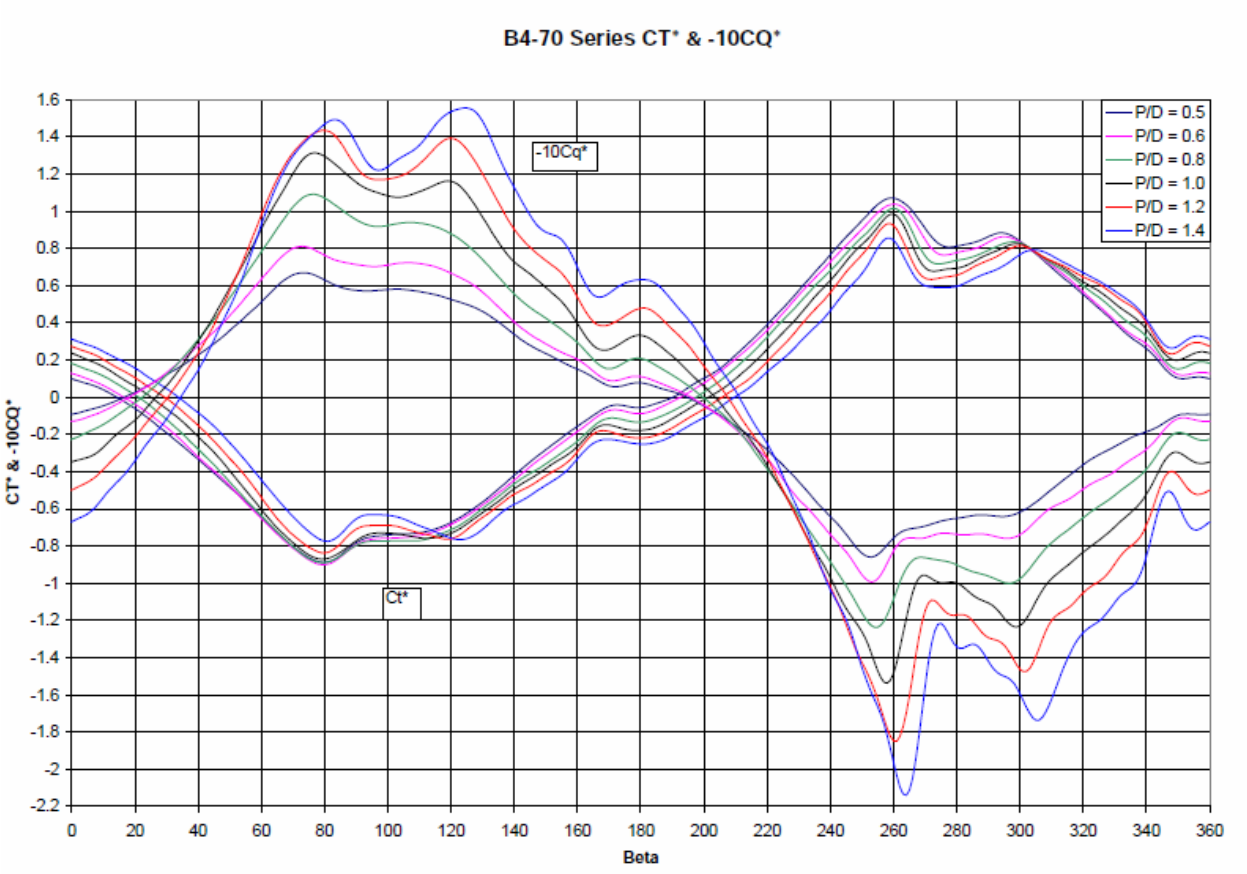

Figure F

To calculate the power generated by the CPP propeller, the torque and propeller speed need to be calculated. These will vary with changing pitch settings, ship speed and allowed speed reduction. The Wageningen B4-70 series four quadrant diagram (figure F) is used because it contains data for most pitch ratios.

D	Propeller diameter	[m]
V_A	Advance velocity	[m/s]
V_S	Intended ship speed	[m/s]
B	Hydro-mechanical pitch angle	[-]
J	Advance ratio	[-]
n_P	Propeller speed	[1/s]
w	Wake fraction	[-]
C_T*	Thrust Coefficient (four Quadrant)	[-]
C_Q*	Torque Coefficient (four Quadrant)	[-]
K_T	Thrust Coefficient (open water)	[-]
K_Q	Torque Coefficient (open water	[-]
R	Resistance	[N]
ρ	Water density	[kg/m^3]

P	Power	[W]
η	Efficiency	[-]

As the ship sails at a certain speed it encounters resistance, R_{int}. When the propeller is trailing it slows the ship down, adding resistance, R_{trail}. At this new speed the ship encounters the new resistance R_{red}, so;

$$R_{trail} = R_{\text{int}} - R_{red} \quad [1.1]$$

At this new ship speed, V_S, the open water diagram intersects with the pitch ratio curves by;

$$K_T = \frac{K_T}{J^2} J^2 \quad [1.2]$$

Combining this with $R_{trail} = -T$, assuming the thrust factor is 0,

$$J = \frac{V_A}{n_p \cdot D} \ , \quad [1.3]$$

$$V_A = V_s \cdot (1-w) \text{ and} \quad [1.4]$$

$$K_T = \frac{T}{\rho \cdot n_p{}^2 \cdot D^4} \text{ this leads to,} \quad [1.5]$$

$$K_T = \frac{-R_{trail} \cdot n_p^2 \cdot D^2}{\rho \cdot n_p{}^2 \cdot D^4 \cdot V_s{}^2 \cdot (1-w)^2} J^2 = \frac{-R_{trail}}{\rho \cdot D^2 \cdot V_s{}^2 \cdot (1-w)^2} J^2 \quad [1.6]$$

Kt relates to CT* through,

$$K_{T,Q} = C_{T,Q}{}^* \cdot \frac{\pi}{8} \cdot [illegible]^2 + 0.7 \cdot \pi^2 \quad [1.7]$$

Combining equations [1.6] and [1.7] with

$$\beta = \arctan\left(\frac{V_A}{0.7 \cdot \pi \cdot n_p \cdot D}\right), \ \beta = \tan^{-1}\left(\frac{J}{0.7 \cdot \pi}\right) \quad (1.8)$$

This leads to

$$C_T{}^* = -\frac{8}{\pi} \cdot \frac{R_{trail}}{\rho \cdot D^2 \cdot V_s^2 \cdot [illegible](1-w)^2} \cdot \frac{J^2}{[illegible]J^2 + 0.7 \cdot \pi^2} = -\frac{8}{\pi} \cdot \frac{R_{trail}}{\rho \cdot D^2 \cdot V_s^2 \cdot [illegible](1-w)^2} \cdot \frac{\tan^2 \beta}{[illegible]\tan^2 \beta + 1} \quad (1.9)$$

Equation [1.9] is plotted in the four quadrant diagram for different ship speeds at different trailing resistances. These curves intersect with the different pitch ratio propeller curves in the four quadrant diagram, at which *CT**, *CQ** and accompanying *B* were determined.

Combining equation [1.7] with [1.8] and [1.3] results in values for K_Q and n_p.
Now P_{prop} can be calculated, with

$$K_Q = \frac{Q}{\rho \cdot n_p^{\ 2} \cdot D^5}$$, resulting in [2.0]

$$P_{prop} = 2\pi \cdot K_Q \cdot \rho \cdot n_p^3 \cdot D^5$$ [2.1]

The power generated by the trailing propeller can now be calculated by taking the shaft, gearbox and generator efficiency into account.

$$P_{gen} = P_{prop} \cdot \eta_s \cdot \eta_{GB} \cdot \eta_{gen}$$ [2.2]

Sailing at an intended speed of 10 kn, and allowing several reductions up to a maximum of 2 kn, the power at the propeller (generated by the trailing propeller) and accompanying shaft speed is shown for varying pitch ratios in figure G. In the same way this is shown for an initial speed of 13 kn in figure H.

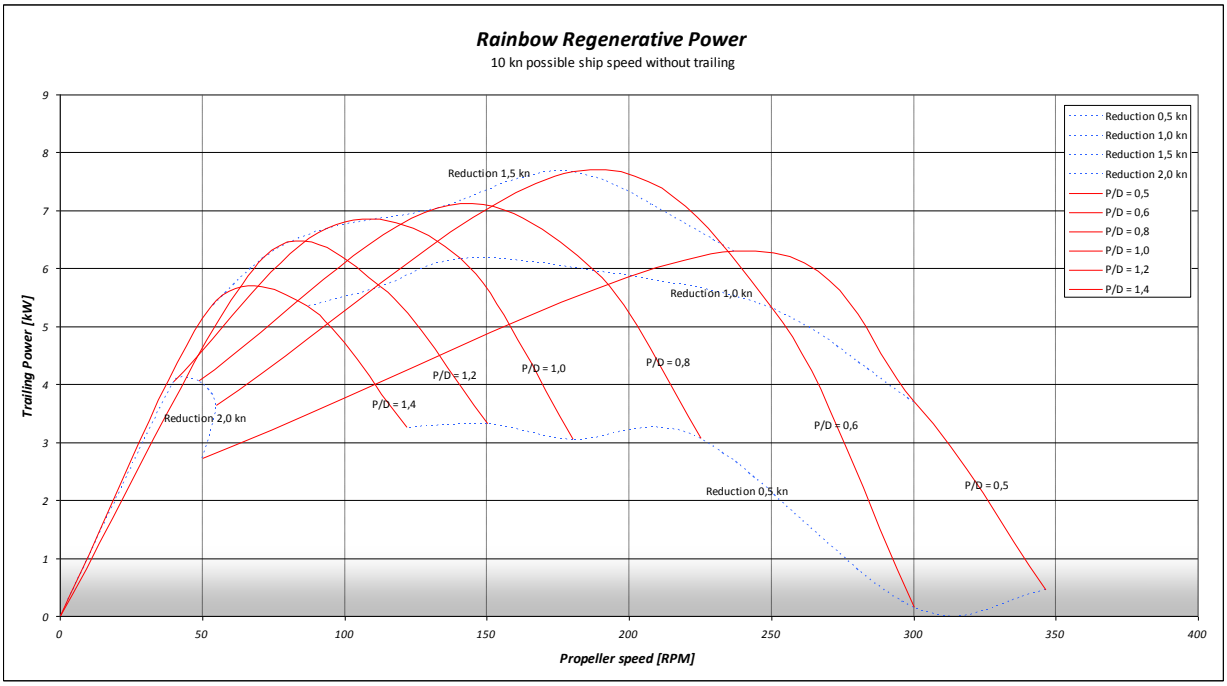

Figure G

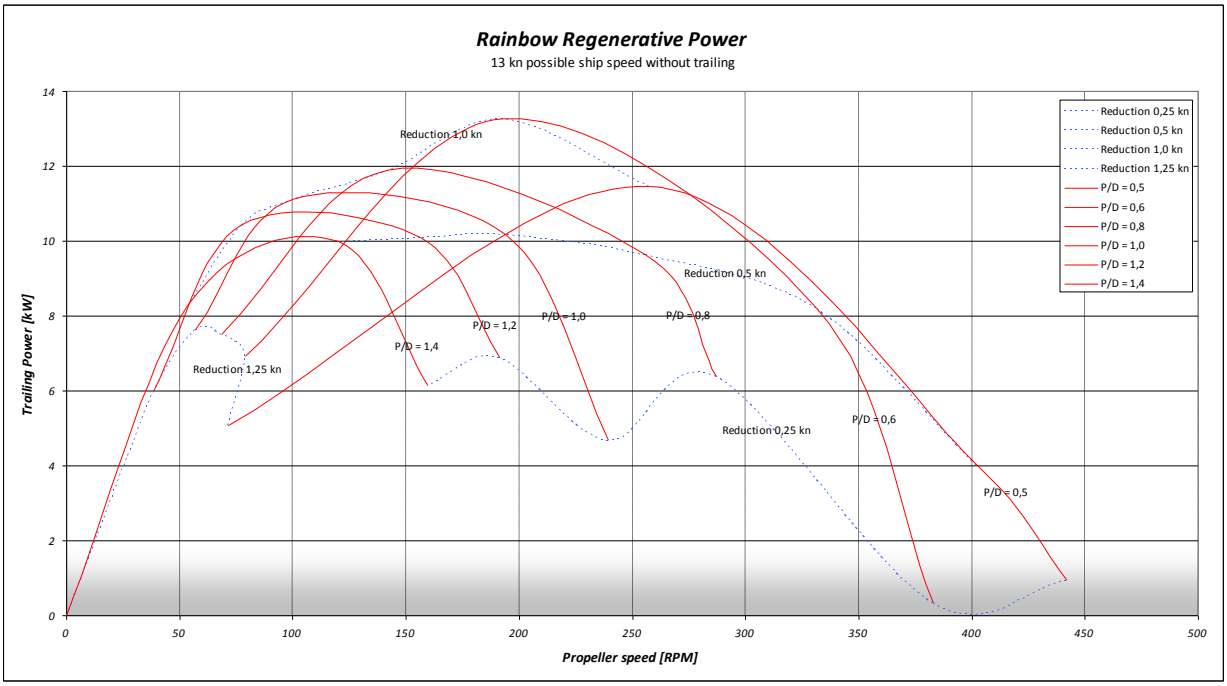

Figure H

When sailing at an intended speed of 10 kn, and allowing for a 1.5 kn reduction, the maximum power can be generated at a pitch ratio of P/D = 0.6. This results in P_{gen} = 7.1 [kW], at a shaft speed of 180 [RPM]. For an intended speed of 13 kn, the maximum power to be generated is at a pitch ratio of about P/D = 0.6 and a speed reduction of about 1.0 kn. This will generate about P_{gen} = *12.2* [kW] at a shaft speed of 193 [rpm].

9. ESSENTIAL SYSTEM FEATURES: THE BATTERIES

In battery-based systems such as our hybrid system, the specifications of the selected batteries are crucial for the performance of both power and propulsion. Traditional lead acid batteries are not good enough for such systems, which is why we use lithium-ion batteries. Common in consumer electronics, they are one of the most popular types of rechargeable battery for portable electronics, with one of the best energy-to-weight ratios, no memory effect, and a slow loss of charge when not in use. Lithium-ion batteries are also growing in popularity for military electric vehicles and aerospace applications due to their high energy density. They are three times smaller, three times lighter and three times more durable than conventional semi-traction lead-acid batteries.

As lithium-ion batteries vary in materials and construction, the type selected depends on the target application. For our hybrid systems we use lithium-ion phosphate type batteries. These are the best choice for frequent high deep discharge and charge cycles, and can handle the heat which comes into the battery the best way. Stacks are engineered in such a way that cooling is optimised.

Our LiFeYPO4 batteries can be charged and discharged by 1/C. To prevent damage and complete malfunction of the batteries, a sophisticated Battery Management System is added which ensures proper cell balancing at charge and discharge. Safety requirements are given a high priority during the engineering process of the system as overcharging and discharging can short circuit the cell, potentially making recharging unsafe.

10. SYSTEM COSTS

We can roughly estimate the price difference between conventional systems and our new hybrid systems. Installing a hybrid system offers a range of benefits: 1/ extended silent time, with no generator running, 2/ peak shaving, and 3/ electrical navigation and manoeuvring. These features cannot be realised with traditional systems. As a rule of thumb we calculate the price of a hybrid system to be at least twice that of conventional system. Orders for large systems in general take 40 to 50 weeks, with smaller systems being available in around 25 weeks.
